Experimental Investigation of Concentrating Solar Baker Using Parabolic Trough Solar Collector Integrated with Thermal Energy Storage

By

Seid Getachew Abate

A Thesis Submitted to the Department of Thermal and Aerospace Engineering

School of Mechanical, Chemical and Materials Engineering

Presented in Partial Fulfillment of the Requirement for the Degree of Master of science in Thermal Engineering

Office of Graduate Studies
Adama Science and Technology University

August, 2021

Adama, Ethiopia

Experimental Investigation of Concentrating Solar Baker Using Parabolic Trough Solar Collector Integrated with Thermal Energy Storage

By

Seid Getachew Abate

Advisor: Dr. Dawit Gudeta

A Thesis Submitted to the Department of Thermal and Aerospace Engineering

School of Mechanical, Chemical and Materials Engineering

Presented in Partial Fulfillment of the Requirement for the Degree of Master of science in Thermal Engineering

Office of Graduate Studies
Adama Science and Technology University

August, 2021

Adama, Ethiopia

DECLARATION

I hereby declare that this MSc. thesis entitled "*Experimental Investigation of Concentrating Solar Baker Using Parabolic Trough Solar Collector Integrated Thermal Energy Storage*" in partial fulfillment of the requirement for the award of the degree of Master of Science in thermal engineering is my original work under the supervision of Dr. Dawit Gudeta, Assistant Professor of Thermal and Aerospace Engineering Department.

The matter embedded in this thesis has not been submitted for the award of a degree or diploma in any other university. All relevant resource information used in this paper has been duly acknowledged.

Seid Getachew Abate	______________	________________
Candidate	Signature	Date

This is to certify that the above statement made by the candidate is correct to the best of my knowledge and belief. This thesis has been submitted for examination with my approval.

Dr. Dawit Gudeta	_________________	________________
Advisor	Signature	Date

APPROVAL OF BOARD OF EXAMINERS

We, the undersigned, members of the Board of Examiners of the final open defense by Seid Getachew Abate has read and evaluated his thesis entitled *Experimental Investigation of Concentrating Solar Baker Using Parabolic Trough Solar Collector Integrated Thermal Energy Storage*" and examined the candidate. This is, therefore, to certify that the thesis has been accepted in partial fulfillment of the requirement of the Degree of Master of Science in Thermal Engineering.

This is, therefore, to certify that the thesis has been accepted in partial fulfillment of the requirement of the Degree of Master of Science in Thermal Engineering.

Seid Getachew Abate	______________	______________
Candidate	Signature	Date
Dr. Dawit Gudeta	______________	______________
Advisor	Signature	Date
______________	______________	______________
External Examiner	Signature	Date
______________	______________	______________
Internal Examiner	Signature	Date
______________	______________	______________
Chairperson	Signature	Date
______________	______________	______________
Head of Department	Signature	Date
______________	______________	______________
School Dean	Signature	Date
______________	______________	______________
Post Graduate Dean	Signature	Date

DEDICATED
TO
MY MOTHER SERKE MENGISU
and
MY FATHER GETACHEW ABATE

ACKNOWLEDGEMENTS

First of all, I would like to give special thanks to God for giving me the patience, courage and strength during my life. I would like to express my deepest gratitude to my advisor, Dr. Dawit Gudeta for his continuous support, encouragement, invaluable comments, and supervision that helped me during the time of the thesis work. I also would like to thank Dr. Addisu Bekele for sharing his academic experience, knowledge and he has been an enormous resource to me in all aspects of my academic life. I express my sincere thanks to Mr. Mekonen Yalelet and Mr. Dessie Tadele of the Thermal and Aerospace Engineering staff, for their outstanding suggestions and continuous inspiration during my study period. I would also like to thanks all my best friends for their encouragement, suggestion, and assistance, and gave a worthy comment on my work and through the process of researching. I am also grateful to express my sincere gratitude to Adama Science and Technology University for allowing me to join a master's program with a full scholarship. Finally, I extend my deep gratitude to thank my family for their support during tough times and motivating me throughout my life, and for their constructive suggestions and inspiration.

ABSTRACT

Energy is one of the building blocks of modern society. The growth of modern society has been fueled by cheap, abundant energy resources. Solar energy is a form of renewable energy which is available abundantly and collected unreservedly. One of the energy-intensive activities is baking. Energy demand for baking is mostly fulfilled by biomass, natural gas, and electricity. Solar energy is also one of the promising solutions for meeting the energy demand. In this thesis, the work aims to design and experimentally test a solar bread baking system. The selected solar collector and the thermal storage are also designed based on: the amount of bread supplied to the family two times throughout the day and the energy needed to bake the demanded bread. The uses of parabolic trough collectors to capture solar radiation to receiver tube and the hot HTF (Shell Thermal oil B) circulates through the receiver tube, baking unit, and thermal storage unit filled with 10kg D-mannitol having a melting temperature of 440.15K. Thermal storage was considered as a heat source for baking at off sunshine hours of the day. Comparative studies on the performance of PTC without and with receiver fin and receiver fin with shield are conducted using the no-load experimental test. The result showed that the maximum outlet HTF temperature, maximum thermal, and exergy efficiency of PTC are found to be 456.45K, 51.9%, and 28.5%, with receiver fin 465.25K, 53.6%, and 29.7% and receiver fin with shield 469.85K, 55.2%, and 31.1% respectively. The experimental result of LHS using D-mannitol showed that the amount of sensible, latent, and total energy stored/released during the charging/discharging processes are, 1.78MJ, 3.15MJ, and 4.93MJ and, 1.41 MJ, 2.85MJ and 4.26MJ respectively. A baking plate surface temperature of 433K was achieved and the corresponding baking time was 55 minutes. Finally, economic analysis was performed and the pay-back period of the bread baker was found to be 2.93 years.

Keywords: Solar thermal bread baker, PTC, PCM, Baking Plate

Table of Contents

Contents **page**

List of Figures

List of Table

ABBREVIATIONS

BCR	Benefit-cost ratio
CFD	Computational fluid dynamics
CSP	Concentrated solar power
DSG	Direct steam generation
EHC	Effective heat capacity
EL	End loss
HTF	Heat transfer fluid
CST	Concentrated solar thermal
LCC	Life cycle cost
LHESS	Latent heat energy storage system
LHS	Latent heat storage
LPM	Littre per minute
LSC	Life cycle saving
LSCA	length of a single solar collector assembly
NPV	Net present value
NPW	Net present worth
NTU	Number of transfer units
PCM	Phase change material
PTC	Parabolic trough collector
PTR	Parabolic trough receiver
PTSC	Parabolic trough solar collector
PTSPP	Parabolic trough solar power plant
RHS	Rectangular hollow sections

RS	Row shading
SCA	Solar collecting assembly
SEGS	Solar electric generation systems
SHES	Sensible heat energy storage
SHS	Sensible heat storage
SPP	Simple payback period
ST	Local solar time
TDH	Total dynamics head
TES	Thermal energy storage

NOMENCLATURE

$\dot{E}_{dest}$	Destroyed exergy rate (W)
$\dot{E}_{in}$	Inlet exergy rate (W)
$\dot{E}_{l}$	Loss exergy rate (W)
$\dot{E}_{out}$	Outlet exergy rate (W)
$\dot{E}_{s}$	Stored exergy rate (W)
h_{12}	Heat transfer coefficient of HTF (W/m^2-k)
h_{34}	Convection heat transfer coefficient from the air (W/m^2-k)
k_1	Thermal conductivity of the HTF
k_{23}	Absorber thermal conductivity at the average absorber temperature (W/m-k)
Nu_{d2}	Local Nusselt number of HTF
Nu_{d3}	Average Nusselt number based on the absorber outer diameter
Pr_1	Prandial number of HTF
Pr_{34}	Prandtl number for air at T_{34}
$q'_{12\ Conv}$	Convection heat transfer from the absorber to the HTF(W/m^2)

$q'_{23\ Cond}$	Conduction Heat Transfer Trough the Absorber Wall (W/m^2)
$q'_{34\ Conv}$	Convection heat transfer from the absorber to the atmosphere (W/m^2)
$q'_{35\ rad}$	Radiation heat transfer from the absorber to the atmosphere (W/m^2)
Ra_{d3}	Rayleigh number for air based on the pipe outer diameter
Re_{d2}	Reynolds number of HTF
V_1	Kinematic viscosity of HTF
v_{34}	Kinematic viscosity for air (m^2/s)
α_1	Thermal diffusivity of HTF
α_{34}	Thermal diffusivity for air (m^2/s)
ε_3	Emissivity of the carbon steel pipe outer surface
Δp	Pressure drops (pa)
Δt_{ch}	Total charging times (hr)
Δt_{dis}	Total discharging times(hr)
a_1 and b_1	Regression coefficients
Aap	Aperture area (m^2)
Aap,r	Aperture receiver area (m^2)
C_r	Concentration ratio
D_2	Inside diameter of absorber pipe [m]
D_3	Outside diameter of absorber pipe [m]
f	Focal length [m]
G	Gravitational acceleration (m/s^2)
H_O	Daily extraterrestrial solar radiation on a horizontal surface(W/m^2/day)
hv	Heat of vaporization of water (kJ/kg)

I_{ext}	Extraterrestrial radiation (W/m^2)
I_O	Extraterrestrial solar radiation on a horizontal surface (W/m^2/day)
I_b	Beam radiation factor (W/m^2)
I_{sc}	Solar constant (W/m^2)
k_1	Thermal conductance of HTF at T_1 [W/m-K]
k_{23}	Thermal conductance of absorber wall at T_{23} [W/m-K]
L	Length of LHS unit (m)
Q_{req}	Required Energy
Qs	Sensible Heat Capacity
Re	Reynolds number
T_1	Mean (bulk) temperature of the HTF (^oC)
Ta	Ambient Temperature (^{o} C)
Tb	Boiling Temperature of Water (K)
T_{max}	Maximum Temperature(K)
T_{min}	Minimum Temperature
C_p	Heat capacity (KJ/kg.K)
Cp_s and Cp_l	Specific heat capacity of PCM at solid-state and liquid state (J/kg.K)
D_{cyl}	Diameter of PCM containment cylinder (m),
$\dot{Ex}_{dest}$	Destructed exergy rate (W)
$\dot{Ex}_{in}$,	Rate of inlet exergy (W)
$\dot{Ex}_{in.f}$	Exergy of collector inlet heat transfer fluid (W)
$\dot{Ex}_{in.rad}$	Exergy of absorbed solar energy from the sun (W)

$\dot{Ex}_{out}$	Outlet exergy rate (W)
$\dot{Ex}_{out.f}$	Exergy of the outlet fluid (W)
H_G	Monthly average daily global solar radiation (W/m^2/day)
H_b	Monthly average daily beam radiation (W/m^2)
H_d	Monthly average daily diffuse radiation on a horizontal surface (W/m^2/day)
I_G	Monthly average hourly global radiation on a horizontal surface (W/m^2)
I_T	Incident solar radiation on an inclined surface (W/m^2)
I_d	Monthly average hourly diffuse radiation on a horizontal surface (W/m^2)
$L_{F.\,pcm}$	latent heat of fusion for the PCM (J/kg)
$\dot{Q}_{loss}$	Rate of heat loss (W)
$\dot{Q}_u$	Useful heat gain (W)
R_o *and* R_i	Outer and inner diameter of HTF tube (m)
T_L	Liquidus temperature (K)
T_S	Solidus temperature (K)
T_{in}	Inlet temperature (K)
T_m	Melting point of PCM (K)
T_{out}	Outlet temperature (K)
Tp,f	Final baking plate temperature (K)
Tp,i	Initial baking plate temperature (K)
U_L	Overall heat loss coefficient (W/ $m^2.K$)
V_{PCM}	Volume of PCM (m^3)
V_{tube}	Tube volume (m^3)
$\dot{m}$	Mass flow rate(kg/sec)

ρ	Density (kg/ m^3)

Greek symbol

a	Solar altitude angle (°)
θ_z	Zenith angle (°)
ω	Hour angle (°)
θ	The angle of incidence (°)
ϕ	Latitude angle (°)
δ	Declination angle (°)
η_{th}	Thermal energy efficiency (%)
η_{ex}	Exergy efficiency (%)
η_o	Optical efficiency (%)
θ_f	Melt fraction (%)
γ	Surface azimuth angle
γ_s	Solar azimuth angle
μ	Dynamic viscosity (Pa.s)
$\boldsymbol{\nu}$	Kinematic viscosity (m^2/s)
Ψ	Rim angle (°)
σ	Stefan-Boltzmann constant (W/ m^2. K^4)

CHAPTER ONE

INTRODUCTION

1.1 Background of the Study

Energy is a crucial input for technological, industrial, social and economic development of a country. All societies require energy services to meet basic human needs like lighting, cooking, mobility, communication, etc., but Greenhouse gas emissions associated with the provision of energy services can be seen as the major cause of climate change. Biomass is the primary source of energy in developing countries. Biomass is often thought of as a renewable energy source; but, in developing countries where deforestation and afforestation are not balanced, this is a misleading concept. According to studies, about 1 billion people who rely on this source of energy are at risk of death and serious health problems (World bank, 2019). There are two types of energy sources i.e renewable and non-renewable. Aside from making a concerted effort to use different forms of resources, the world's attention is now focused on mitigating environmental problems by improving energy quality and lowering carbon emissions. Household energy consumption accounts for more than 30% of overall energy consumption in developing countries. cooking is one of the most energy-intensive everyday activities, accounting for roughly 90% of domestic energy consumption in these countries (Newell *et al*.,2019). The majority of rural households rely on biomass fuels for heating and cooking, with firewood accounting for nearly all of the fuel used in village kitchens. Each year, about 16 million hectares of forest are burned as cooking fuel, resulting in three million deaths worldwide due to toxic pollution from the burning of this biomass fuel (Sedighi and Salarian, 2017). The majority of people in developing countries cook their food with biomass as their primary energy source. Cooking accounts for more than half of Ethiopia's total primary energy consumption. Because of population growth, the number of people dependent on biomass for cooking will rise to 2.7 billion by 2030 unless new renewable and cleaner sources of energy are used (Adem and Ambie, 2017). Several threats associated with the use of non-renewable energy sources have compelled world public unions, international and national institutions, and other organizations to urgently seek alternative renewable energy sources and convert current energy systems to a more sustainable foundation. Exploiting other available and renewable energy resources at the local level via appropriate energy technology designs appears to be a more long-term solution. Solar energy is a clean, plentiful, and easily accessible renewable energy source among alternative energy sources. However, because of its intermittent and dynamic nature, it is difficult to effectively utilize the energy. The thermal energy storage (TES) system provides a solution to these issues, as well as the time gap between energy demand and supply.

1.1.1 Bread Baking Method

Bread is a popular food made from wheat flour and water dough by the baking process. During baking, a variety of physicochemical and biological transformations occur concurrently, including water evaporation, starch gelatinization, volume expansion, crust formation, protein denaturation, and browning reactions. As a result of the complicated baking process, bread baking is a very difficult issue. Since bread baking is a non-reversible method, the key problem is manufacturing high-quality bread. Since it is a non-reversible process, unsatisfactory products must be discarded, which is economically unfavorable (Chhanwal *et al*., 2010; Pinelli and Suman, 2017). Baking is a heat and mass transfer process that occurs simultaneously. Water evaporates during baking, and the vapor condenses on the cooler side of the chamber. This evaporation–condensation process will proceed until the entire crumb reaches a temperature of 100 °C**.**

Bread is a basic need for people all over the country, especially in Ethiopia. It, along with *injera*, accounts for a large portion of food consumption in all parts of the countries. Bread (*Difo Dabo*) was baked for Holydays, Birth Days, Religious, and other ceremonies in addition to regular household consumption. Baking is often performed in Ethiopia using traditional methods such as fossil fuels, and biomass (firewood), all of which are rapidly depleting and a major cause of global warming. As a result, due to the impending energy cost and crisis, there is a crucial need for the production of alternative, suitable, and affordable baking systems. The majority of published researches on the bread baking process does not give attention to the use of solar thermal systems for bread baking.

1.1.2 Concentrating Solar Thermal collector

Concentrating solar thermal (CST) technologies produce high-temperature, high-quality energy that can be used to drive a variety of engineering processes. CST is attractive because of free and abundant solar radiation. The four main commercial CST technologies are distinguished by the way they focus the sun's rays and the technology used to receive the solar energy: parabolic-trough collector (PTC), solar tower (ST), linear Fresnel (LF) and parabolic dish (PD). They can be classified according to the focus type (line focus or point focus).

Parabolic trough concentrator is one of the most common solar concentrators to generate high temperature of HTF for CST technology.

Parabolic trough concentrator (PTC) comprises of a cylindrical concentrator of parabolic cross-sectional shape and a circular cylindrical receiver located along the focal line of the parabola. It reflects direct solar radiation onto a receiver tube located in the focal line of the parabola. Since the collector aperture area is bigger than the outer surface of the receiver tube, the direct solar radiation is thus concentrated.

The parabolic trough concentrator (PTC) converts solar beam radiation into thermal energy in its linear focus receiver. The focal line onto which the beam radiation is reflected is comprised of all focal points at each cross-sectional location of the concentrator. The trough assembly tracks the sun in a single axis so as to always keep the trough aperture towards the sun. The trough is generally mounted with its focal axis parallel towards either east- west direction or north-south direction (Kalogirou, 2009).

1.1.3 Thermal Energy Storage System

Solar energy is a renewable energy source that is clean, plentiful, and free to use. However, because of its intermittent and dynamic nature, it is difficult to effectively utilize the energy. The thermal energy storage (TES) device becomes a solution to those naturals and the time-mismatch between energy demand at night and usable solar energy during the day (Kousksou *et al.*, 2007). TES retains energy by melting, or vaporizing a storage medium, then cooling or solidifying the storage medium to use the stored energy for different applications later. Due to the changing nature of solar radiation during the day, a TES must be adequately built to ensure a constant supply of heat (Dawit, 2018). Thermal energy storage can minimize the gap between supply and demand in this case. These thermal storage systems include sensible and latent heat storage systems as shown in figure 1.1. In sensible heat storage systems, the energy is stored by changing the temperature of storage material like concrete, sand-rock minerals, ferroalloy materials, bricks, etc. whereas, in latent heat storages, the heat transfer occurs when substances like salt nitrates, paraffin wax, etc. change their phase from solid to liquid and vice versa. Latent heat storage systems store higher amounts of energy per unit storage material compared to sensible heat storage systems (Swami *et al*., 2018). Phase change material (PCM) is a kind of latent energy storage material that undergoes an isothermal or near isothermal phase transformation, which has attracted considerable attention due to the high energy storage density and compactness of the material (Wang *et al*., 2015). As a result, TES systems are used to completely harness solar energy while still providing coverage during off-peak hours.

To improve the sustainability of renewable energy sources it is important to incorporate the concept of energy storage. The importance of energy storage is to (Tesfay, 2015):

- Meet short-term fluctuating energy demand requirements.
- Redistribute the energy required during on-peak demand conditions through the energy.
- Make use of the energy generated from renewable sources during fluctuating load.

Thermal energy storage can be classified by storage mechanism; those are sensible heat storage (SHS), latent heat storage (LHS), and chemical or bond heat storage.

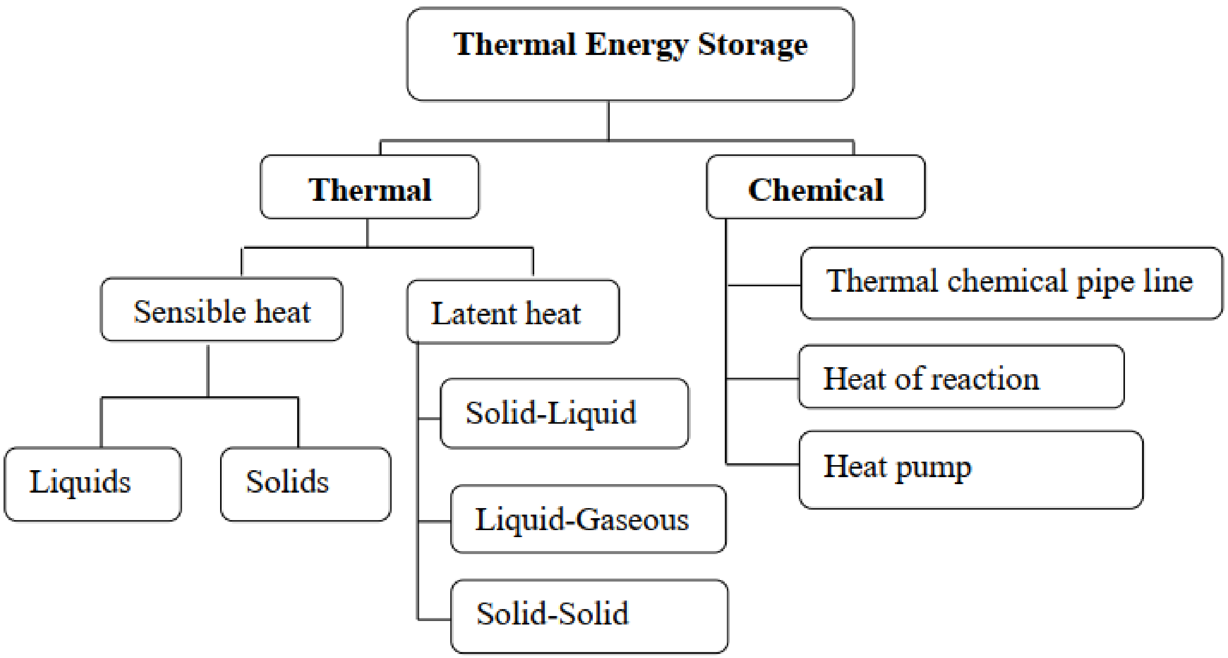

Figure 1. 1:- Classification of the forms of thermal energy storage (Swami *et al*., 2018).

1.2 Statement of the Problem

In Ethiopia, bread baking requires a bulk of domestic energy. It apparent that bread baking energy usage mainly depends on biomass, fossil fuels, and electricity. Due to the limited access to electricity, bread baking is mainly through biomass. In most households, the bread baking system is carried out using an open fire /three stones/ stove which is inefficient and a waste of energy. To bake bread, the heat supplied to the baking pan comes usually from burning firewood, animals' dung, and agricultural residue in biomass bakers using the traditional *Mitad* stoves for centuries.

Due to the growing scarcity of wood fuel, people are forced to travel long distances from their homes to fetch wood; this struggle is carried almost entirely by women and children. Recent field observation shows that improvements in air control and firebox design are currently the most effective and socially acceptable stove design modifications. However, their usefulness in saving the resource base from depletion is limited in the face of the growing population and urbanization because they use firewood as the source of energy. In addition, the wood firing causes health problems due to inhalation of carbon monoxide, smoke, and emission of Carbon dioxide into the atmosphere which results in the greenhouse effect**.** Thus, to reduce and avoid the addressed problems, it is important to look for a new means of fuel source by utilizing energy from the solar. Converting the solar radiant energy to heat is the most common and well-developed solar energy conversion to alleviate the stated problems. Therefore, the present thesis effort has been made to properly design a solar bread baker which utilizes a parabolic trough collector as a heat source and phase change material-based thermal energy storage system for the off-sunshine operation of the baker.

1.3 Objective of the Study

This section describes the general and specific objective of the thesis.

1.3.1 General Objective

The general objective of this study is to carry out an experimental investigation on solar bread baker by using a parabolic trough solar collector which is integrated with thermal energy storage.

1.3.2 Specific Objectives

The specific objectives of this study are:

- Designing and fabricating of parabolic trough solar collector and solar bread baking system.
- Evaluating and analyzing the performance of parabolic trough solar collector with and without fin and shield.
- Evaluating the thermal performance of the Phase change material-based Latent heat storage system.
- Experimentally investigating solar bread baking system for average family size.

1.4 Significance of the Study

The majority of Ethiopia's population lives in rural areas. Women and children spend much of their time collecting firewood and they are exposed to health problems due to smoke inhalation from the burning wood while cooking. The use of solar bread baking systems where there are no other alternatives like electric power helps to conserve time that can be used for production purposes and avoids the health problems that may be caused by smoke inhalation. Applying a solar baking system is expected to solve the problem of energy sustainability by replacing the current dependency on firewood, cow dung, crop, and petroleum oil residues and this contributes to a reduction in air pollution and greenhouse gas emissions in the long-range through avoidance of forest deforestation.

1.5 Scope of the Study and Its Limitation

The scope of this study will be designing and selecting components for solar bread baker, parabolic trough solar collector for harvesting of solar energy and a PCM based thermal energy storage system, development of the prototype from easily and locally available materials for conducting an experimental investigation. During the thesis works, Some limitation makes the study hard. Lack of accessibility of measuring equipment like Pyranometer, flow meter, and others. The baking temperature distribuation on the baking plate was not considered in this study.

1.6 Organization of the Study

This thesis is composed of eight chapters. After the previous chapter introduces the concept of solar energy, bread baking technology, and thermal energy storage, a literature survey on the same was presented in chapter two with its summary. The third chapter presents the material and methodology section of the work followed by chapter four which presents the estimation of solar potential for the selected site. The fifth chapter formulates the theoretical design and sizing of system components for individual performance investigation. Then, the sixth chapter describes the conceptual design, construction process, and the experimental setup of the prototype. Chapter seven presents the major findings and results of the experimental analysis conducted with their implication. The last chapter includes the conclusion of the whole work and recommendations for further study.

TWO

LITERATURE REVIEW

2.1 Introduction

This chapter concerns some general information about solar thermal energy utilization that has been done in the past years. In this part earlier works related to solar energy and its application, parabolic trough solar collector, bread baking technology, solar thermal energy storage system, phase changing material, heat transfer fluid, and thermal insulation were reviewed. Finally, a summary of all the literature and its gap is also included.

2.2 Basics Solar Energy

Earth receives about 170 x 10^{12} kW of energy from the sun out of this,30% is reflected in the outer atmosphere, 23% is utilized in the photosynthesis process and 47% is received as low-temperature energy at the surface (Duffie and Beckman, 2013). The energy demands for the last two centuries are met mainly by utilizing carbon fuels. Due to the forecast of fossil fuel depletion, researchers are focusing their attention on other energy sources like nuclear energy and non-conventional energy (Cardinate *et al*., 2003). The increasing environmental concern due to global warming and the harmful effect of carbon emission have also created new demand for clean and sustainable energy, i.e.., solar, wind, biomass, and geothermal sources of energy. Among the various sources, solar energy is widely accepted as a clean, environmentally friendly, cheap, and limitless energy source (Keyanpour *et al*., 2000).

2.3 Applications of Solar Energy

Solar energy is considered to be the most promising source of energy. Solar energy can be used for various applications of solar thermal technology as illustrated in Figure 2.1. These are generally for heat applications and power applications. Depending upon the application temperature, solar thermal technology for heat applications is further categorized into low, medium, and high-temperature systems. Nowadays, solar power has provided the most efficient and most reliable solar products available in the market. Different industries and researchers are actively involved in research in the area of solar energy.

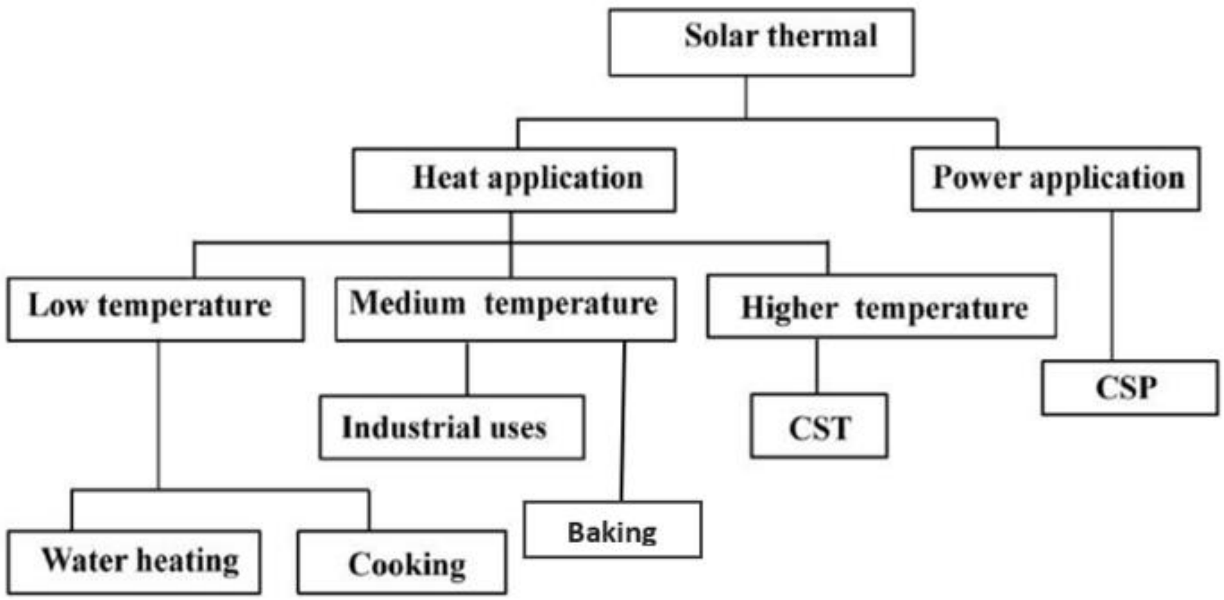

Figure 2.1: - Application of solar thermal technology (Dawit, 2018).

Solar energy is very cheap compared to other sources of energy. It is also abundant and appropriate for many applications. The maintenance cost for solar energy systems is also low. The main disadvantage is the fact that they are subject to weather intermittency; hence will require an energy storage system that will add to the overall cost of the technology (Wilberforce *et al*., 2019).

Zhang (2020) reported that the potential of solar thermal systems in sectors such as the food industry, agro-industries, textiles, and chemical industry. And the systems were evaluated in economic terms in comparison with energy equivalent systems. After the review, it was observed that the installation of different solar harvesting devices such as solar dryers, parabolic through collector systems, and flat plate collectors for different applications can be economically attractive for the users. As the report proved that the use of such systems offers significant energy savings and provides environmental benefits to society.

Mollahosseini *et al.,* (2019) investigated that the environmental problems related to the use of conventional sources of energy and the benefits offered by renewable energy systems. Various types of collectors like flat-plate, compound parabolic, evacuated tube, parabolic trough, Fresnel lens, parabolic dish, and heliostat field collectors were explained. Optical, thermal, and thermodynamic analysis of the collectors and a description of the methods used to evaluate their performance were described. As a result, solar energy collectors can be used in a wide variety of systems and can provide significant environmental and financial benefits, and should be used whenever possible.

2.4 Parabolic Trough Solar Collector

Parabolic trough collectors focus direct solar radiation onto a focal line on the collector axis. To transport high temperatures with good efficiency a high-performance solar collector is required. Systems with light structures and low-cost technology for process heat applications up to 400℃ could be obtained with parabolic trough collectors (PTCs). PTCs can effectively produce heat at temperatures between 50 and 400℃ (Kalogirou, 2013).

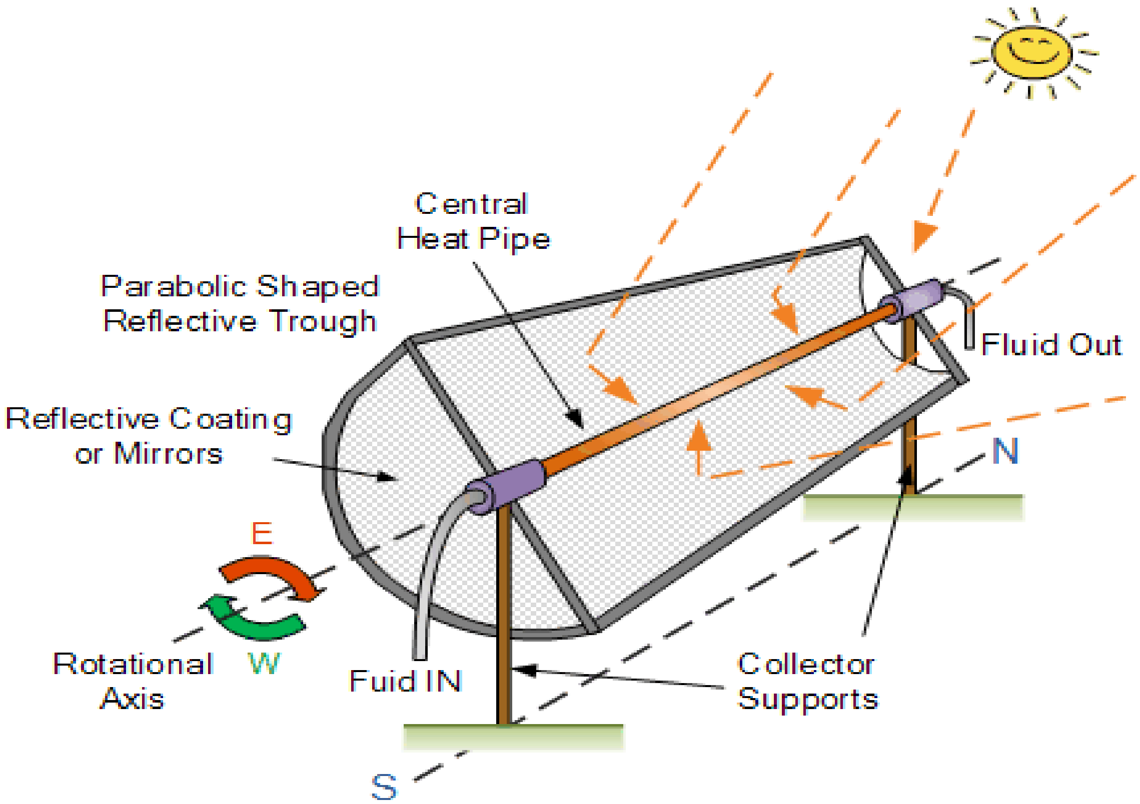

Figure 2.2: - Schematic of a parabolic trough collector (Islam *et al.*, 2015).

Sekhar *et al*., (2018) reported that the solar collector in the shape of a parabolic mirror reflects the incident solar energy on the longitudinal axis of the solar collector. This feature enables the parabolic collectors to achieve high outlet temperatures of the water working fluids, sometimes 120ºC or as high as 140ºC. This feature allows the parabolic concentrators to be integrated with solar thermal systems.

Sandeep and Arunachala (2017) investigated that parabolic trough collectors (PTC) thermal efficiency optimization methods that use evacuated receivers, Nanofluids with/ without inserts, and use of inserts with base fluids. PTC with evacuated receivers has thermal efficiency within the range of 65–70% which is about 10% over PTC with the non-evacuated receiver. Further rise in efficiency is observed for Nanofluids with insert due to the mutual effect. The improved heat transfer in the laminar regime was 20–30% for base fluid with insert compared to it in the plain receiver. Similarly, the increase was 30–50% for Nanofluid with insert. It is often concluded that for PTC application use of insert with base fluid is useful within the laminar region and Nanofluid with insert is justified for the turbulent regime.

Abbood and Mohammed (2019) carried out an experimental investigation on a Parabolic trough solar collector (PTSC) to test the thermal performance of the system. Different parameters of the PTSC system were selected for tests such as heat transfer fluid (HTF) type (hydraulic oil, ethylene glycol, and water) and three flow rates of working fluid (1 LPM, 2 LPM, and 3 LPM). The experiments showed that the maximum heat gain and high efficiency can be happening with using hydraulic oil and the highest value of fluid flow rate. The results showed that the maximum useful heat gain is 1.035 kW, 0.879 kW, and 0.734 kW for the case of using hydraulic oil, ethylene glycol-based water, and water respectively, with a 3 LPM flow rate. The peak experimental efficiencies close to 46.2%, 43.5%, and 40.7% were obtained for PTSC with hydraulic oil, ethylene glycol-based water, and water respectively at the highest value of fluid flow rate.

Marif *et al.,* (2014) investigated the optical and thermal performance of a solar parabolic trough collector under the climate conditions of Algerian Sahara one dimensional implicit finite difference method with an energy balance approach. The absorber model is based on an energy balance in each section of the glass envelope, absorber pipe, and the fluid developed. They found out that the high optical efficiency was obtained with full tracking equal to 73.92% and the one axis polar East-West and horizontal East-West tracking systems were most desirable for a parabolic trough collector throughout the whole.

Alguacil *et al.,* (2014) studied parabolic trough collectors for direct steam generation applications with thermal oil as an HTF. The study developed temperatures higher than 400 ℃ due to operating by the second generation of parabolic troughs at, Abengoa solar power plant is assessing, it is the use of direct steam generation (DSG) inside parabolic troughs to achieve higher temperatures; the first time heating up to 450 ℃ and the second time heating up to 550 ℃.

2.5 Parabolic Trough Solar Collector Enhancement Method

Tijani and Roslan (2014) have numerically simulated the convective and radiation thermal losses in a parabolic trough collector and studied the effect of wind speed on its losses. Results showed that the wind speed does not have a great effect on thermal losses; convective losses and radiation losses account for 64 and 36%, respectively for the wind speed of 2 m/s.

Gong *et al.,* (2017) studied the improvement of the performance of a PTR (Parabolic Trough Receiver) by the use of attached fins to the inner surface of the absorber tube. Results were validated by comparing the numerical results to those experimental data with an acceptable error of 5%. The results showed that the addition of the fins improves the heat transfer performance; the Nusselt number increased by 9%; the heat transfer coefficient increased by 12% and the thermal index is increased with the increase of the fins number.

Laaraba and Mebarki (2020) have studied the improvement of the thermal performance of the parabolic collector by adding the rectangular fins attached to the lower half to the inner surface of the absorber tube. Results showed that the addition of fins increases the thermal performance of the PTR compared to the smooth case. The increase in turbulence intensity increases the heat transfer and the fins with greater height increase the heat transfer.

Demagh *et al.,* (2015) have developed a new technique to improve the efficiency of the PTR, by replacing the planar absorber with another corrugated. Results showed that the corrugated absorber increases the heat transfer coefficient and the friction coefficient by 63% and 60% respectively. With the corrugated absorber, a larger amount of solar flux is received, so the corrugated surface increases the movement of heat transfer fluid in the absorber.

2.6 Bread Baking Technology

Many technologies exist for bread baking systems conventionally the bread baking systems are either electric-powered, biomass power, and fuel powered for mass production, relatively few exist for baking using a renewable energy source. These are electric power baking systems, fossil fuel-powered, biomass-based (firewood), and solar baking systems. The electric power baking system is very expensive and also has a shortage of power the major obstacle. Fossil fuel-powered; the biomass-based baking system is not environmentally friendly. Therefore, it is better to see a renewable source of energy such as solar baking system which is environmentally friendly.

2.6.1 Open Fire Baking System

Baking using open fire system in most of the households of the country, traditional baking is carried out using an open fire (three stone, locally ‟Gulecha‟) bread baking system and biomass is used as a fuel. The heat supplied to the *mitad* in this system is lost through a variety of paths such as: through the sides, through the exhaust gases from the fuel, through convective and radiative heat losses from the pan surface. The fraction of energy that flows into the bread batter is very limited and therefore this technique is inefficient and wasteful; and also, is unhealthy because of carbon inhalation to the lungs and irritation of the eyes.

Figure 2. 3: - Open fires (Gulicha method) bread baking system (Kedir *et al*., 2019).

The working principle of open fire biomass baking systems is similar to that of fuel-powered ones. There is a combustion chamber to burn a large mass of biomass or wood and the fire and hot air are sent to the baking chamber through conduction, convection, and radiation. Biomass-dependent energy sources lead to deforestation and cause global warming. CFD simulation of the flow field in biomass (wood) powered bakery ovens presented by (Manhiça *et al*., 2012).

Lucas *et al*., (2012) studied the analysis of wood-fired bakery ovens' baking process and its wood consumption. Thus, the specific firewood consumption of both indirect and semi-direct bakery ovens was found to be 0.55 and 0.90 kg of wood per kg of wheat flour baked, respectively.

Patel (2020) reported that manufactured *miret* stoves from cement and local aggregates such as sand panels or the oven can be made by pressing clay around the mold. This stove is suitable for mass production by casting light concrete. Each Miret saves approximately 10 kg of wood per Injera baking session for an average household. Most household bakes Injera twice a week. Thus, the Miret saves at an average per household nearly 1040 kg of wood per year. This is a significant saving for the average Ethiopian urban household. However, the Miret saves commercial Injera bakers over 3.5 tons of fuelwood per year.

Even though the Miret stove is better and efficient compared to the open fire baking system; it has the following drawbacks:

- Since it uses biomass (wood or animal dung) it has contributed to deforestation and limits the advantage of dung as plant fertilizer.
- It may also produce smoke and may result in producing pollutants if baking is indoor.

Figure 2. 4: -Miret baking stove (Ayub, 2018).

Biomass gasification was used as the incomplete oxidation thermochemical conversion process of biomass energy sources, like cattle dung or agricultural residue, into gas and solid phases. The solid phase includes char and the inert material present in the biomass (ash). The gas-phase was a combustible gas and used for power generation or biofuel production. The combustible gas produced, when using air as a gasifying agent, consists mainly of CO, H_2, CH_4, CO_2, and N_2 (Bhattacharya and Leon, 2005).

The main challenges of biomass-based bread baking system are health risks due to incomplete burning of biomass, the rising cost, and a cause for deforestation. This creates global warming which is the one major trait of our planet. Due to the limited supply of electric power, and the above challenges of conventional bread bakeries it is critical to use solar bread bakeries as a viable option.

2.6.2 Electrical Baking System

The electric oven is direct-fired which have efficient heat distribution, and results in higher energy cost. An electrically powered bakery system depends solely on the grid system which has its own drawbacks. The bakery consists of steel heating elements of different capacities on the top and bottom surfaces of the oven. These generally work on natural convection phenomena for heat transfer mechanism which also aids the moisture removal from the oven (Chhanwal *et al.*, 2010; Boulet *et al.*, 2010).

The other type of technology for the baking systems is an electric ‟Mitad‟; which is mainly used by people in the urban and near urban areas where electric power is available. However, the majority of the population (more than 80%) in Ethiopia uses wood or biomass fuel for baking. Though this system reduces the problem of carbon inhalation and deforestation (Mekonnen, 2011). The heating element generates heat and the heat generated is dissipated within the pan chamber. The basic operational principle of the electric baking pan is the process of heat transfer. Heat transfer through conduction, convection, and radiation, tends to occur whenever there is a temperature difference. Electric injera and bread baker has certain disadvantages like: -

- People in rural areas do not have the access to electricity. Hence, the electric braking system is used only in urban areas.
- There is heat loss due to the non-optimum of insulation through the sides and bottom.

Figure 2. 5: - Electrical Injera and bread baking method (Mekonnen, 2011).

Generally, most bread baking systems in Ethiopia are electric-powered and biomass powered. An electrically powered bakery oven depends only on the grid system which has its own drawbacks. In electric ovens, cooking time and quality are generally dependent on the airflow in the oven. And also, a sudden power fluctuation and failure greatly affects the bread quality which is undesirable to all bread products. Nowadays the electric tariff is increasing by more than fifty percent this year and a hundred by the coming year. This increases the baking cost of bread and price of bread for consumers.

2.6.3 Fuel Energy Baking System

In a fuel-powered bakery system, the combustion chamber is integrated with the baking chamber itself. The forced air is circulated into the combustion chamber from the atmosphere, and then the hot air along with the flue gases is sent to the baking cavity of the oven where the dough is placed in trays. Convection is the dominating mode of energy transfer inside the baking oven. Typical fuel powered bread bakery consumes 0.02 L of fuel per kg of bread making which would be even more in the case of electric bakery considering the transmission losses Morakinyo *et al*., (2017).

Ganitha *et al*., (2014) developed a domestic gas-fired oven and evaluate the performance of the baking process. The result showed a temperature of 180℃ with a baking time of 28 min and showing a better energy efficiency by minimizing energy loss, and baking time. An improved heating system design of novel gas-fired industrial tunnel ovens was developed and CFD simulations have been used to model the fuel burner and baking chamber (Williamson and Wilson, 2009). The result showed that bread quality was highly sensitive to moisture content of the baking chamber, radiative and convective heat flux incidents on the dough surface.

Dual powered bread baking oven was developed which is possible to use an alternative heat source that of electricity and fuel (gas) (Okafor, 2014). It has two chambers: the upper chamber is powered by electricity while the lower chamber is powered by a gas or biomass burner located outside the baking chamber and having a performance of 95.2%.

The main drawback of fossil fuels are used as a heat source that emits harmful GHG to the environment after combustion and is the major concern of the world. The resource is also depleting and the increasing price needs to see alternative sustainable energy source of the baking industry.

2.6.4 Solar Energy Baking System

There are two types of solar energy applications for baking. These are direct solar baking and indirect solar baking (solar thermal baking) systems. Direct solar bakeries are devices that bake food when solar radiation is available. In this method, solar energy is concentrated using high concentration solar collector such as parabolic dish at one focal point and this energy is directly sent to the baking chamber (Minaye, 2020).

Hassen *et al*., (2016) investigated that solar thermal energy is transferred to the kitchen using a circulating heat transfer fluid heated by solar energy concentrated by a parabolic trough. For experimental simplicity and investigation of the possibility of baking on a glass stove, the heat transfer fluid is heated by simulating the solar power with electricity, and the heated fluid is allowed to circulate through the closed-loop of the baking pan assembly. Surface temperatures of heated plate were achieved on top of the glass baking pan and Injera baking experiments were performed successfully.

Tsegay (2011) stated that solar thermal energy for household energy consumption has not been well developed and adopted. One reason for this is that the system can only be used outdoor and at the time of sunshine. The prototype for direct steam-based baking was developed and tested at Mekelle University (Ethiopia) and Phase-change material-based heat storage prototype was developed and tested at NTNU. Both experiments show the possibility of solar energy for Injera baking and its sustainability by including latent heat storage.

Tesfay *et al*., (2014) conducted that an experiment that investigated a parabolic dish solar collector coupled with latent heat storage constructed. A solar salt (40% KNO3 and 60% NaNO3) was selected as heat storage material and the storage was charged with a self-circulating steam loop. A cooking pan was integrated with an aluminum block with three steam channels and ten salt cavities. They conducted the experiment and the result was compared with the simulation results of COMSOL Multiphysics. The aluminum block efficiently separated the salt from the high-pressure steam, but the numbers of steam channels are few and this limits the heat transfer process

The baking temperature influenced the quality of the bread as well as its shelf life, making it unsuitable for extended periods. The CFD analysis of solar thermal powered bread baking oven using parabolic trough collector by (Mishra *et al*.,2019) was done without integrating thermal energy storage and achieved a baking temperature of 168℃. Therefore, it is mandatory to integrate thermal energy storage, because solar power fluctuation greatly affects bread quality which is the main concern for bakers.

Hailessilase *et al*., (2015) presented a solar thermal-based direct baking and proves the possibility of baking in a temperature range of 120-160℃ using aluminum plate as a baking pan.

Gallagher (2011) developed the solar fryer, which was specifically designed for cooking Injera. He used a 460 mm diameter *Mitad* and 1200 mm diameter mirror for his prototype, which was designed for cooking 420 mm diameter slices of Injera. A mirror below the *Mitad* directs the radiation to the *Mitad* bottom, which was coated with a low-emissivity black absorber. The the mirror uses flat, hexagonal panels of aluminized-Mylar to provide uniform illumination across most of the *Mitad* bottom. This system was mainly designed for cooking outdoors.

Among different types of collectors available PCM thermal storage is dominating in the solar thermal baking application, thus the main challenging task is the charging and discharging process. Depending on the type of collector used the storage is charged either through direct illumination or by the help of HTF. The Scheffler collector and parabolic dish with secondary reflector (beam down reflector) can charge their storage by direct illumination whereas parabolic dish and parabolic trough collectors can charge their thermal storage by the circulation of HTF using a heat exchanger system.

2.7 Thermal Energy Storage System

Up to now, the world energy demands are satisfied mainly using fossil fuels. Due to the number of problems while using fossil fuels, viz., varying prices, emission of harmful gases, and depleting resources, researchers have focused their attention on developing technologies to take advantage of renewable energy sources. Due to the unpredictable and fluctuating nature of renewable energy sources, the thermal energy storage system provides a sustainable option (Niyas *et al*., 2017).

The nature of solar energy is diluted and intermittent, thermal energy storage (TES) required stores energy for a particular time and provides this energy for later usage. Energy storage is used to correct the mismatch between the time of energy supply and energy demand. Solar energy can be stored in different forms like electrical, chemical, mechanical, and thermal energy. The heat that is not required by the process during sun hour can be stored to use later when there is no solar irradiation. This stored heat is used for water heating, space heating, desalination, cooking, thermal power system, etc. Based on the nature of the change that occurs on the storage material different techniques are used for thermal energy storage (Stutz *et al*., 2017).

The desired properties while selecting thermal energy storage include:

- High energy density (per-unit mass or per-unit volume) in the storage material
- Good thermal properties
- Mechanical and chemical stability of storage material
- Compatibility between storage material, HTF, and other materials
- Complete reversibility for a large number of charging/discharging cycles
- Minimum thermal Losses
- Minimum cost.

Table 2. 1: Typical parameters of thermal energy storage methods (IRENA -ETSAP, 2013).

Type	Storage capacity (kWh/t)	Power (MW)	Efficiency (%)	Storage period
Sensible heat storage	10-15	0.001-10	50-90	Day/month
Latent heat storage (PCM)	50-150	0.001-1	75-90	Hour/month
Chemical storage	120-250	0.01-1	75-100	Hour/ day

2.7.1 Sensible Heat Energy Storage (SHES)

Sensible heat storage materials are defined as a group of materials that undergo no change in phase over the temperature range encountered in the storage process. The ability to store sensible thermal energy for a given material depends strongly on the (density and heat capacity), the thermal capacity of the material. For a material to be useful in a thermal energy storage application, it must be inexpensive and have good thermal capacity. Another important parameter in sensible thermal energy storage is the rate at which heat can be released and extracted. This characteristic is the function of thermal diffusivity. The material here can be a liquid or a solid (Mohamed *et al*., 2017)

Hence, the storage capacity of sensible heat storage material (Q_{sh}) is given by;

$$Q_{sh} = \int_{T_1}^{T_2} m\, C_p dT = \int_{T_1}^{T_2} \rho V\, C_p dT \qquad 2.1$$

Where m is the mass of the storage material

C_p is the specific heat capacity

dT is the rise in temperature during the charging process

ρ, V – are density and volume of the storage material respectively

The amount of thermal energy stored in the form of sensible heat depends on mass, the value of the specific heat of the material used to store the thermal energy, and the temperature change. Some of the most common sensible heat storage materials are water, mineral oil, molten salts, liquid metals and alloys, rock, concrete, sand, and bricks (Alva *et al.*, 2018).

Duffie and Beckman, (2013) conducted one of the sensible heat storage systems, which is a basic theoretical introduction on using water as a thermal energy storage material in various solar thermal energy storage systems as well as analytical models for the water storage stratification.

2.7.2 Latent Heat Energy Storage System (LHESS)

A latent heat energy storage system (LHESS) is used to store the existing thermal energy for later usage and increases its utilization. Further, it provides a favorable solution for smoothing the inconsistency between energy demand and supply. LHESS uses phase change materials (PCM) as energy storage mediums. Energy is stored during melting and released during solidification. Several types of research have used LHESSs for various applications such as solar domestic hot water systems (Mazman *et al*., 2009).

Latent heat storages store thermal energy when a material changes from one stage to another. The amount of heat stored or released when a material change from solid to liquid or vice versa is called the latent heat of fusion and from liquid to vapor or vice versa is called the latent heat of vaporization (Lingayat and Suple, 2013). Compared to sensible heat storage, latent heat storages are attractive since they provide a high energy storage density and can store energy at a constant temperature which is the phase transition temperature of the material. Latent heat storage systems are also known as phase change materials (PCMs) store energy by using phase change material which allows storing a significant amount of energy over a narrow temperature range (John *et al*., 2015).

The use of an LHSS system using PCMs is an effective way of storing thermal energy and has the advantages of high-energy storage density and the isothermal nature of the storage process. The main benefit of using LHSS is their storage capacity of heat up to 14 times more energy than SHS over relatively a small temperature interval (Sharma *et al*., 2009; Sarbu and Sebarchievici, 2018). Initially, these materials act like sensible heat storage materials in that the temperature rises linearly with the system enthalpy; however, later, heat is absorbed or released at an almost constant temperature with a change in physical state. PCMs are characterized by their high thermal energy storage capacity and ability to absorb energy during the heating process and release it to the environment during the cooling process. During solid-liquid phase change, for example, fusion absorbs energy, and solidification releases it. Molten salts, paraffin waxes, eutectic salts, magnesium nitrate hexahydrate, Galactitol, magnesium chloride hexahydrate, stearic acid, acetamide, acetanilide, and erythritol are some of the latent heat storage materials that can be selected for solar cooking (Khadiran *et al*., 2015).

Wang *et al.*, (2013) numerically studied that the charging and discharging energy characteristics of a shell-and-tube phase change material heat storage unit to study the effect of inlet temperature and mass flow rate of HTF on the thermal performance of a shell and tube latent heat storage systems. The study finally concluded from the obtained result was the inlet temperature of the HTF had more effect on thermal energy storing capacity and melting rate than the mass flow rate.

Medrano *et al.*, (2010) have investigated that thermal energy storage and solar energy applications. Investigated different thermal energy storage materials both sensible and latent heat storage materials; steam, mineral oil, metals, earth materials, molten salts, organic and inorganic material, etc. From the investigation molten salts (especially the nitrates) are currently the most attractive thermal energy storage materials in CSP plants which, are cheap, giving them high energy storage density, lower vapor pressure than water and are capable of operating at high temperatures in the liquid form up to 400 °C. This permits the improvement of the efficiency of the Rankine cycle at high temperatures in the plant.

A latent heat thermal storage system has the following three main components (Tyagi *et al*., 2012):

i. PCM: A suitable material having all the desired properties of a phase change material and having its melting point in the required temperature range.
ii. Heat Exchanger: A suitable heat exchange surface or a suitable heat-carrying fluid for transferring the heat effectively from the heat source to the heat storage. Also, a lot of PCMs have poor thermal conductivity and thus require a large heat exchange area.
iii. Container: A container for storage that is compatible with the PCM as sometimes the PCMs are corrosive and thus require special containers.

The two main advantages of latent heat storage are

- It is possible to store a large amount of heat with only a small temperature change and therefore to have a high storage density.
- As the change of phase at a constant temperature takes some time to complete, it becomes possible to smooth temperature verities.

2.8 Phase Change Material Energy Storage

Phase change materials absorb or release a large amount of heat at constant phase transition temperature when they undergo a phase change. Phase change materials exhibit solid-liquid, liquid-gas phase change, and vice versa. Although liquid-to-gas phase change also involves heat absorption, yet they show large volume changes during phase change. Thus, to exploit the heat from liquid-gas phase change, very large containment volumes are required. Solid-liquid phase change material is particularly promising as they show very little volume change during phase change which enables heat to be stored in a smaller volume. Absorption of a large amount of heat at a constant temperature during a phase change is one of the main advantages of phase change material. The isothermal nature of heat absorption and release renders phase change material a suitable candidate for thermal energy storage and temperature control applications (Hassan, 2010). A PCM is the heart of any latent heat storage system. Having a high latent heat is not the only requirement to use material as a thermal energy storage material. The desired PCM properties are (Arabacigil *et al.*, 2015):

- Melting point should be in the desired temperature range. For example, if we want to incorporate PCM in building materials, then the melting point of the PCM should be around the required room temperature.
- High latent heat of fusion per unit volume to store high energy in a given volume.
- High thermal conductivity to assist charging and discharging of energy.
- Low changes in volume during phase change and low vapor pressure to avoid containment problems.
- Non-flammable & non-toxic.
- Low cost and low containment cost.

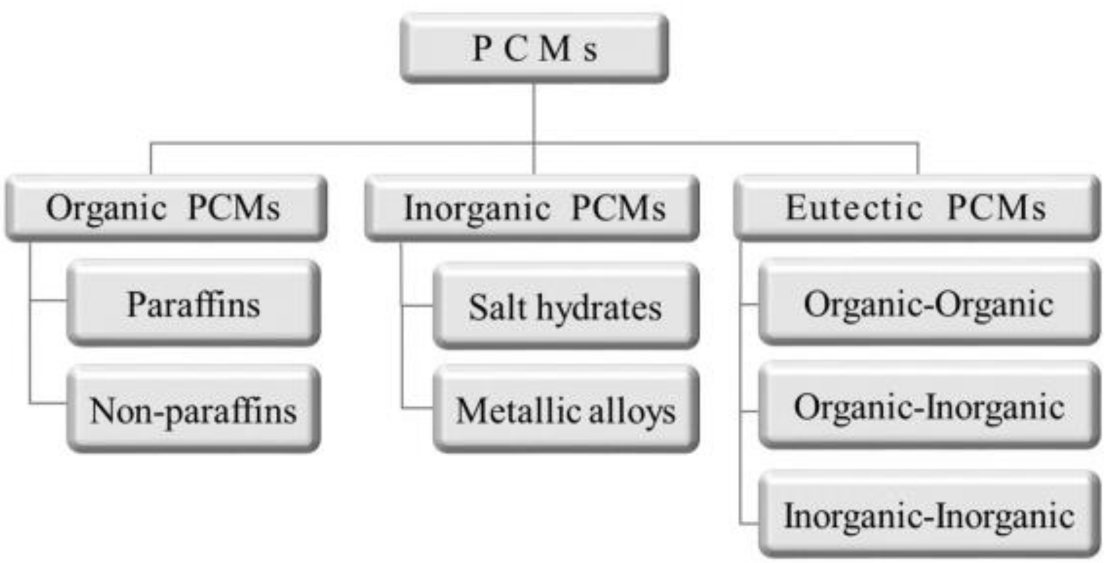

Figure 2. 6: Phase-change material (PCM) classification (Hassan, 2010)

Phase change materials (PCMs) can absorb, store and release large amounts of latent heat over a well-defined temperature range when the material changes phase or state. A fabric containing a PCM can act as a transient thermal block that controls the heat flux. The heat absorption by PCMs results in a delay in microclimate temperature and hence a substantial decrease in the amount of sweat produced by the skin of the wearer. Both principal to an enhancement of the wearing comfort and prevent heat stress (Bendkowska *et al.*, 2005).

2.9 Heat Transfer Fluid (HTF)

Heat transfer fluids serve as the collection and transport of heat from solar absorbers to the storage tank. It is the most important part of any solar system which extracts heat from the solar collector. This section discusses heat transfer fluid, which is one of the critical components for storing and transferring thermal energy in concentrating solar systems. Heat transfer fluid is used to transfers the thermal energy delivered by the solar collector to the thermal energy storage system. There are various HTF available and used for solar thermal systems such as air, water, thermal oils, molten salts, and liquid metals but thermal oils and molten salts are the more dominant HTFs (Kotyla, 2017).

Selection criteria of HTF include (Kotyla, 2017; Vignarooban *et al*., 2015);

- Extended working temperature range and high thermal stability,
- Good thermal conductivity is desired for efficient heat transfer,
- Low viscosity is beneficial to pressure drop,
- Large heat capacity would allow for direct thermal storage,
- Low vapor pressure,
- Low hazard properties and good material compatibility,

a. Water

Water was used as heat transfer fluid for single fluid direct steam generation solar thermal systems. Even if it has high heat capacity, low viscosity, cannot be used for high-temperature application and used for direct steam generation systems.

Table 2. 2: Advantages and Disadvantages of water as HTF

Advantages	**Disadvantages**
♣ Inexpensive, non-toxic, non-combustible and widely available ♣ High specific heat and high density ♣ Simultaneous charging and discharging of the storage tank is possible	♣ Superheated steam at high temperature ♣ Highly corrosive ♣ Working temperatures are limited to less than 100°C and suitable only for direct steam generation solar systems

a. Molten salts

As compared with water and thermal oils, molten salts are the best heat transfer fluids. This is due to molten salts have high density, high heat capacity, high thermal stability (> 500℃), and very low vapor pressure even at elevated temperatures. Another important property of molten salts is the avoidance of fire and contamination hazards due to leaks of thermal oil in piping and vessels because molten salts recently used (binary mixture of potassium nitrate and sodium nitrate) have been traditionally used by farmers as fertilizer. Additionally, when molten salt is poured onto the ground it freezes immediately and remains as a thick solid film that can be easily recovered and reused, thus avoiding the high decontamination costs related to oil leakages on the ground (Vignarooban *et al.*, 2015).

Solar Salts have a high melting point usually above 200℃ which results in freezing in pipelines when there is no solar energy during the night and cloudy time. Using molten salt have higher efficiency than oils, but it has a high freezing problem and needs a freeze protection system, which increases the operation and maintenance cost (McLaughlin, 2020).

b. Thermal oils

Thermal oils such as mineral oil, silicone oil, and synthetic oils have been used in concentrated solar thermal system applications as heat transfer fluids (Vignarooban *et al*., 2015). These thermal oils are not commonly used for high-temperature solar thermal applications. This is because these oils can be thermally stable only up to 400℃ and are also highly expensive. Thermal oil has low viscosity and good flow properties so that can be circulated easily with low pumping power.

Table 2. 3: Typical heat transfer fluids used for solar thermal systems (Hassen *et al*., 2016; Tian and Zhao, 2013; Purlis, 2012).

Type	Operating Temperature ℃	Density (kg/ m^3)	Thermal conductivity (W/m. ℃)	Specific heat (kJ/kg. ℃)
Therminol VP-1	12-400	900	0.11	2.3
Shell Thermia oil B	-18-320	868	0.12	2.6
Molten salt	250-500	1870	0.52	1.6

2.10 Thermal Insulation System

Insulation is defined as a material or combination of materials, which retard the flow or loss of heat and is used in heating, air conditioning, and refrigeration systems to insulate piping, ducts, vessels, thermal storage devices, and equipment's to conserve thermal energy, prevent surface condensation and control heat input to the contained fluids. Generally, the thermal insulation can be used to control heat flow in wide temperature ranges when the appropriate insulating material is selected (ATIMA, 2005; GSU, 2005).

2.10.1 Advantages of Insulation Systems

The following are the basic advantages of insulating systems (GSU, 2005; Molla, 2020):

i. **Energy Savings:** Energy Savings: Significant quantities of heat energy are wasted because of un-insulated heated surfaces. Properly designed and installed insulation systems will immediately reduce the need for energy and benefits to the industry include enormous cost savings, improved productivity, and environmental quality.

ii. **Process Control**: By minimizing heat loss or gain, insulation can help maintain process temperature to a pre-determined value or within a predetermined range

iii. **Personnel Protection:** Thermal insulation is one of the most effective means of protecting workers from burns resulting from skin contact with surfaces of hot surfaces and equipment working at higher temperatures. Insulation minimizes the surface temperature of piping or equipment to a safer level, consequential in increased worker safety and the avoidance of worker downtime due to injury. downtime due to injury.

iv. **Fire Protection:** Used in mixture with other materials, insulation helps provide fire protection in fire stop systems designed to provide an effective barrier against the spread of flame, smoke, and gases at penetrations of fire-resistance-rated assemblies by ducts, pipes, and cables. The most abundant insulation materials that can withstand high temperatures such as fiberglass (glass wool), mineral wool, calcium silicate, foam glass, and firebricks (Li *et al.,* 2017).

Desired properties of insulating materials to be considered during the selection of insulation materials include;

- Low thermal conductivity,
- Non- corrosive,

- Non-toxic, non-flammable and
- exhibit little or no decomposition at a long period

In addition, cost & structural considerations must be undertaken during of selection insulation material. Here, insulation is required at various sections of the system and these include circulation pipe, thermal storage tank, receiver back, and storage tank cover insulation plate.

Table 2. 4: Insulating materials with their thermal conductivity at room temperature

Material	Thermal conductivity (w/m.℃)
Cork	0.048
Fiber glass/Glass wool	0.040
Foam	0.026
Wood ash	0.015

Glass wool insulation is made from recycled glass bottles, sand, and other materials. Glass wool is also called fiberglass insulation. Researches proved that the thermal insulation performance of glass wool is not affected by high temperature and moisture conditions.

For this particular design, glass wool is used as an insulating material for circulation pipe as well as energy storage containers due to the following important insulation properties;

- Good thermal insulating properties,
- Low moisture-vapor permeability,
- High resistance to water absorption,
- High mechanical strength and low density and low cost and simplicity of installation.

2.11 Literature Summary

In the literatures, biomass systems, electrical systems, and solar baking systems have been discussed. In most of the literatures associated with the biomass-based bread baking system are health risks due to incomplete burning of biomass, the rising cost, and a cause for deforestation and global warming. Even though an electric oven which is mainly used by people in the urban and near urban areas where electric power is available. Though electric system reduces the problem of carbon inhalation and deforestation; it has certain disadvantages like electric conception, electric cost, availability, and sudden power fluctuation. Comparatively, literature showed that solar bakers have an advantage of being able to bake bread using solar without suffering a problem associated with biomass and electric system. Surveys of literatures indicated that considerable efforts have been invested in research and development of direct solar bakers and indirect solar baker. However, limited research works were reported on indirect solar bread baking, particularly, parabolic trough collector type solar bread baker with a thermal energy storage system. Besides, those limited works in literature focuses only on energy efficiency of the systems even if exergy efficiency is the true performance measure of solar-thermal system which indicate the quality of energy converted into useful form of energy. Generally, in this study experimental investigating on solar bread baker by enhancing the performance of parabolic trough solar collector using receiver fin with shield and integrating with PCM based thermal energy storage system for off-sunshine.

CHAPTER THREE
MATERIALS AND METHODS

3.1 Introduction

The present study applies theoretical and experimental analysis as the main approach which is used as a methodology. The theoretical approach uses governing equation for the design, sizing, selection, and formulation of the solar thermal baking system components. The thermal performance of the parabolic trough collector (PTC) and latent heat storage (LHS) system is evaluated experimentally. In this section the research design techniques, process model, different data sources and collection methods, material and equipment used, and experimental data presentation and analysis methods which will be employed for experimental investigation and performance evaluation of the present solar thermal bread baking system are presented.

3.2 Materials and Equipment

Materials, measuring devices, and system components required for developing the experimental prototype and measuring the system parameters are obtained by purchasing from the local market in Adama and Addis Abeba cities (Ethiopia).

Materials used to construct the experimental setup were selected based on local availability and cost-effectiveness. The main materials used are presented below.

- **Aluminum sheet:** used for constructing the baking plate and cover of the setup.
- **Glass mirror:** used for the fabrication of the reflector surface of the parabolic trough reflector system by using adhesive tape.
- **Stainless steel sheet**: due to its corrosion resistance property at high temperature, used for construction of storage container walls and parabolic trough shape.
- **D-mannitol:** used as a thermal storage medium due to its better thermal properties
- **Galvanized steel pipe:** used for HTF circulation from cold storage tank to the solar collector and then to the thermal storage unit.
- **Flat Iron**: used for parabolic solar collector supporter.
- **Iron Angles and RHS:** used for making stand frame for the solar collectors.
- **Shell Thermal oil:** used for heat transfer fluid due to its better thermophysical properties.
- **Valves:** used for proper flow control.
- **Epoxy:** used to seal linkage.

- **Fiber Glass:** The fiberglass was used for insulating hot oil carriage pipes, baking units, and thermal energy storage tanks.
- **Green and silver color paint**: used for painting the supporting stand and storage tank.

Measuring Instruments

- **Digital Thermocouples:** used for measuring the temperature profile at the various sections of the baking system at different stages of baking and the daily ambient temperature variation.
- **Weight Balance:** used for measuring the weight of the dough and weight (difference) loss of bread sample after baking.

3.3 Methodology and Research Design

The procedures of the research are mixed analytical and experimental research design where both qualitative and quantitative research techniques are employed. The solar thermal bread baking system is evaluated based on the existing hypothesis and experiential testing of the hypothesis. The general process layout of the methodology followed in the research is presented in Figure 3.1.

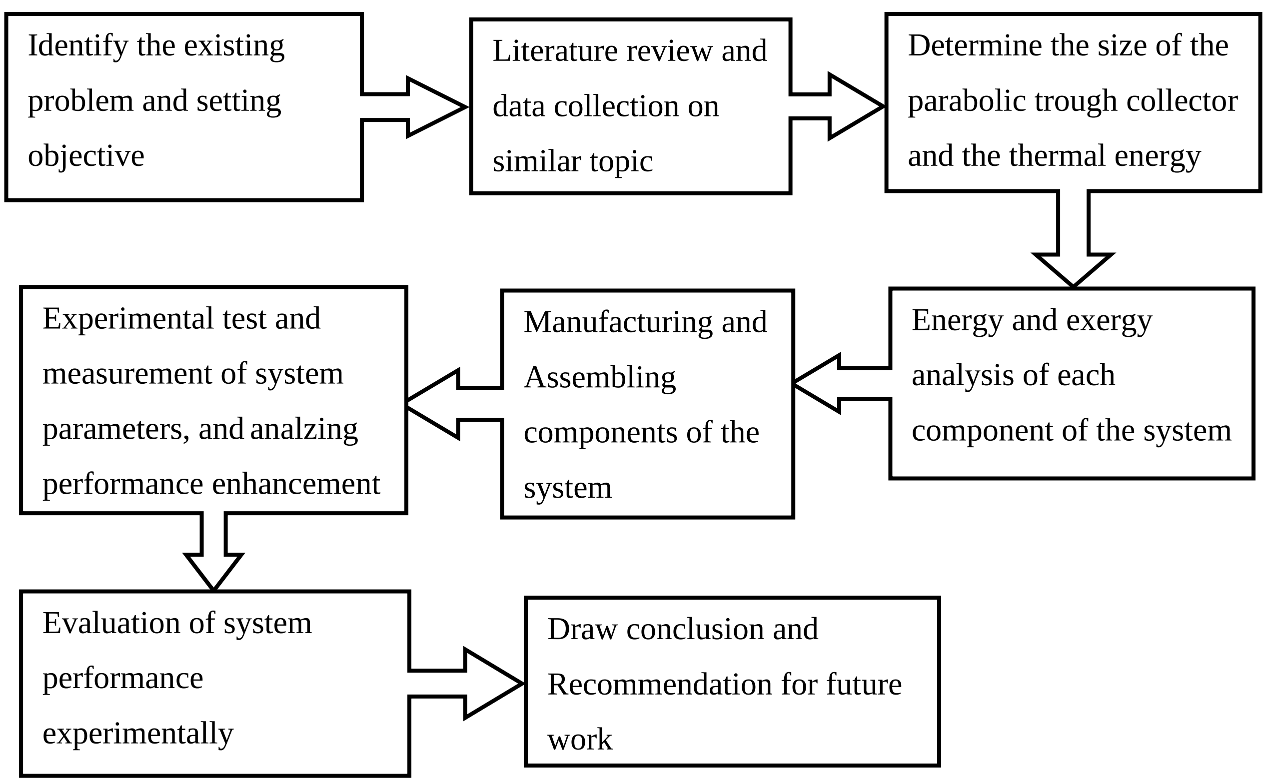

Figure 3. 1: Methodology of the study.

3.4 Data Collection Method

The data required for the whole work is obtained from both primary and secondary sources of data. The Primary data sources would be taken by direct measure temperature such as the ambient temperature of the air, the temperature of inlet and outlet of heat transfer fluid from parabolic trough solar collector, charging and discharging of thermal storage and plate surface temperature is obtained by direct measuring. Secondary data are obtained from different sources on the internet such as books, documents from websites, literature from local and international journal articles, and data from the deep literature reviews. Metrological and solar radiation data for the site is obtained from National Meteorology Agency Eastern and Central Oromia Metrological Services Center. In this thesis Excel (spreadsheet) is the basic software that is used as a data storage, estimation, analysis, and interpretation tool for the solar radiation data and timely varying measured parameters during the experimental tests.

CHAPTER FOUR

SOLAR POTENTIAL ESTIMATION

4.1 Solar Energy Resource in Ethiopia

Ethiopia is located in the eastern part of Africa between 3^o to 15^o North and 33^o to 48^o East which is within the solar belt (Le Houerou, 2012), With a surface area of 1.1 million square kilometers, It is the third-largest country in Africa, which is mostly distributed in northern, central and southwestern highlands. Ethiopia receives solar irradiation of 5000-7500Wh/m^2 according to region and season and thus has great potential for the use of solar energy. The average solar radiation is more or less uniform, around 5.2kWh/m^2/day. The seasonal variation is from 4.55-5.55 kWh/m^2/day and with location from 4.25Wh/m^2/day in the extreme eastern lowlands to 6.25kWh/m^2 /day in Adama area in southeast Ethiopia (Argaw, 1996).

4.2 Assessment of Solar Energy Intensity

The absence of devices for recording the hourly values of solar and climatic data made it necessary to use the estimated values of global radiation, diffuse radiation, and beam radiation of the specific site. Estimation of solar energy intensity is required to calculate the total amount of solar energy incident on a collector. The rate at which solar radiation is striking a surface per unit area of the surface is called the total solar irradiation on the surface. Sun–earth angles are essential for estimating solar intensity throughout the year for any surface at any place with a desired inclination and orientation. Those angles generally depend on the location on earth, day of the year, and time of the day.

4.2.1 Solar Geometry

The geometric relationships between a plane of any particular orientation relative to the earth at any time and the incoming solar radiation, that is, the position of the sun relative to that plane, can be described in terms of several angles (Duffie and Beckman, 2013).

Latitude angle (ϕ) is the angular location of any place on earth which is north or south of the equator, north positive; $-90° \leq \phi \leq 90°$. The latitude of Adama is 8.54° north of the equator.

Declination angle ($\boldsymbol{\delta}$) is the angular position of the sun at solar noon concerning the plane of the equator, north positive; -23.45° ≤ $\delta \leq 23.45$ The declination, δ, in degrees for any day of the year calculated as (Duffie and Beckman, 2013):

$$\delta = 23.45 \sin \left(\frac{360(284+n)}{365}\right) \quad \text{………………………………..……………………………4.1}$$

where n is the day of the year (counted from January 1)

The Representative Day of each month in the year and the value of the declination angle on its day can be obtained by Table 4.1.

Table 4. 1:-Recommended average days for months in the year (Duffie and Beckman, 2013)

Month	n for i^{th} Day of the Month	For the average Day of the Month		
		Date	n, Day of the Year	δ, Declination
January	i	17	17	-20.9
February	31 + i	16	47	-13.0
March	59 + i	16	75	-2.4
April	90 + i	15	105	9.4
May	120 + i	15	135	18.8
June	151 + i	11	162	23.1
July	181 + i	17	198	21.2
August	212 + i	16	228	13.5
September	243 + i	15	258	2.2
October	273 + i	15	288	-9.6
November	304 + i	14	318	-18.9
December	334 + i	10	344	-23.0

Slope or tilt angle (β) is the angle between the inclined plane surface under consideration and the horizontal; -180° ≤ β ≤ 180°.

Hour angle (ω) is the angular displacement of the sun east or west of the local meridian due to the rotation of the earth on its axis at 15° per hour; positive in the afternoon and negative in the forenoon (Kalogirou, 2013).

ω = [solar time – 12:00] (hours)x15°……………………………………………………………4.2

Zenith angle ($\boldsymbol{\theta_z}$) is the angle between the vertical and the line to the sun, that is, the angle of incidence of beam radiation on a horizontal surface.

$\cos \boldsymbol{\theta_z} = \cos \delta \cos \phi \cos \omega + \sin \phi \sin \delta$..4.3

Surface azimuth angle (γ) is the deviation of the projection on a horizontal plane of the normal to the surface from the local meridian.

$\gamma = 0$ for surfaces facing south.

The angle of incidence (θ) is the angle between the sun's ray's incident on the plane surface and normal to that surface.

$\cos \theta = (\cos \phi \cos \beta + \sin \phi \sin \beta \cos \gamma) \cos \delta \cos \omega + \cos \delta \sin \omega \sin \beta \sin \gamma + \sin \delta (\cos \beta \sin \phi + \cos \phi \sin \beta \cos \gamma)$ 4.4

Solar altitude angle ($\boldsymbol{\alpha_s}$) is the angle between the horizontal and the line to the sun, that is, the complement of the zenith angle ($\theta_Z + \alpha_s = 90^o$).

Solar azimuth angle (γ_s) is the angular displacement from south of the projection of beam radiation on the horizontal plane. Displacements east of south are negative and west of south are positive.

Sunshine hour (N) is the total duration in hours of the Sun's movement from sunrise to sunset. It is defined in terms of the hour angle as (Kalogirou, 2013):

$N = \frac{2\omega_s}{15}$..4.5

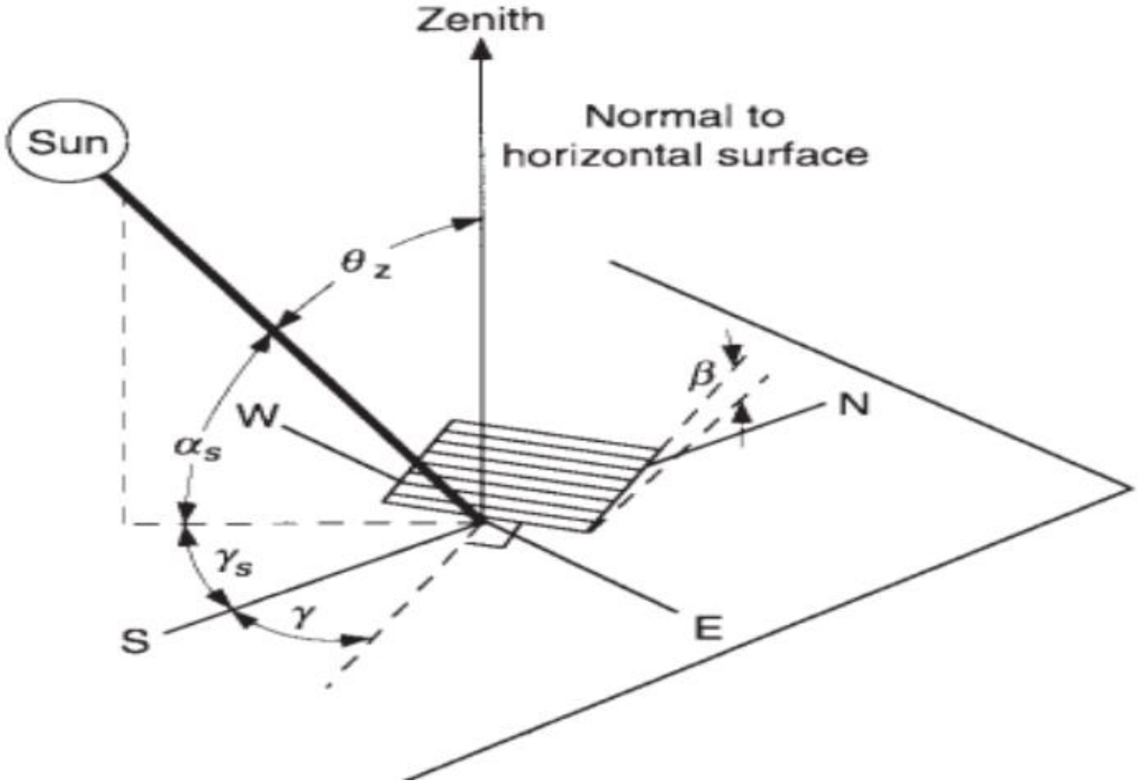

Figure 4. 1: Zenith angle, slope, surface azimuth angle, and solar azimuth angle for a tilted surface (Duffie & Beckman, 2013)

4.3 Solar Radiation Analysis

i. **Beam Radiation** is the solar radiation received from the sun without having been scattered by the atmosphere. (Beam radiation is often referred to as direct solar radiation; to avoid confusion between subscripts for direct and diffuse, we use the term beam radiation.)

ii. **Diffuse Radiation** is the solar radiation received from the sun after its direction has been changed by scattering by the atmosphere

iii. **Total Solar Radiation** is the sum of the beam and the diffuse solar radiation on a surface. The most common measurements of solar radiation are total radiation on a horizontal surface, often referred to as global radiation on the surface (Duffie and Beckman,2013).

4.3.1 Solar Radiation Estimation

Extraterrestrial radiation is the amount of solar radiation received if the earth's atmosphere had not been there, or, the atmosphere transmittance is unity. i.e., the radiation outside the earth's atmosphere.

4.3.2 Estimation of Daily Extraterrestrial Radiation on a Horizontal Surface

The extraterrestrial radiation on a surface normal to the sun's rays kept at the actual sun-earth distance at a specific day and time which is modified to take into account the varying distance between the sun and the earth is given by (Duffie and Beckman, 2013):

$$I_{ext} = I_{sc}[1.0 + 0.033\cos(\frac{360(n)}{365})] \quad \text{……………………………………………………….……………4.6}$$

Where, n is the day of the year (counted from January 1) and I_{sc} is solar constant =1367 W/m2.

Extraterrestrial solar radiation that would fall on a horizontal surface at the location is given by:

$$I_o = I_{ext}\cos\Theta_z \quad \text{……………………………………………………………4.7}$$

$$I_o = I_{sc}[1.0 + 0.033\cos(\frac{360(n)}{365})]\,[\cos\delta\cos\emptyset\cos\omega + \sin\emptyset\sin\delta] \quad \text{…..……………4.8}$$

The daily extraterrestrial solar radiation on a horizontal surface can be obtained by integrating equation (4.9) from sunrise to sunset and expressed as:

$$H_O = \frac{24*3600}{\pi} I_{sc}[1.0 + 0.033\cos(\frac{360(n)}{365})]\,[\cos\delta\cos\emptyset\sin\omega_s + \frac{\pi*\omega_s}{180}\sin\emptyset\sin\delta \quad \text{………………………………4.9}$$

Where, sunset hour angle $\omega_s = \cos^{-1}(\tan\emptyset\tan\delta)$ ……………………………………………………………………………4.10

4.3.3 Estimation of Monthly Average Daily Global Radiations on a Horizontal Surface

To estimate the monthly average daily global radiations on a horizontal surface of the selected site, it is crucial to get the data of the hourly sunshine duration of the day. Thus, the daily sunshine duration (sunshine hours) data of the site (Adama city with latitude 8.54° north of the equator, longitude =39.28°E; and altitude = 1648 m above sea level) for five years was obtained from National Metrology Agency Eastern and Central Oromia Metrological Services Center. The five-year daily sunshine hour data was then monthly averaged as shown in Figure 4.2 for the ease of estimation of monthly average daily global radiations.

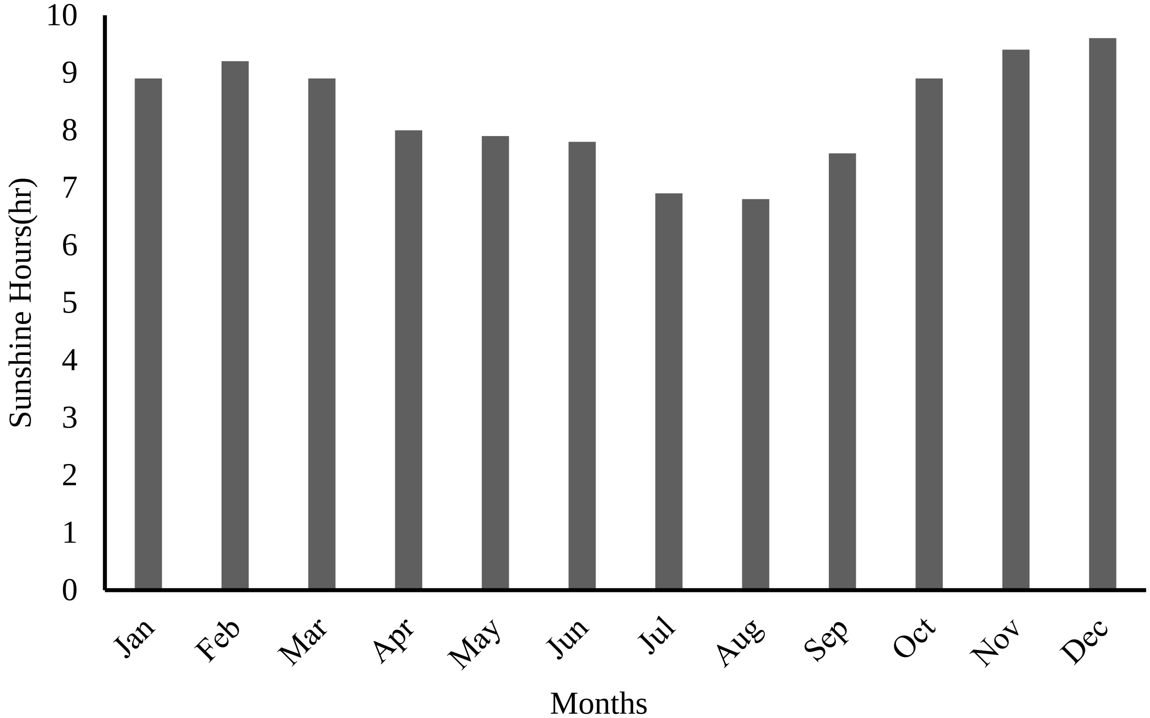

Figure 4. 2: Monthly average daily sunshine hours of Adama city

Global solar radiation (I_G) is the sum of the beam and the diffuse solar radiation on a surface, or simply it is the most common measurements of total solar radiation on a horizontal surface, often referred to as global solar radiation on the surface. The solar energy reaching the earth's the surface is reduced while crossing the atmosphere because of absorption, reflection, and scattering by liquid and solid aerosols, etc., especially in the case where a cloud cover is present. The monthly average daily global radiation on a horizontal surface may be estimated from sunshine records by the Angstrom correlation, as (Tiwari, 2018):

$$\frac{H_G}{H_O} = a_1 + b_1\left(\frac{\bar{n}}{\bar{N}}\right) \qquad 4.11$$

Where, H_G is monthly average daily global solar radiation on a horizontal surface,

H_o is monthly average radiation outside of the atmosphere (ETR on the horizontal surface) for the same location.

$\bar{n}$ is the monthly average daily hours of bright sunshine.

$\bar{N}$ is the monthly average of maximum possible daily hours of bright sunshine.

a_1 and b_1 is empirical constant, (values are obtained by regression).

given by,

$$a_1 = -0.11 + 0.235 \cos\emptyset + 0.32\left(\frac{\bar{n}}{\bar{N}}\right) \quad \ldots\ldots 4.12$$

$$b_1 = 1.449 + 0.235 \cos\emptyset + 0.694\left(\frac{\bar{n}}{\bar{N}}\right) \quad \ldots\ldots 4.13$$

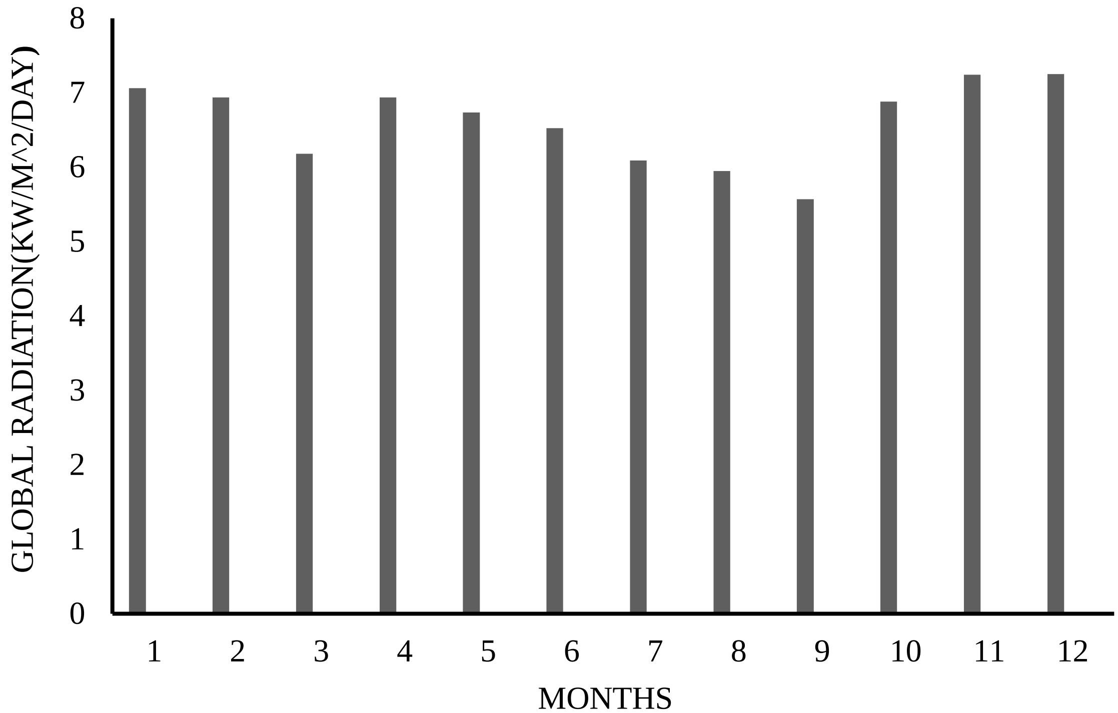

Figure 4.3:- Monthly average daily global radiation on a horizontal surface of Adama city

4.3.4 Estimation of Monthly Average Daily Diffuse and Beam Radiations on a Horizontal Surface

The monthly average daily diffuse radiation on a horizontal surface can be determined from the monthly average daily global radiation on a horizontal surface and the number of bright sunshine hours and is given by the correlation (Tiwari *et al.*, 2016):

$$\frac{H_d}{H_G} = 0.931 - 0.814\left(\frac{\bar{n}}{\bar{N}}\right) \quad \ldots\ldots 4.14$$

The monthly average daily beam radiation on a horizontal surface is the difference between the monthly average daily global and diffuse radiations.

$$H_b = H_G - H_d \quad \ldots\ldots 4.15$$

Figure 4.4 shows estimated variations of monthly average daily global, diffuse, and beam radiations on a horizontal surface.

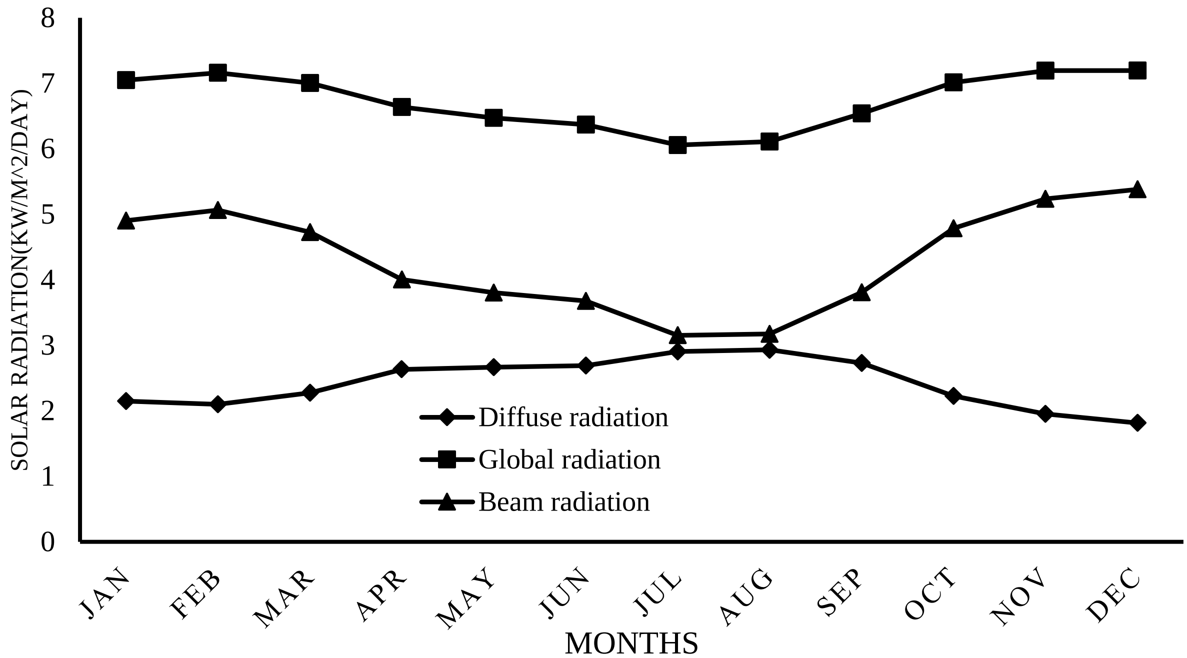

Figure 4.3: Monthly average daily global, diffuse, and beam radiations on a horizontal surface.

4.3.5 Estimation of Monthly Average Hourly Global Radiation on a Horizontal Surface

The monthly average hourly global radiation on a horizontal surface can be determined from the monthly average daily global radiation (Duffie and Beckman, 2013) as shown in Figure below.

$$\frac{I_G}{H_G} = \frac{\pi}{24} \left(a_2 + b_2 \cos\omega\right)\left(\frac{\cos\omega - \cos\omega_s}{\sin\omega_s - \frac{\pi}{180}\omega_s \cos\omega_s}\right) \quad \text{4.16}$$

Where, $a_2 = 0.409 + 0.5016 \sin(\omega_s + 60)$ ……………………………………………4.17

$b_2 = 0.6609 + 0.4767 \sin(\omega_s + 60)$ ……………………………………………4.18

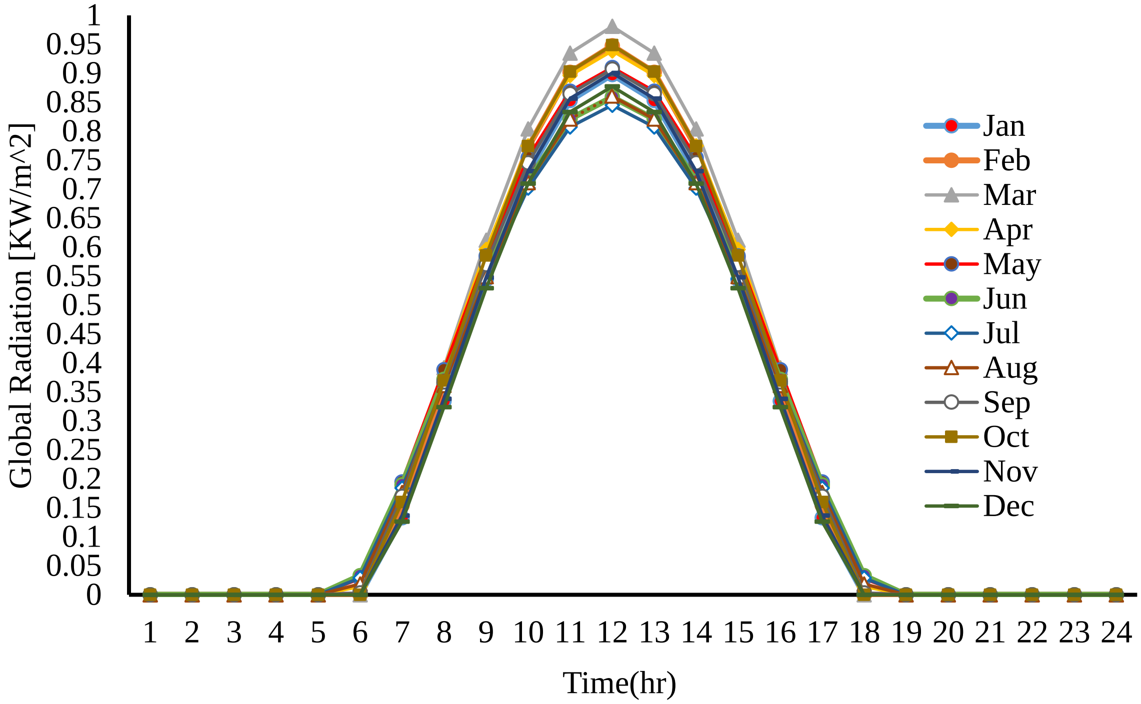

Figure 4. 4: Monthly average hourly global radiation on a horizontal surface

4.3.6 Estimation of Monthly Average Hourly Diffuse and Beam Radiations on a Horizontal Surface

The monthly average hourly diffuse radiation on a horizontal surface can be determined from the monthly average daily diffuse radiation on a horizontal surface (Duffie and Beckman, 2013) and presented in figure 4.5.

$$\frac{I_d}{H_d} = \frac{\pi}{24}\left(\frac{\cos\omega - \cos\omega_s}{\sin\omega_s - \frac{\pi}{180}\omega_s\cos\omega_s}\right) \quad \text{.......4.19}$$

The monthly average hourly beam radiation on a horizontal surface is the difference between the monthly average hourly global and diffuse radiations as shown in Figure 4.5.

$$I_b = I_G - I_d \quad \text{.......4.20}$$

Hourly variation of diffuse and beam radiation at each representative day of the month for each of 24 hours in an hour interval is presented in figure 4.6 and 4.7 respectively. As the graph shows solar the radiation intensity is detected from 6 AM up to 18 PM of the day (maximum at solar noon and minimum at sunset and sunrise.

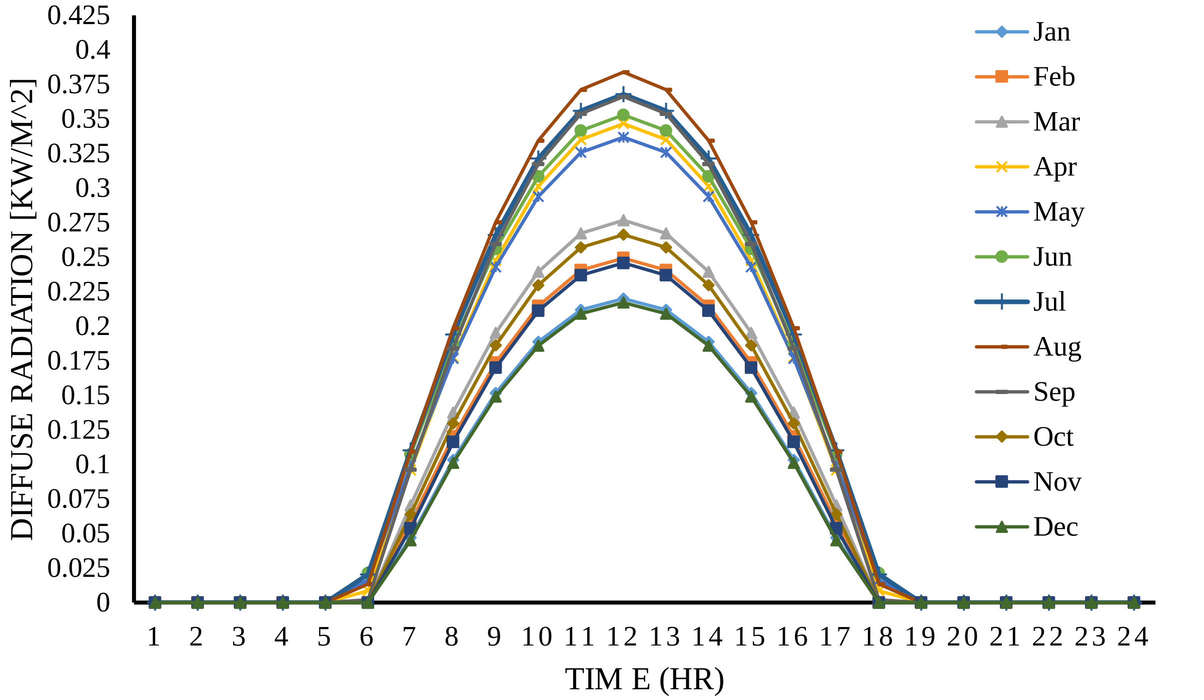

Figure 4. 5:-Variation of monthly average hourly diffuse solar radiation on a horizontal surface

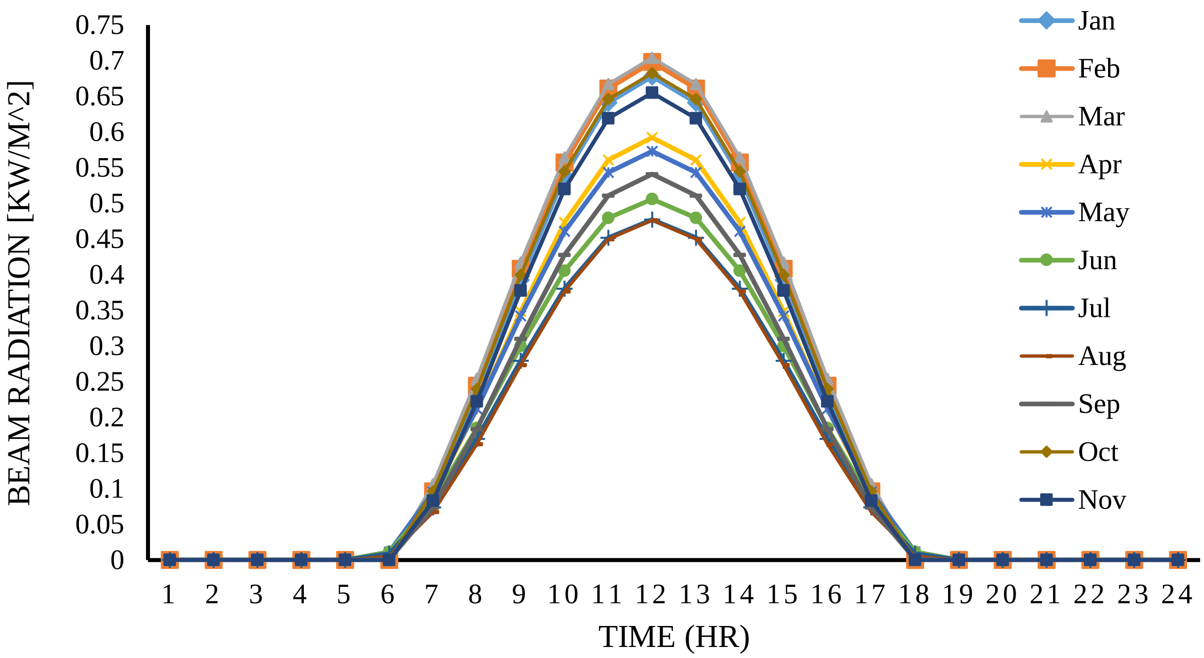

Figure 4. 6:-Variation of monthly average hourly beam radiation on a horizontal surface

CHAPTER FIVE

THEORETICAL FORMULATION OF PARABOLIC TROUGH SOLAR COLLECTOR AND LATENT HEAT STORAGE

5.1 Introduction

The theoretical study of both a parabolic trough solar collector (PTC) and a thermal storage device that can be used in a solar thermal bread baker system is presented in this chapter. The design, sizing, selection, and specifications for both a parabolic trough solar collector (PTC) and the thermal energy storage unit are presented in detail. Theoretical formulations and governing equations used for energy and exergy analysis of the PTC and LHS units are discussed. Selection of PCM and HTF and sizing of LHS unit is also addressed. Lastly, numerical analysis for LHS using COMSOL software is presented.

5.2 Description of Solar Bread Baking System

The solar bread baking system developed in this study uses solar radiation as the source of energy. Solar energy is collected and converted to usable heat using a parabolic trough collector. The parabolic trough collector is used to collect incoming solar radiation and increased the temperature of oil which circulates in the receiver. The heated thermal oil passes through the thermal energy storage tubes and the shell is filled with D-mannitol then be supplied to the baking unit. Heat transfer oil pumped from the baker unit outlet to PTC receiver inlet. The heat transfer fluid (thermal oil B) is also sent from the outlet of PTC to the thermal storage tank. Heat is transferred from the heated thermal oil to the PCM through the tubes during the charging process and the process is reversed during the discharging time. The heat was stored during the daytime when the solar radiation was available to heat the thermal oil in the parabolic trough collector and this stored heat will then be supplied to the baking unit when there is no more heat supply from the parabolic trough solar collector. A removable well-insulated cover made of fiberglass was used to prevent heat loss from thermal energy storage, baking unit, and connecting pipe during charging and discharging time. The oil pump is used to circulate the thermal oil through the overall system of solar thermal bread baker and as opening/closing valve in the system to control the flow rate of the HTF.

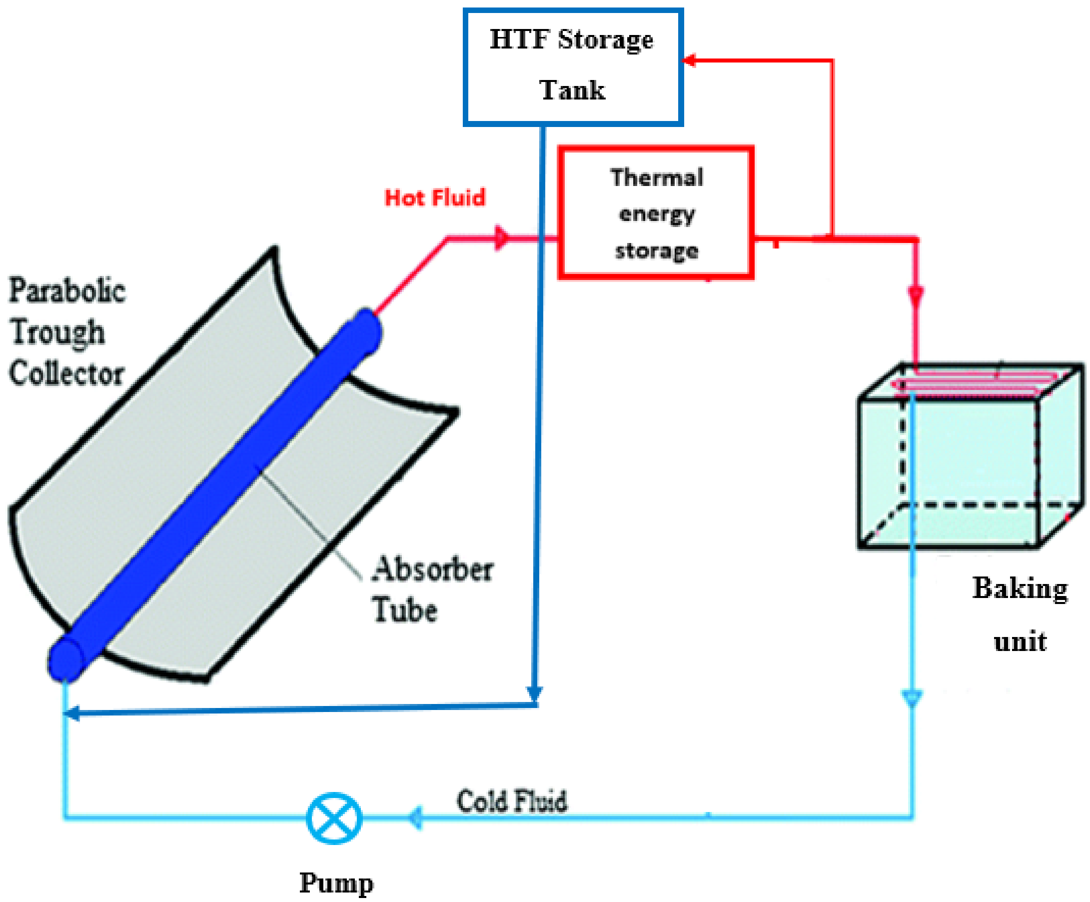

Figure 5. 1: Solar bread baker system

5.3 Design Specifications of Solar Bread Baking System

The subject of this study is experimental testing of solar bread baking systems. The capacity of the bread baking system is directly proportional to the number of bread baked per day and baking plate dimensions that means the size of the backing plate and the dough weight.

- For this analysis, the average weight of bread dough considered for this study was 2.1 kg, based on data collected at small-scale bakeries interviews.
- The time required for baking one batch of bread was 35- 45minutes for conventional baking system and 45-60 minutes for solar thermal-based baking (Tesfay *et al*., 2014).
- The required baking plate surface temperature for bread baking is 433K (Morakinyo *et al*., 2017 and Tesfay *et a*l., 2014).
- The ambient temperature is 297.15 K throughout this analysis.

- The flow is considered to be laminar flow since solar thermal systems work on low fluid flow to maximize the heat gain of the fluid at the receiver tube.

5.3.1 Energy Required for Bread Bakery

Bread baking requires intensive energy and this energy is necessary to raise the dough to a particular temperature, and evaporate the amount of water that is to be lost during the baking process. Thus, to find the energy required in bread baking, the initial mass of dough, and the mass of bread after baking were determined. The mass of water vapor can be the difference between the mass of the bread product and the initial mass of dough.

Bread baking is an energy-intensive process due to water evaporation occurring in the product (e.g., latent heat of water vaporization is 2.26 MJ/kg at $100^{o}C$) (Purlis, 2012). It is assumed that the energy utilized in bread baking is the energy required in raising the temperature of the dough from room temperature to the boiling point of water which is called sensible heat, plus the energy required to evaporate water which is called latent heat. It is also assumed that the heat capacity of dough is the same as that of water to calculate the energy required to raise the dough temperature to boiling point. Mass loss of the dough after the baking process is estimated to be 16% of the initial mass (Nicolas *et al.*, 2017). The time required for baking one bread is 45 min (Chhanwal *et al.*, 2011).

Mathematically, this baking energy is given by (Hailu *et al.*, 2017):

$$Q_{req} = m_{dough} * C_{pw} * (T_b - T_\infty) + (m_{dough} - m_{bread})h_v \quad \text{.......} 5.1$$

Where, m_{dough} = is the mass of the dough before baking =2.1 kg.

m_{bread} = is the mass of bread after baking = 1.764 kg.

T_b = is the boiling temperature of water in Adama city = 367.15K.

C_{pw} = is the heat capacity of water=4.18kJ/$kg^{o}C$

T_∞ = is ambient temperature = 297.15K.

h_v = is the heat of vaporization of water =2.26MJ/kg

The required energy becomes, Q_{req} = 1373.82kJ.

A baking Patra is a cylindrical shape commonly size about 30 to 50cm in diameter. The baking plate (Patra) considered in this case, baking Patra was 0.5mm thick, 400mm in diameter, and 40mm in height, it has high thermal conductivity than the one which is available in the local market. Direct contact of the Patra with the hot heat transfer oil cover tank; therefore, the baking plate was made up of Aluminum sheet because of its high thermal conductivity.

The system design for the average family size. The amount of energy required for heating a baking plate (0.5 mm thick aluminum sheet) to a plate temperature of 433.15K is given by;

$Q_{plate} = m_{plate} * C_{p.plate} * \left(T_{p.f} - T_{p.i}\right)$……………….…………………………………………5.2

Where,

$C_{p.plate}$ = Specific heat capacity of aluminum sheet plate = 0.888kJ/$kg^{o}C$.

$T_{p.i}$ = Initial plate temperature.

$T_{p.f}$ = required baking temperature.

m_{plate} = Mass of the baking plate.

Therefore, the energy required to heat the baking plate to the desired temperature could be 60.38kJ. The total thermal energy required for the baking process is the sum of heat energy utilized for baking and heat the baking plate.

$Q_{total} = Q_{req} + Q_{plate}$……………………………….....…………………………………5.3

The total energy supplied for one cycle of baking could be 1434.2kJ. And thus, by assuming a safety factor of 10% for various heat losses during a baking process (Tsegay, 2011). The total energy required becomes 1576.62kJ.

The amount of heat transfer fluid (shell thermal oil B) required for the baking process can also be determined from the energy balance equation:

$Q_{total} = m_f * C_{pf} * \left(T_{baking} - T_{initial}\right)$………………...…………………………….….……5.4

Where, m_f is mass of heat transfer fluid (shell thermal oil B) in kg,

T_{baking} and T_{intial} are baking bread temperature and initial temperature of air corresponding to an equilibrium state in K.

C_{pf} is the specific heat capacity of heat transfer fluid (shell thermal oil B) in kJ/kg.

Substituting the values of Q_{total} = 1576.62 KJ, T_{baking} =433K, $T_{initial}$ =297K and C_{pf} = 2.6 kJ/$kg^{o}C$ into Eqn. (5.4) gives m_f = 4.59 kg of hot thermal oil is required for this bread baking.

The mass flow rate of heat transfer fluid needed for the system was determined by (Forson *et al*., 2007):

$\dot{m}_f = \frac{m_f}{t_b}$……………………………………………………………………………….5.5

Where, t_b is the bread baking time in second.

Substituting the values of $\dot{m}_f = 0.0017$ kg/s.

5.4 Design of Latent Heat Storage System

The design of a latent heat storage system involves the selection of storage material, design of the geometrical configuration of containment, and heat exchanger type. The intermittent nature of solar energy needs thermal energy storage systems for baking bread in the door and non-sunny days. In this section, the overall size of solar thermal storage system to bake bread for one baking session of average family size.

5.4.1 Phase Change Material Selection

The operational temperatuure range required by the baking system is the first criterion to consider when selecting a PCM for a specific solar application, followed by availability and cost. The thermophysical properties of the PCM to be used in the design of thermal storage systems should be achieved (Arabacigil *et al*., 2015).

The thermal energy storage selected as PCM to store heat was a D-Mannitol. It melts at 440.15K. D-Mannitol is available in the Ethiopian local market and was purchased from Fine Chemical Trading found in Addis Ababa. Table 5.1 shows the Thermophysical properties of D-mannitol.

Table 5. 1: Thermophysical properties of the D-Mannitol (Eames and Cunha ,2016).

Property	unit	D-mannitol
Density	[Kg/ m^3]	1520
Melting temperature	[℃]	167
Latent heat of fusion	[KJ/Kg]	297
Thermal conductivity	[W/m℃]	2.07
Specific heat capacity	[KJ/Kg℃]	2.5

5.4.3 Selection of Heat Transfer Fluid

Conditions to be considered when selecting the heat transfer fluid are coefficient of expansion, viscosity, thermal capacity, freezing point, boiling point, flash point; it should not exhibit a high level of toxicity behavior (Purlis, 2012). Fluids capable of operating at high temperatures with low vapor pressure are commonly used as heat transfer fluid in solar thermal systems. Shell Thermal oil B was a highly refined mineral oil chosen for its best performance in indirect closed fluid heat transfer systems. Shell Thermal oil B has a high heat transfer coefficient, low viscosity, and low vapor pressure is non-toxic, non-corrosive, and easy to dispose of than synthetic oils. Thus, due to the above reasons shell Thermal oil B was used as heat transfer fluid for this application.

Table 5. 2: Thermophysical Properties of Shell Thermal oil B (Hassen *et al*., 2016; Tian and Zhao, 2013; Purlis, 2012).

Property	unit	Value
Operating temperature	℃	320
Thermal conductivity	W/m.℃	0.12
Specific heat capacity	kJ/kg. K	2.6
Density	kg/m^3	868

5.4.4 Sizing of Thermal Energy Storage

Thermal energy storage is a shell and tube, heat exchanger. The heat transfer fluid (HTF) passes through the tubes and the shell is filled with PCM. Heat is transferred from the hot HTF to the PCM through the tubes during the charging process and the process is reversed during the discharging time. The heat was stored during the daytime when the solar radiation was available to heat the HTF in the solar collector. The latent heat thermal energy storage system was designed for storing the heat needed in the baking unit for the baking process. Assuming the storage will store the heat for 2 off sunshine hours per day, the quantity of heat needed to be stored in the latent heat thermal energy storage system can be estimated by considering a safety factor of 1.5 for the change in temperature ΔT = $T_{desired}$ - $T_{initial}$ (Niyas *et al.*, 2017).

$$Q_s = \dot{m}_f C_{pf} 1.5t(\Delta T) \quad \text{……5.6}$$

The mass of the PCM m_{pcm} is determined from the amount of heat stored expressed as;

$$Q_s = m_{pcm}\left[Cp_{pcm}(T_m - T_{ini}) + L_{F.pcm}\right] \quad \text{……5.7}$$

The volume of the PCM can be calculated from:

$$V_{PCM} = \frac{m_{pcm}}{\rho_{pcm}} \quad \text{……5.8}$$

The volume of the tank is the sum of the volume of the PCM and the volume of the tubes.

$$V_{storage} = V_{PCM} + V_{tube} \quad \text{……5.9}$$

To find the volume of storage required, the tube volume (V_{tube}) should be determined as follows;

$$V_{tube} = \pi L n R_O^2 \quad \text{……5.10}$$

The storage volume of the LHS unit can be determined from the mass of PCM by the expression;

$$V_{storage} = \left(\frac{\pi}{4} D_{cyl}^2 L\right) 1.5 \quad \text{……5.11}$$

Where D_{cyl} diameter of containment cylinder, L is the length of LHS unit, R_o *and* R_i are the outer and inner diameter of HTF tube inside the shell, n is the number of tubes, and allowance factor 1.5 is induced accounting the thermal expansion of the PCM whenever phase change occurs.

Using the above relationships, the storage volume of the LHS can be determined by determining the mass of PCM required to store the required heat. Using Eqn.5.7 the mass of PCM required was found to be 10 kg. Using Eqn.5.8 volume of the PCM is determined to be $0.00657 m^3$. To store 10 kg of PCM inside the shell and tube storage unit.

5.4.5 Design Parameters of LHS Unit

In the design of latent heat storage systems, effectiveness(ε) and the number of transfer units (NTU) are principal design parameters. Effectiveness is the measure of how efficient the LHSS. According to Joseph (2010), NTU of LHSS is defined only using the fluid side of the heat transfer coefficient(h_i), rather than the usual overall heat transfer coefficient in a conventional heat exchanger (HX). For a total length of tube L and number of tubes n in the heat exchanger, the equation for the NTU and the definition of the effectiveness applied to the LHHS is given by (Sham Sundar *et al.*, 1992);

$$\mathrm{NTU} = \frac{\pi d_i h_i L n}{m_f C_P} \quad \text{5.12}$$

$$\varepsilon = \frac{T_f - T_i}{T_m - T_l} \quad \text{5.13}$$

The number of transfer units (NTU) was expressed as:

$$\varepsilon_{max} = 1 - \exp(-NTU) \quad \text{5.14}$$

Where d_i is the inside diameter of the tube

h_i is inside heat transfer coefficient

L is the length of the tube

n is the number of tubes

m_f *and* C_P are the mass flow rate and specific heat capacity of HTF

T_f and T_i is outlet and inlet temperature of HTF

T_m is the melting point of PCM

In a sizing latent heat storage unit, the following dimensionless parameters should be well defined.

$$Parameter\ (\beta) = \frac{h_i R_i}{K_{pcm}} \quad \text{5.15}$$

$$Biot\ number\ (Bi) = \frac{h_i R_o}{K_{pcm}} \quad \text{5.16}$$

$$\text{Nusselt number Nu} = \frac{h_i R_o}{K_f} \quad \text{5.17}$$

where; k_{pcm} and k_f is the thermal conductivity of the PCM and the HTF respectively;

R_i and R_o are the inner and outer radius of the HTF tube.

To estimate parameter β, the Nusselt number (Nu) should be first estimated depending upon the type of flow regime in the tube is either laminar or turbulent. If the fluid flow inside the tubes are considered as laminar and fully developed, the recommended assumption for Nu is 1.835. Nusselt number (Nu) is the ratio of convective to conductive heat transfer across the boundary.

For turbulent flow $Nu = 0.023Re^{0.8}Pr^{0.4}$……………………………….…………………5.18

Thus, $\beta = \text{Nu}\left(\frac{K_f}{K_{pcm}}\right)\left(\frac{R_i}{R_o}\right)$…………………………………………………………..………5.19

The outside radius R_o of the tube heat exchanger can be determined by (Joseph, 2010);

$R_o = \left(\frac{K_{PCM}(T_m - T_{in}.t)}{\tau\rho_{pcm}L_f}\right)^{1/2}$ ……………………………………………………………………5.20

Where t = storage period;

ρ_{pcm} = density of the PCM;

L_f = heat of fusion of the PCM;

K_{PCM}= thermal conductivity of the PCM;

T_m = melting point of the PCM;

T_{in} = inlet temperature of HTF;

Where τ_o is the nondimensional time variable which was expressed as:

$\tau_o = \left(\frac{F_o}{2\beta}\right) + \frac{1}{4}[(1 - F_o)ln(1 - F_o) - F_o]$……………………………………...…………………5.21

The number of tubes was determined from the length of the pipe as:

$n_t = \left(\frac{NTU\dot{m}_{HTF}C_{pa}}{2\pi hR_iL}\right)$……………………………………………………………..…………………5.22

h is the heat transfer coefficient:

$h = \frac{k_a N_u}{R_o}$ ………………………………………………………………………..……………..……..5.23

τ is a non-dimensional time variable which depends on the parameter β and initial PCM solidification fraction (Fo). F_o is the amount of PCM solidified at the tube inlet at the end of the discharge period and its value is usually between 0 and 10. In the process of sizing the LHS unit, the inner diameter of the tube, length of the tube, and diameter of shell were simply chosen depending on the volume of PCM which is required to obtain the value of the required storage volume of the LHS unit.

and its dimensional parameters were determined based on the procedure in APPENDIX B. Table 5.3 summarizes the design parameters and specifications of the shell and tube LHS unit.

Table 5. 3: Design parameters of LHS unit

Parameter	**Value**
Length of LHS(m)	0.7 m
Diameter of the shell (D_{cyl})	0.10 m
The outer radius of the tube (R_o)	0.012 m
The inner radius of the tube (R_i)	0.011 m
Number of tube(n)	5
Mass of PCM (m_{pcm})	10kg
Volume of PCM (V_{PCM})	$0.00657 m^3$
Tube volume (V_{tube})	$0.00158 m^3$
The volume of LHS unit ($V_{storage}$)	$0.00815 m^3$

5.4.5 Performance Parameters of Latent Heat Storage System

Performance parameters of LHS include determination of melt fraction, charging, and discharging time. These are presented below.

Charging is the process of storing heat energy in the latent heat storage material while it changes its phase from the solid state to the liquid state. Charging time implies the total time it takes for the LHS material or PCM to completely melt into the liquid state. The LHS is said to be fully charged when the entire PCM is completely melted, i.e., when the melt fraction reaches a value of one. Discharging is the process of releasing heat energy in the latent heat storage material while it changes its phase from the liquid state to the solid-state. Discharging time for LHS is defined concerning the temperature decrease of the PCM. The LHS is said to be fully discharged when the entire PCM is solidified, i.e., the melt fraction becomes zero.

Melt fraction (θ_f) is generally referred to as the liquid fraction of the PCM when it exists in a 2-phase form. The highest temperature below which the material is completely in the solid state is called solidus temperature (T_S) and the lowest temperature above which the material is in the liquid state is called liquidus temperature (T_L). Melt fraction (θ_f) of the PCM was obtained from the relationship (Dawit, 2018).

$$\theta_f = \frac{T-T_S}{T_L-T_S} = \frac{T-T_m+\Delta T_m}{2\Delta T_m} = \begin{cases} 0 & for\ T < T_S \\ 0-1 & for\ \ T_S \leq T \leq T_L \\ 1 & for\ T > T_S \end{cases} \quad \ldots\ldots\ldots\ldots\ldots\ldots 5.24$$

Where T_m is the melting point of PCM.

Energy stored and discharged: energy gets stored in the PCM during the charging time and discharged from the PCM to the HTF during the discharging time in the form of sensible and latent heat.

5.4.6 Energy Analysis of Latent Heat Storage System

Energy analysis of latent heat storage system applies the first law of thermodynamics for both charging and discharging modes of the PCM.

i. Energy Stored

The total heat stored in the LHS system ($E_{T.C}$) consists of the sensible heat ($E_{S.C}$) and the latent heat ($E_{L.C}$). These can be obtained from the relationship (Niyas *et al.*,2017).

$$E_{S.C} = mC_p(T - T_{int}) \ldots\ldots\ldots\ldots \quad 5.25$$

$$E_{L.C} = mL_F\theta_f \ldots\ldots\ldots\ldots 5.26$$

$$E_{T.C} = m\left[C_p(T - T_{int})\right] + L_F\theta_f \ldots\ldots\ldots\ldots 5.27$$

ii. Energy recovered

The total heat discharged from the LHS system ($E_{T.D}$) consists of the sensible heat ($E_{S.D}$) and the latent heat ($E_{L.D}$). These are expressed as (Niyas *et al.*, 2017).

$$E_{S.D} = mC_p(T_{int} - T) \quad \text{......5.28}$$

$$E_{L.D} = mL_F(1 - \theta_f) \quad \text{......5.29}$$

$$E_{T.D} = m[C_p(T_{int} - T) + L_F(1 - \theta_f)] \quad \text{......5.30}$$

5.4.7 Energy Efficiency of Latent Heat Storage System

The overall efficiency of the LHS also called the percentage of the energy recovered, is defined as the ratio of the net heat recovered during the discharging period to the net heat input during the charging period.

$$\eta_{LHS} = \frac{Q_{dis}}{Q_{ch}} \quad \text{......5.31}$$

5.4.8 Exergy Analysis of Latent Heat Storage System

Exergy analysis takes into account the temperature at which the exergy is available for storing as it uses the difference between the inlet temperature of HTF and environment temperature (T_a) rather than the difference between the inlet and outlet temperatures of HTF.

i. Exergy Stored During Charging

The rate of exergy supplied by HTF during the charging period of the LHS system is given by (Suresh *et al.*, 2014):

$$\dot{Ex}_{in.HTF} = \dot{m}_f C_p \left[\left(T_{f,o} - T_a\right) - T_a\left(ln\frac{T_{f,o}}{T_a}\right)\right] \quad \text{......5.32}$$

During the charging mode of operation, the exergy stored at any time instant is computed from the instantaneous heat transfer rate expressed as:

$$\dot{Ex}_{ch} = Q\left[1 - \frac{T_a}{T_{fin.ch\,pcm}}\right] - Q_{loss}\left[1 - \left(\frac{T_a}{T_{fin.ch\,pcm}}\right)\right] \quad \text{......5.33}$$

Therefore, the total exergy stored in PCM during charging can be readily obtained by performing time integration of Eq. (5.33) from initial charging time to final. However, it requires the computation of heat loss to the surrounding. An alternate form, simpler than the time-integrated form of Eq. (5.33) can be found in (Suresh *et al.*, 2014):

$$\dot{Ex}_{ch} = mL_f\left[1 - \frac{T_a}{T_m}\right] + mC_{p.s}\left[\left(T_m - \bar{T}_{ini-ch.pcm}\right) - T_o\left(ln\frac{T_m}{T_{in.ch\,.pcm}}\right)\right] +$$
$$mC_{p.l}\left[\left(\bar{T}_{fini-ch.pcm} - T_m\right) - T_o\left(ln\frac{\bar{T}_{fin.ch.pcm}}{T_m}\right)\right] \quad \text{......5.34}$$

ii. Exergy Released During Discharging

Expressions for exergy stored during the discharging process can be obtained in the similar way corresponds to the charging process as (Suresh *et al*., 2014);

$$\dot{E}x_{dis} = mL_f\left[1-\frac{T_a}{T_m}\right] + mC_{p.s}\left[\left(\bar{T}_{ini-ch.pcm} - T_m\right) - T_o\left(ln\frac{T_{in.ch\,.pcm}}{T_m}\right)\right] + mC_{p.l}\left[\left(T_m - \bar{T}_{fini-ch.pcm}\right) - T_o\left(ln\frac{T_m}{\bar{T}_{fin.ch.pcm}}\right)\right] \quad 5.35$$

iii. Exergy Efficiency of Latent Heat Storage System

The overall exergy efficiency of latent heat storage is expressed as;

$$\eta_{exe\ LHS} = \frac{\dot{E}x_{dis}}{\dot{E}x_{ch}} \quad 5.36$$

5.5 Design of Parabolic Trough Solar Collector

In this section about parabolic trough system components and mathematical geometry of PTC, optical efficiency, thermal efficiency and Thermal Analysis will be discussed.

5.5.1 Geometry of parabolic trough collector

The parabolic trough collector is a trough that has the shape of a part of a parabola. More exactly, it is an asymmetrical section of a parabola around its vertex. The following four parameters are commonly used to characterize the form and size of a parabolic trough (Günther *et al*., 2011).

- Focal length,
- Trough length,
- Aperture width and
- Rim angle.

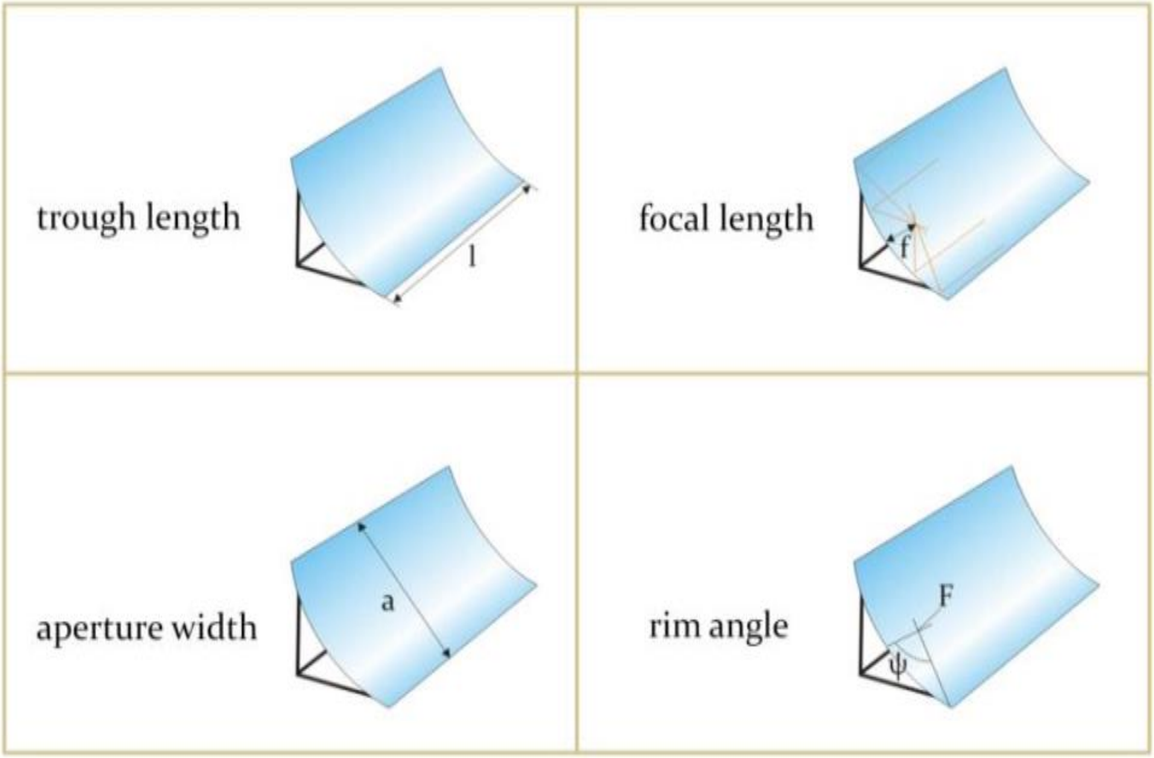

Figure 5. 2: Geometrical parabolic trough parameters (Günther *et al*., 2011)

i. Reflector Aperture Area

Most solar concentrator's thermal efficiency ranges from 40%-60%. Let the thermal efficiency (η_{th}) assumed to be 50% (Padhy *et al.*, 2021). Average beam radiation of Adama (I_b) in Ethiopia sunshine hour is 556.64W/m^2.

$$\eta_{th} = \frac{Q_u}{A_{ap} I_b} \quad \text{5.37}$$

where: Q_u -useful energy

I_b - beam radiation

A_{ap} - is the aperture area of the parabolic trough reflector

Based on equation (5.37), the aperture area of the parabolic trough is:

$$A_a = \frac{Q_u}{\eta_{th} I_b} \quad \text{5.38}$$

The aperture area is calculated as the product of the aperture width and the collector length (Günther *et al*., 2011).

$$A_{ap} = a * l \quad \text{5.39}$$

Where: l-is the aperture length of the parabolic trough

a-is the aperture width of the parabolic trough

ii. Focal length

Parabolic troughs have a focal line, which consists of the focal points of the parabolic cross-sections. Radiation that enters in a plane parallel to the optical plane is reflected in such a way that it passes through the focal line. Focal length f is the distance between the vertex of the parabola and the focal point (Günther *et al.*, 2011).

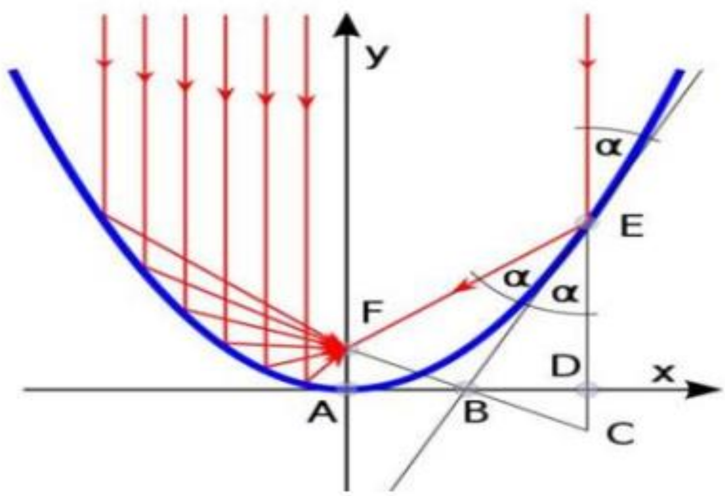

Figure 5. 3: Path of parallel rays at a parabolic mirror (Günther *et al.*, 2011)

$$f = \frac{a^2}{16h} \qquad 5.40$$

where: a - width of the parabolic trough

h - the height of the parabolic trough

iii. Rim Angle

The rim angle has a great impact on the solar radiation concentrated by the parabolic trough. The value of the rim angle depends on the size of the aperture width. It is the angle between direct incident radiation on the reflective surface and the line joining focal point and extreme point of the reflective surface at the aperture width. The rim angle determines the shape of a parabolic trough and, ideally, it should neither be too small nor too large. If the rim angle is very small, then the parabolic trough is very narrow and this increases solar radiation incidence but at the same time increases the heat loss due to convection and radiation. Hence a small rim angle in the parabolic trough solar collector is not advantageous. It is calculated by using the width and focal length of the parabolic trough (Kumar and Shukla, 2016).

The rim angles the angle between the optical axis and the line between the focal point. The rim angle ψ can be expressed as a function of the ratio of the aperture width to the focal length (Gnther *et al.*, 2011).

$$\tan\psi = \frac{a/f}{2-\frac{1}{8}(\frac{a}{f})^2} \text{...} 5.41$$

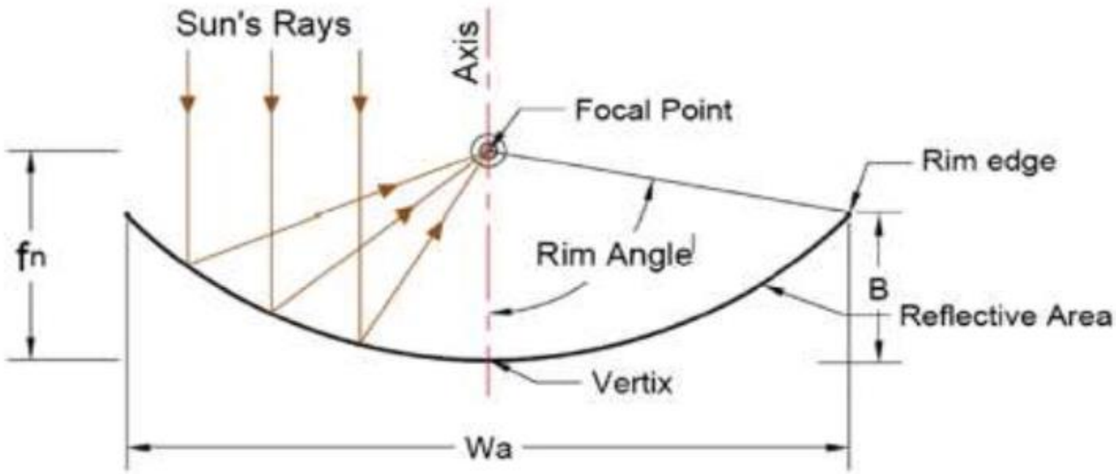

Figure 5. 4: A schematic cross-section of the parabolic trough collector (Gnther *et al.*, 2011).

So, there are several criteria, which together determine the rim angle. The rim angle of real parabolic troughs are around 80°.

Parabola curvilinear length is given by:

$$\mathrm{l} = 2\mathrm{f}\,[\mathrm{a}\sqrt{1+\mathrm{a}^2} + \frac{1}{2}\ln\left(\frac{\sqrt{1+\mathrm{a}^2}+\mathrm{a}}{\sqrt{1+\mathrm{a}^2}-\mathrm{a}}\right)] \text{...} 5.42$$

The surface area of a parabolic trough may be important to determine the material need for the trough. The area is calculated as follows (Günther *et al.*, 2011).

$$A = (\frac{a}{2}\sqrt{1-\frac{a^2}{16f^2}} + 2f * In(\frac{a}{4f} + \sqrt{1-\frac{a^2}{16f^2}})) * 1 \text{...} 5.43$$

iv. **Concentration Ratio**

The geometrical concentration ratio is a useful approximation. It is defined as the ratio of the collector aperture area to the receiver aperture area.

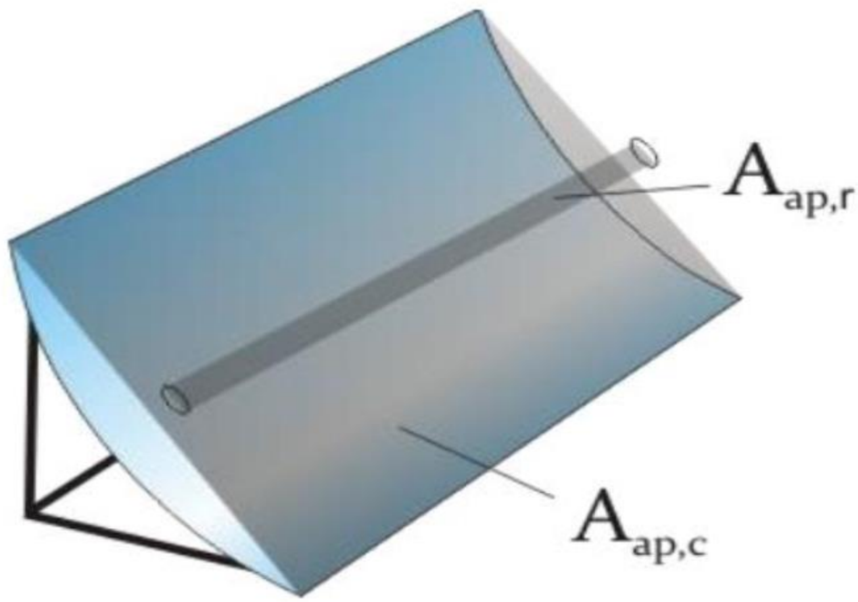

Figure 5. 5**:** Collector aperture area and receiver aperture area

In many cases, the projected area of the absorber tube is chosen. In this case the receiver area is a rectangle with the area d ∗ l, where d is the absorber tube diameter.

Another possibility is to take the irradiated absorber surface area as the receiver aperture area. In real parabolic troughs, this would mean that the whole absorber tube surface area π · d · l is the receiver aperture area.

$$C_G = \frac{A_{ap.c}}{A_{ap.r}} \quad \text{...5.44}$$

$$C_G = \frac{w.l}{\pi.d.l} = \frac{w}{\pi.d} \quad \text{...5.45}$$

This definition would lead to a lower geometrical concentration ratio. However, the concentration ratio according to the projected areas is more commonly used.

5.5.2 Sun Tracking System

Like any collector of a CSP system, parabolic troughs have to track the Sun to reach a continuous concentration of direct solar radiation. As line concentrating collectors, parabolic troughs have a one-axis tracking system. The following figure gives a general idea of the tracking of a parabolic trough. The rotational axis is normally at the vertex line of the parabolic trough or in a parallel position slightly below it.

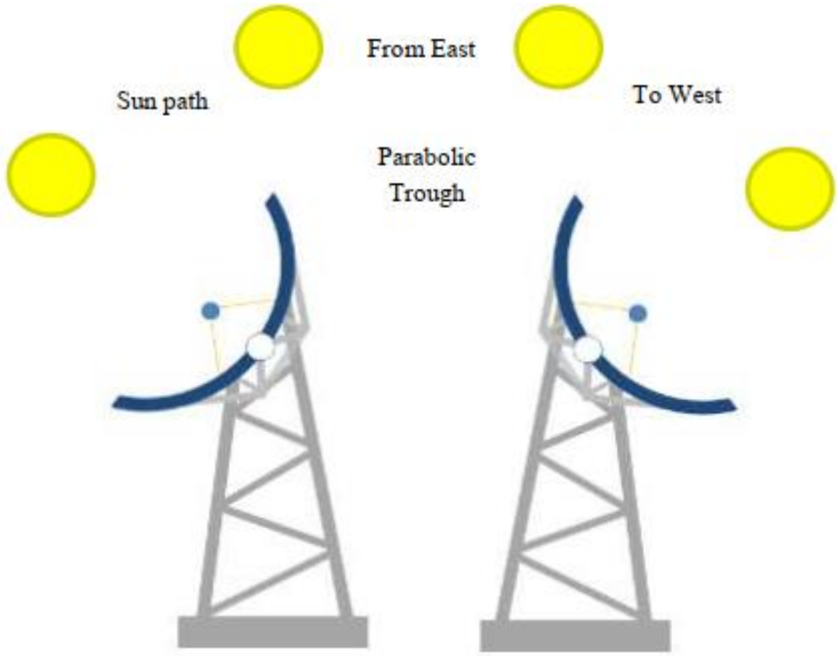

Figure 5. 6: Single-axis tracking of parabolic troughs (Petrov, 2011).

Theoretically, the parabolic troughs in the solar field of a CSP plant can have any horizontal orientation. Sun tracking is always possible. However, there is a preferred orientation, which is the north-south alignment with the respective east-west tracking. East-West alignment with the respective north-south tracking was applied only for experimental purposes.

5.5.3 Incidence Angle Modifier

The incident angle modifier K is the ratio of collector efficiency at any angle of incidence, to that at normal incidence. It is measured experimentally by varying the angle of incidence under noontime solar irradiance conditions with ambient tempersature heat transfer fluid passing through the collector. A regression analysis of the data is used to obtain an equation of the form (Duffie and Beckman, 2013):

$K = \cos(\theta) - B(\theta) - C(\theta)^2$ 5.46

Where: K = Incident angle modifier; the value ranges from 0 to1

θ = Solar beam incident angle (0 to 60 degrees)

B = Coefficient for the linear term

C = Coefficient for nonlinear term

Test results for SEGS LS-2 SCA yield an incident angle modifier expression as given in equation (Cengel and Boles, 2007). The equation is applied for temperatures between ambient and 400^{o}C, at any insolation level from 100 to 1100 W/m^{2}, and at any incident angle from 0 to 60 degrees.

$$K = \cos(\theta) - 0.0003512(\theta) - 0.0003137(\theta)^2 \quad \text{.......} 5.47$$

5.5.4 End Losses

At zero angle of incidence, the solar radiation that reflected from the concentrator hit the entire heat collection element (HCE). However, when the angle of incidence starts to increase, some areas near the end of the receiver are not illuminated by the solar radiation as illustrated in figure 5.7. These losses are addressed with the term of end losses.

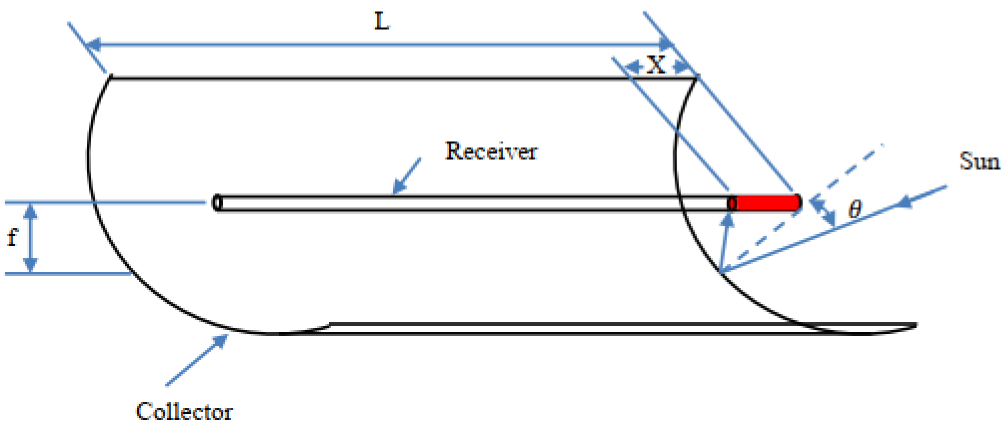

Figure 5. 7: End losses from an HCE (Mesfin and Assefa, 2010).

The end losses are a function of the focal length of the collector, the length of the collector, and the incident angle (Mesfin and Assefa, 2010).

$$EL = 1 - \frac{f \tan\theta}{L_{SCA}} \quad \text{.......} 5.48$$

Where: f = focal length of the collectors

θ = incident angle

L_{SCA} = length of a single solar collector assembly

Table 5. 4: Parameters used for simulation of parabolic trough solar collector

Parameter	Symbol	Value
Width of the PTC	a	0.90 m
Length of the PTC	L	2.00 m
Aperture area of PTC	A_{ap}	1.80 m^2
The focal length of the PTC	F	0.252 m
Rim angle of PTC	ψ	82.88^o
The concentration ratio of the PTC	C	11.82
Receiver diameter	D	0.024m

5.6 Heat Transfer Enhancement Methods for Parabolic of Trough Collector

The heat losses from the receiver tube of PTC largely affect the overall performance of the system. Effective reduction of these losses significantly influences the efficicy of the system. So, the various techniques for the enhancement of heat transfer are developed these are:

i. Inserts the longitudinal internal fin of the receiver tube is used for enhancing heat transfer.
ii. Shield one-third upper part receiver is used for heat transfer enhancement.

Both thermal enhancement techniques are passive methods in PTSC. Here, the objective is to enhance the rate of heat transfer from the surface of the receiver tube to the working medium which lowers the tube surface temperature. This temperature reduction weakens the heat losses, consequently enhances the thermal performance. Also, the uniform temperature distribution is achieved due to which thermal strain decreases. Due to the non-uniform concentration of solar radiation, the lower part of the receiver tube becomes hotter. This passive method of heat transfer enhancement makes a uniform distribution, by increasing the heat transfer coefficient and by providing a proper path to the receiving heat. Due to this method of heat transfer enhancement, there occurs a decrease in thermal boundary layer thickness, consequently turbulence increases. Moreover, passive methods do not require any external power source for their work. It only consumes energy from inside the system which contributes to a rise in fluid friction. Various types of fin direct inserts into receiver tubes such as wavy type, twisted type, internal fins, perforated plates, and porous inserts. Among various types of fins, the internal fin is better than others.

Huang *et al*., (2015) have studied the effect of inclusion dimples on heat transfer in the absorber tube of a parabolic trough collector and conducted a comparison between the obtained results for finned absorber and smooth one. The study shows that the performance of a collector with dimples is higher than that of a collector with projections and helical fins. Smith *et al*., (2016) have found the multi-criteria evaluation of a parabolic trough collector with the finned absorber. The study was carried out by software, and the model was validated by comparing obtained results to literature results. The results show that higher length and thickness lead to higher thermal performance and higher pressure losses. It was observed that the values were 10 mm for fin's length and 2 mm for fin's thickness.

Wang *et al*., (2017) suggested the use of a radiation shield upper surface of absorber to reduce the thermal losses. This idea aims to reduce the radiation thermal losses because the shield is warmer than the ambiant. However, this technique reduces the absorbed solar energy in the upper part of the absorber, something which is not so important due to the non-concentration in this part. This idea seems to be beneficial in temperatures high because in great temperatures the radiation losses are higher. Moreover, they stated that the decrease of the radiation shield emittance is important for achieving a higher temperature in the shield and so to reduce the radiation losses of the absorber.

Figure 5.8 (b) shows the radiation shield which has 2 mm thickness and length has 10mm, its inner surface has 41 mm distance from the tube center and it covers one-third of the total periphery (120^o). In the end, figure 5.8 (c) shows the combination of the shield and the internal fins. At this point, it has to be said that the down part of the shield is a reflecting surface to increase the heat input in the upper absorber surface due to the radiation and the thermal radiation reflection.

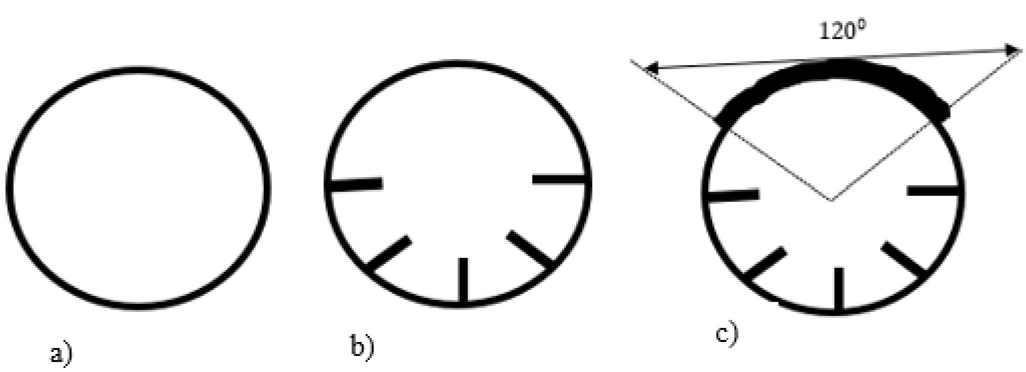

Figure 5. 8: -The observed receivers a) Smooth case (reference) b) Internally finned absorber c) Internally finned receiver with the reflecting shield

5.7 Optical Efficiency of Parabolic Trough Solar Collector

The Optical performance of PTCs depends on factors such as tracking error, geometric error, and technical failure.

The optical efficiency of PTC is defined as the ratio of energy reaching the absorber tube to that received by the collector. It indicates how much energy is absorbed by its receiver out of the total solar energy incident on the aperture of its mirror (Amine *et al.*, 2018).

$\eta_o = \gamma\tau\,\alpha r_m k(\theta)$……………………………………………………………………………5.49

Where γ is intercept factor, $\tau\ \alpha$ is a transmittance-absorbance product, r_m is the reflectance of the mirror and k (θ) is the incident angle modifier.

5.8 Thermal Analysis of Parabolic Trough Collector

A parabolic trough concentrator works by focusing a direct sunbeam onto a linear receiver. The direction of the reflector surface should be arranged according to the position of the sun at each instant in time. A heat transfer fluid (HTF) gets heated up as it flows through the receiver.

5.8.1 Analytical Heat Loss Model for the Receiver

The objective of the analytical modeling is to understand the heat transfer phenomena of the collectors. Figure 5.9 shows the one-dimensional steady-state energy balance for a cross-section of an HCE, without the glass envelope intact, and Figure 5.10 shows the thermal resistance model and subscript definitions.

The effective incoming solar energy (solar energy minus optical losses) is absorbed by the receiver tube. Some energy that is absorbed into the receiver tube is conducted through the absorber ($q'_{23\ cond}$) and transferred to the HTF by convection ($q'_{12\ conv}$), and along with the energy absorbed by the receiver tube is lost to the environment by convection ($q'_{34\ conv}$) and radiation ($q'_{35\ rad}$). If the glass envelope is missing, the heat loss from the absorber is lost directly to the environment. The model assumes all temperatures, heat fluxes, and thermodynamic properties are uniform around the circumference of the HCE.

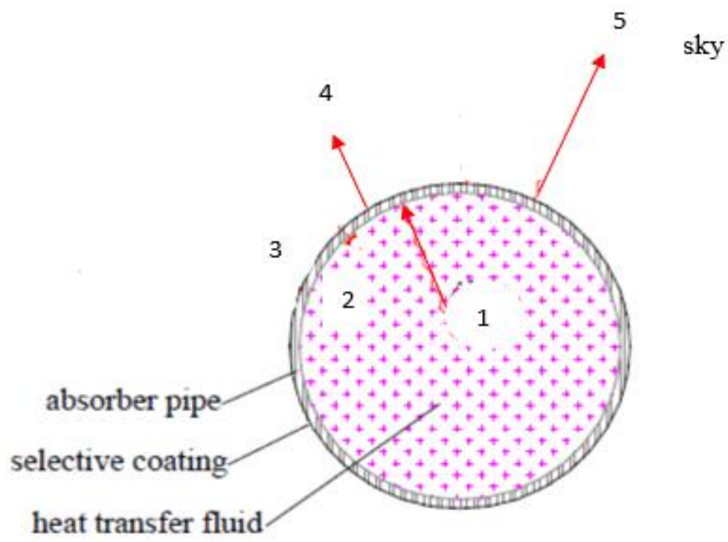

Figure 5. 9: One-dimensional energy balance (Mesfin and Assefa, 2010).

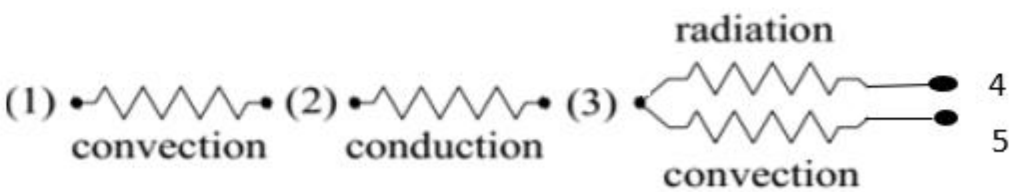

Figure 5. 10: Thermal resistance model (Mesfin and Assefa, 2010).

If the glass envelop is missing, the heat loss from the absorber is lost directly to the environment. The model assumes all temperatures, heat fluxes, and thermodynamic properties are uniform around the circumference of the HCE.

i. Convection heat transfer from the absorber to the HTF

Considering convection for internal flow, the heat transfer per unit length ($q'_{12\ conv}$) is calculated through the Dittus-Boelter equation assuming fully developed (hydrodynamically and thermally) turbulent flow in the smooth circular tube (Frank, 2002).

Hence, the local Nusselt number (Nu_{d2}) is given by

$\mathrm{Nu_{d2}} = 0.023(\mathrm{Re_{d2}})^{0.8}(\mathrm{Pr_1})^{\mathrm{n}}$……………………………………………………………5.50

Where: n= 0.4 for heating (T2 > T1) and

n = 0.3 for cooling (T2 < T1)

The Reynolds number, Re_{d2} for flow in the circular tube is given by

$$Re_{d2} = \frac{4m}{\pi d_2 \mu_1} \ldots 5.51$$

Where μ_1 id viscosity of HTF

The prandial numberPr_1 is determined by

$$Pr_1 = \frac{V_1}{\alpha_1} \ldots 5.52$$

Where: V_1 is the kinematic viscosity of HTF.

$$V_1 = \frac{\mu_1}{\rho_1} \ldots 5.53$$

And thermal diffusivity of HTF is given by

$$\alpha_1 = \frac{k_1}{\rho_1 c_1} \ldots 5.54$$

Where: k_1 is the thermal conductivity of the HTF

The heat transfer coefficient, h_{12} is calculated by using the local Nusselt number, $N_u d_2$

$$h_{12} = \frac{Nu_{d2} k_1}{d_2} \ldots 5.55$$

Where: d_2 is the inside diameter of the receiver tube.

Finally, the absorber energy per length $q'_{12\, conv}$ becomes

$$q'_{12\, Conv} = h_{12} \pi d_2 (T_2 - T_1) \ldots 5.56$$

ii. Conduction Heat Transfer Trough the Absorber Wall

Fourier's law of conduction through a hollow cylinder describes the conduction heat transfer through the absorber wall (Frank, 2002).

$$q'_{23\, cond} = 2\pi k_{23} (T_2 - T_3) / \ln(d_3/d_2) \ldots 5.57$$

Where k_{23} = absorber thermal conductivity at the average absorber temperature $(\frac{T_2+T_3}{2})$ (w/m-k)

T_2 = absorber inside surface temperature (K)

T_3 = absorber outside surface temperature (K)

In this equation, the conduction heat transfer coefficient is constant and is evaluated at the average temperature between the inner and outer surfaces. The conduction coefficient depends on the absorber material type. The conduction coefficient is calculated with the following equation.

$$K_{23} = (0.013)T_{23} + 15.2 \qquad 5.58$$

iii. Heat Transfer from the Absorber to the Atmosphere

The heat will transfer from the absorber to the atmosphere by convection and radiation heat transfer. The convection will either be forced or natural depending on whether there is wind or not. Radiation heat loss occurs due to the temperature difference between the absorber and the sky.

a. Convection heat transfer

The convection heat transfer from the absorber to the atmosphere ($q'_{34\ conv}$) is the largest source of heat loss, especially if there is wind (Frank, 2002).

From newton's law of cooling

$$q'_{34\ \mathrm{Conv}} = h_{34} d_3 \pi (T_3 - T_4) \qquad 5.59$$

$$h_{34} = Nu_{d3} \frac{k_{34}}{d_3} \qquad 5.60$$

Where T_3 = absorber outer surface temperature (k)

T_4 = ambient temperature (k)

h_{34} = convection heat transfer coefficient from the air at $(T_3$-$T_4)/2$ (W/m^2-k)

k_{34} = thermal conductance of air at $(T_3$-$T_4)/2$ (W/m-k)

d_3 = absorber outer diameter (m)

Nu_{d3} = average Nusselt number based on the absorber outer diameter

The Nusselt number depends on whether the convection heat transfer is natural (no wind) or forced (with the wind).

No Wind Case: natural convection

If there is no wind, the convection heat transfer from the receiver tube to the environment will be by natural convection. For this case, the correlation developed by Churchill and Chu will be used to estimate the Nusselt number (Frank, 2002).

$$\overline{\mathrm{Nu}_{d3}} = \left\{0.6 + \frac{0.387\mathrm{Ra}_{d3}^{\frac{1}{6}}}{\left[1+(0.559/\mathrm{Pr}_{34})11^{\frac{9}{16}}\right]^{\frac{8}{27}}}\right\}^{2} \quad \text{......5.61}$$

$$\mathrm{Ra}_{d3} = \frac{g\beta(T_3-T_4)d_3^3}{(\alpha_{34}v_{34})} \quad \text{......5.62}$$

And

$$\mathrm{Pr}_{34} = \frac{v_{34}}{\alpha_{34}} \quad \text{......5.63}$$

Where Ra_{d3}= Rayleigh number for air based on the pipe outer diameter, d3

g = gravitational constant (9.81) (m/s^2)

α_{34} = thermal diffusivity for air at T_{34} (m^2 /s)

β = volumetric thermal expansion coefficient (ideal gas) $1/T_{34}$ (1/K)

Pr_{34} = Prandtl number for air at T_{34}

v_{34} = kinematic viscosity for air at T_{34} (m^2/s)

T_{34} = film temperature (T_3-T_4)/2 (K)

This correlation is valid for $10^5 < \mathrm{Ra}_{d3} < 10^{12}$, and assumes a long isothermal horizontal cylinder. Also, all the fluid properties are determined at the film temperature (T_3 + T_4)/2.

Wind case: Forced convection

If there is wind, the convection heat transfer from the receiver tube to the environment will be forced convection. The Nusselt number, in this case, is estimated with Zhukauskus' correlation for external forced convection flow normal to an isothermal cylinder (Frank, 2002).

$$\overline{\mathrm{Nu}_{d3}} = \mathrm{C}\mathrm{Re}_{d3}^{m}\mathrm{Pr}_{4}^{n}\left(\frac{\mathrm{Pr}_4}{\mathrm{Pr}_3}\right)^{\frac{1}{4}} \text{.......} 5.64$$

With

Table 5. 5: Reynolds Number (Forristall, 2003)

R_eD	C	m
1-40	0.75	0.4
40-1000	0.51	0.5
1000-200000	0.26	0.6
200000-1000000	0.076	0.7

And

n = 0.37, for p_r <=10

n = 0.36, for p_r >10

b. Radiation heat transfer

The useful incoming solar irradiation is included in the solar absorption terms. Therefore, the infrared radiation transfer between the receiver tube and sky is caused by the temperature difference between the receiver tube and sky (Frank, 2002).

$$\mathrm{q}'_{35\,\mathrm{rad}} = \sigma\pi\varepsilon_3 \mathrm{d}_3(\mathrm{T}_3^4 - \mathrm{T}_5^4) \text{.......} 5.65$$

Where σ = Stefan-Boltzmann constant = 5.670 x 108 W/m^2-K^4

d_3 = pipe outer diameter (m)

ε_3 = emissivity of the carbon steel pipe outer surface

T_3 = pipe outer surface temperature (K)

T_5 = effective sky temperature (K)

The effective sky temperature is approximated as being 6^{0}C below the ambient temperature**.** The effective income of solar energy is equal to the solar energy minus the optical loss.

5.8.2 Energy Analysis of Parabolic Trough collector

The theoretical useful energy from parabolic trough solar collector calculated by equation writing as (Yassen, 2012; Kibaara *et al*., 2012):

$$Q_{u,th} = F_R A_a [S- U_l \frac{Ar}{Aa} (T_r - T_a)] \qquad 5.66$$

$$S= I_b \eta_0 \qquad 5.67$$

The overall heat loss coefficient (U_l) is one of the most important parameters and can be found out through the following equation:

$$U_l = h_{rc} + h_{rr} \qquad 5.68$$

The temperature of the absorber surface can be calculated from the written equation as (Garg, 2000):

$$T_r = T_{f,m} + \frac{\dot{m}C_p(T_O - T_i)}{h_{c,i}\pi D_O L} \qquad 5.69$$

The heat removal factor FR is the ratio of the heat delivered to that delivered if the receiver pipe were at a uniform temperature equal to that of the inlet fluid. It is obtained by (Yassen, 2012);

$$F_R = \frac{mC_p}{A_0 U_1}\left[1 - \exp\left(\left(\frac{-A_0 F' U_1}{mC_p}\right)\right)\right] \qquad 5.70$$

For a tubular absorber with inside diameter (D_i) and outside diameter (D_o) having $h_{c,i}$the convective heat transfer coefficient between the absorber and the fluid, the collector efficiency the factor is given as (Garg, 2000):

$$F' = \frac{1/U_1}{\frac{1}{U_1} + \frac{D_O}{h_f D_i} + (\frac{D_0}{2k}\ln\frac{D_0}{D_i})} \qquad 5.71$$

The actual useful energy obtained from parabolic trough solar collector is given as:

$$Q_{actual} = \dot{m}C_p(T_o - T_i)\text{..}5.72$$

5.8.3 Thermal Efficiency of a PTC

The instantaneous thermal efficiency (η_{th}) of a solar concentrator may be calculated from an energy balance on the receiver (Vijayan and Kumar, 2017).

The experimental thermal efficiency (η_{exp}) is given as (Yassen, 2012):

$$\eta_{exp} = \frac{Q_{act}}{I_b A_{ap}}\text{..}5.73$$

Where, I_b= Total solar radiation intensity (W/m^2) and A_{ap}= aperture area (m^2)

The theoretical thermal efficiency is writing as:

$$\eta_{th} = \frac{Q_{u,th}}{I_b A_{ap}} = \frac{F_R A_a\,[S - U_l \frac{Ar}{Aa}(T_r - T_a)]}{I_b A_{ap}}\text{..}5.74$$

5.8.4 Exergy analysis of Parabolic Trough Collector

Exergy is determined as the maximum amount of work that can be produced by a system or flow of mass or energy as it regards equilibrium with a reference point at surrounding (Kotas, 2013). The main form of exergy equilibrium equation is as:

$$\dot{E}_{in} + \dot{E}_{s} + \dot{E}_{out} + \dot{E}_{l} + \dot{E}_{dest} = 0\text{..}5.75$$

where, $\dot{E}_{in}$, $\dot{E}_{s}$, $\dot{E}_{out}$, $\dot{E}_{l}$ and $\dot{E}_{dest}$ are the inlet, stored, outlet, loss, and destroyed exergy rate, respectively. The inlet exergy rate is the sum of the inlet exergy rate with fluid flow and the absorbed solar radiation exergy rate. The inlet exergy rate with the fluid flow is obtained by (Kotas, 2013; Sadaghiyani, 2018).

$$\dot{E}_{in,f} = \dot{m}c_p\left(T_{in} - T_a + T_a\,ln\left(\frac{T_{in}}{T_a}\right)\right)\text{..}5.76$$

Also, according to the Petela theorem, the absorbed solar radiation exergy rate is calculated by (Najian, 2000):

$$\dot{E}_{in,Q} = \eta_o I_T A_{ap}\left[1 - \frac{4}{3}\left(\frac{T_a}{T_{sun}}\right) + \frac{1}{3}\left(\frac{T_a}{T_{sun}}\right)^4\right]\text{..}5.77$$

The term in the bracket is named the Petela efficiency (η_p). However, this equation contravenes the second law of thermodynamics in some systems. If the sun is assumed as an infinite thermal source, the corrected form of eq. (5.77) will be:

$$\dot{E}_{in,Q} = \eta_o I_T A_{ap}\left(1 - \frac{T_a}{T_{sun}}\right) \ldots\ldots 5.78$$

where T_{Sun} is the apparent sun temperature and equals 75% of black body temperature of sun 4500K (Bavil, and Razavi, 2017). The summations of Eqs. (5.76) and (5.77) will result in the total inlet exergy rate of the solar collector. The stored exergy rate is negligible at steady-state conditions. Also, the outlet exergy rate of outlet fluid flow in the solar collector is:

$$\dot{E}_{out,f} = -\dot{m}c_p\left(T_{out} - T_a + T_a \ln\left(\frac{T_{out}}{T_a}\right)\right) \ldots\ldots 5.79$$

The loss exergy rate consists of two terms: the first is created by the heat loss rate from the absorber tube to the environment because of wind blast. It is calculated by (Dutta and Saha, 1990):

$$\dot{E}_{l,w} = -U_l A_C (T_r - T_a)\left(1 - \frac{T_a}{T_r}\right) \ldots\ldots 5.80$$

The second is created by the temperature difference between the receiver tube and the sun. In other words, the radiation loss makes these terms of exergy loss:

$$\dot{E}_{l,\Delta T_s} = -\eta_o I_T A_C T_a\left(\frac{1}{T_r} - \frac{1}{T_{sun}}\right) \ldots\ldots 5.81$$

where η_o is optical efficiency of collector and calculated by $\eta_o = \tau\alpha$.

And the second term is concluded by the temperature difference between the receiver tube surface and the working fluid which is obtained by:

$$\dot{E}_{dest,\Delta T_f} = -\dot{m}c_p\left(\ln\left(\frac{T_{out}}{T_a}\right) - \frac{T_{out} - T_{in}}{T_r}\right) \ldots\ldots 5.81$$

Therefore, the eq. (5.75) is discretized to more terms as:

$$\dot{E}_{in,f} + \dot{E}_{in,Q} + \dot{E}_s + \dot{E}_{out,f} + \dot{E}_{l,w} + \dot{E}_{l,\Delta T_s} + \dot{E}_{dest,\Delta T_f} = 0 \ldots\ldots 5.82$$

If the absorbed solar radiation exergy rate (E_{in}, Q) supplants to the right hand and two hands of resulted equation divided to E_{in}, Q then:

$$\frac{\dot{E}_{in,f}+\dot{E}_{out,f}+\dot{E}_{l,w}+\dot{E}_{l,\Delta T_s}+\dot{E}_{dest,\Delta T_f}}{-\dot{E}_{in,Q}} = 0 \quad \text{...5.83}$$

5.8.5 Exergy efficiency of parabolic trough solar collector

Exergy efficiency is defined as the ratio of output exergy to input exergy, as follow:

$$\eta_{ex} = \frac{\dot{E}_{out}}{\dot{E}_{in}} = 1 - \frac{\dot{E}_{dest}}{\dot{E}_{in}} \quad \text{...5.84}$$

The exergy efficiency has been defined as the increase of fluid flow exergy to the radiation source in solar collectors. In other words:

$$\eta_{ex} = \frac{\dot{E}_{in,f}+\dot{E}_{out,f}}{-\dot{E}_{in,Q}} \quad \text{...5.85}$$

Subtitling Eq. (5.75), (5.78), and (5.79) into Eq. (5.85), the exergy efficiency of the solar collector is calculated by:

$$\eta_{ex} = \frac{\dot{m}\left[c_p\left(T_{out}+T_{in}+T_a ln\left(\frac{T_{out}}{T_a}\right)\right)\right]}{I_T A_c\left(1-\frac{T_a}{T_{sun}}\right)} \quad \text{...5.86}$$

5.9 Performance of Solar Thermal Bread Baking unit

The baking experiment was performed to know the energy distribution and energy loss at various sections of the baking system such as energy absorbed by the receiver, amount of energy supplied to the storage, amount of energy stored and energy utilized for baking. As energy transfers from one medium to another energy loss should occur. It needs to calculate the amount of energy loss of the system performance.

Heat energy supplied is the energy given to the storage through circulating HTF and given by;

$$Q_s = \dot{m}C_p\left(T_{in,bu} - T_{out,bu}\right) \quad \text{...5.87}$$

Where,

m - mass flow rate of HTF, kg/s

C_p – Specific heat capacity of HTF, KJ/kg.k

$T_{in,bu}$ - Inlet temperature of the HTF to the baking unit, K

$T_{out,bu}$ - Outlet temperature of the HTF from baking unit, K

The energy utilized for bread baking ($Q_{utilized}$) is given by (Ayub *et al*., 2018; ERKEK and GÜNGÖR, 2013).

$$Q_{utilized} = \frac{T_s - T_b}{{}^{1}/_{hA} + {}^{t}/_{kA}} \quad \text{5.88}$$

Where,

T_s – HTF temperature, K

T_b – baking plate temperature, K

A- Area of the baking plate, m^2

h- Heat transfer coefficient, $w/m^2.k$

k – Thermal conductivity of the baking plate, w/m.k

The efficiency of the baking unit or energy utilization ratio can be determined by the relation (Ayub *et al*., 201).

$$EUR = \frac{heat\ utilized}{heat\ stored} = \frac{Q_{utilized}}{Q_s} \quad \text{5.89}$$

$$EUR = \frac{Q_{utilized}}{Q_s} \quad \text{5.90}$$

Where, EUR – the energy utilization ratio (%)

5.10 Pumping Power

To circulate the HTF through the system, it must be equipped with a pumping system that can overcome the pressure drop throughout the whole system which is specified by ΔP. pressure drop in the system was determined by the relationship (Dawit, 2018).

$$\Delta p = f\frac{\rho V^2 \Delta L}{2d} + K\frac{\rho V^2}{2} \quad \text{5.91}$$

Where V is the mean flow velocity of the fluid, d is tube diameter, ρ is density, f is friction factor, Δl is the length of the tube and K is the head loss coefficient.

Frictional factor f which is is caused by the viscosity of fluid during laminar flow inside the tube was determined by the relation;

$$f = \frac{64}{R_e} \quad \text{5.92}$$

where R_e is the Reynolds number and is expressed as:

$$Re = \frac{\rho V d}{\mu} \quad \text{.........} 5.93$$

The mean velocity of the fluid (V) can be determined by:

$$V = \frac{4m}{\rho \pi d^2} \quad \text{.........} 5.94$$

Therefore: the pumping power can be determined as follows:

$$P_{pump} = \frac{\dot{m}\Delta p}{\rho} \quad \text{.........} 5.95$$

Thus: the required pumping power can be determined as follows:

5.10.1 Pressure Props

Pressure drop in the system is the sum of pressure drop in the collector, thermal storage, fittings, and bendings.

i. Pressure Drop in the Collector

A quantity of interest in the analysis of pipe flow is the pressure drop (Δp) since it is directly related to the power requirements of the pump to maintain flow (Mekonnen, 2011).

$$\frac{dp}{dx} = \frac{p_2 - p_1}{L} \quad \text{.........} 5.96$$

The pressure drop for a fully laminar flow can be expressed as:

$$\Delta p = p_2 - p_1 = \frac{32 v L V_o}{D_{PJ}^2} \quad \text{.........} 5.97$$

Where:

ΔP - pressure drop

ν - viscosity of the oil

L - length of the pipe

V - average velocity of the fluid

D_p - internal diameter of the pipe

The pressure drop is proportional to the viscosity (ν) of the fluid, and ΔP would be zero if there were no friction. Therefore, the drop of pressure from P_1 to P_2 is due to entirely viscous effects (Mekonnen, 2011). The pressure loss for fully developed internal laminar flows can be expressed:

$$\Delta p = f\frac{L\rho V_o^2}{2D_{PJ}} \qquad 5.98$$

Where: f-friction factor

ρ-density of fluid

The pressure loss can be calculated from equation (5.84):

$$\Delta p = 1649.05\ Pa$$

ii. Pressure Drop in LHS System

The LHS system had 5 HTF tubes with 700mm length, 16mm diameter inside a 760mm length, and 120mm shell. Volume flow rate inside the LHS can be determined by assuming uniform flow inside the HTF tubes.

$$\dot{Q}_{LHS} = \frac{\dot{Q}}{5} = 1.704 * 10^{-6}\ m^3/_s$$

$V_{av,LHS} = \frac{\dot{Q}_{LHS}}{A_t} = 0.004$ m/s

$Re = \frac{\rho.v_{avLHS}.d}{\mu} = 77.09 < 2300$ laminar flow and the pressure drop developed can be estimated as

$$\Delta P_{LHS} = f\frac{\rho.V_{avLHS}{}^2L}{2D} \qquad 5.99$$

$\Delta P_{LHS} = 464.21$ Pa

iii. Pressure Drop in Connections Fitting and Bending's in the Whole System

The length of the total connecting tubes is 10-meter 25mm diameter with 13 right angle bending's. Thus, the pressure drop developed can be estimated by assuming uniform flow inside the pipes;

$$\Delta P_{com} = f\frac{\rho.V_{av}{}^2L}{2D} + K_f\frac{\rho V_{av}^2}{2} \qquad 5.100$$

$\Delta P_{com} =$ 5.968 Pa + 2.61 Pa = 8.578 Pa

Hence, the total pressure drops of the system

$$\Delta P_{tot} = \Delta P_{PTC} + \Delta P_{LHS} + \Delta P_{conn}$$

$$\Delta P_{tot} = 2121.838\ Pa$$

An allowance factor of 1.5 is given for the reliability of the pump $\Delta P_{tot} = 3182.757\ Pa$

The total specific work Y = $\frac{\Delta P_{tot}}{\rho} = 4.266\ {m^2}/{s^2}$

Total dynamic head TDH $\equiv \frac{Y}{g} = 0.435m$

Total volume flow rate $\dot{Q} = 8.52 \times 10^{-6}\ {m^3}/{s} = 0.031\ {m^3}/{hr}$

Therefore, a proper pump with the requirement of head more than 0.435m and a flow rate of $0.031\ {m^3}/{hr}$ can perform the required pumping effect. In the market the least power of pump(centrifugal) available is 0.5hp. But it was costly with fixed motor speed. For the present solar bread baking system, the available electrically driven drum pump with the following specification was selected.

Table 5. 6: Specification of the selected pump

Pump specification		**Motor specification**	
Normal speed	1000rpm (adjustable)	Frequency	50hz
Flow rate	100L/min	Voltage	220V
Shaft power	700W	Speed	1000rpm
Lift distance	8m	Rated power	0.8kW
Efficiency	50%	Electric current	4A

5.11 Numerical Modeling of Latent Heat Storage System

The procedure that has been taken in COMSOL Multiphysics 4.3a simulation software in the developed TES models is as shown in Figure 5.11.

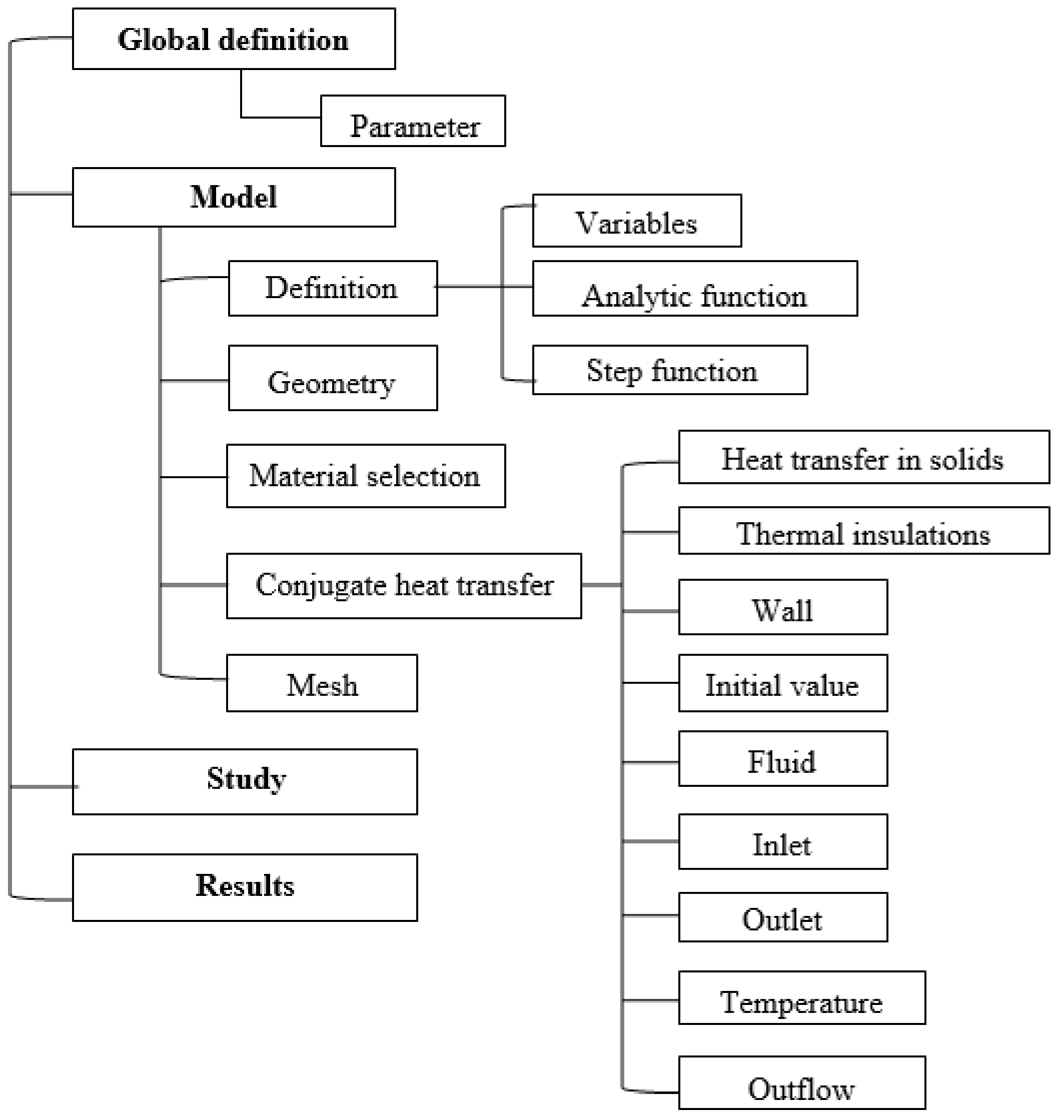

Figure 5. 11:- Flow chart integrated with COMSOL Multiphysics 4.3a simulation software

5.11.1 Model geometry for the latent heat storage system

Figure 5.12 illustrates the sectional view of the 3D shell and tube type storage system filled with the heat transfer medium in the shell and thermal oil B in the HTF tube. Since the developed model is symmetric about the X-axis, only $1/_{4th}$ of the model was taken for the investigation. The diameter of the LHS shell and the HTF tube, length of the LHS shell, and thickness of HTF was 100, 12, 700, and 1mm, respectively which are similar to the fabricated storage system. D-mannitol was used as a PCM for the LHS model.

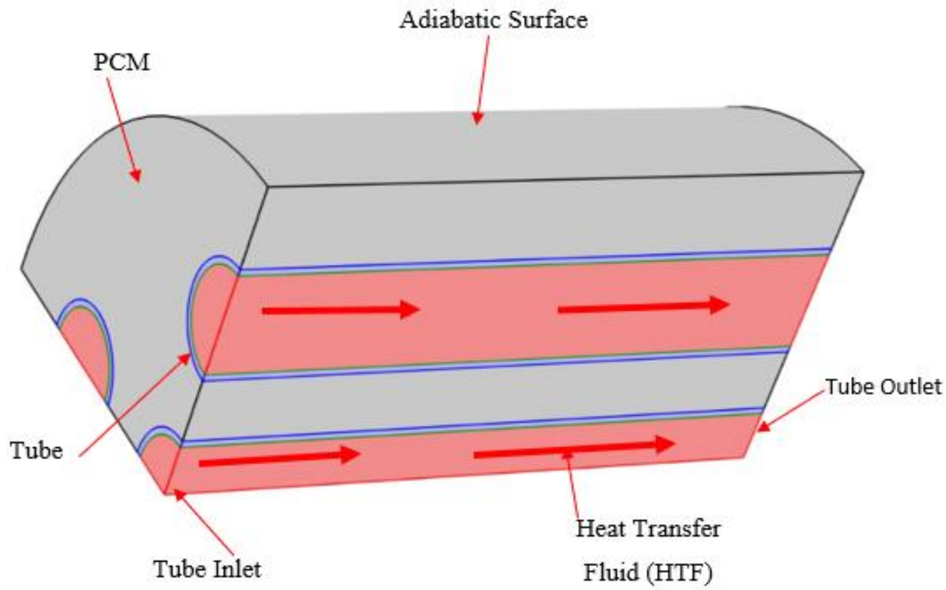

Figure 5.12: - Numerical model of the LHS system

5.11.2 Meshing for Latent Heat Storage System

The numerical solution of D-mannitol and thermal oil B based LHS depends on the number of mesh elements. Grid generation was performed using tetrahedral cells for both the domain and boundaries which is presented in figure 5.13. The smaller section such as HTF tube thickness was highly refined with sufficient volume elements. To capture the boundary layer in the near-wall regime, Special meshing features of COMSOL Multiphysics, viz., boundary layers were used for the developed model. This feature helped for predicting the near-wall velocity and thermal gradient with almost accuracy and precision.

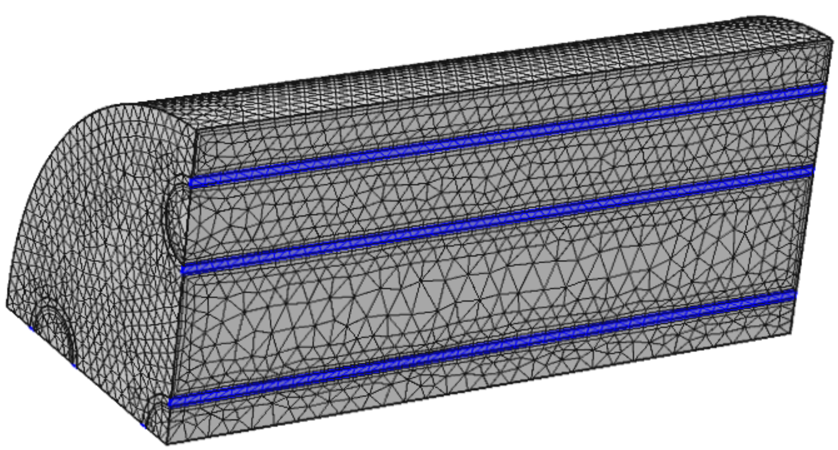

Figure 5.13: - Meshed part of the LHS model

5.11.3 Governing Equations for Latent Heat Storage System

The thermal energy storage behavior of latent heat storage can be studied by simulating four physical processes, HTF flow, phase change, convection, and conduction. The thermal model was developed based on the following assumptions:

- HTF is incompressible and Newtonian.
- HTF flow is laminar and exhibits negligible viscous dissipation.
- The initial temperature of PCM is uniform.
- Phase change during melting/solidification occurs in a temperature interval.
- Thermal losses through the outer wall of the PCM are negligible.
- PCM is homogeneous and isotropic.

The developed LHS physical model was solved by the coupled conjugate heat transfer problems which simultaneously solve both the flow behavior of the HTF and the phase change behavior of the PCM. This was solved by implementing the equivalent heat capacity (EHC) method, which comprises both the specific heat and latent heat of the PCM in a single term called EHC.

Bonacina *et al.*, (1973) used the EHC method for the first time for solving the problem. The modified heat capacity of the PCM and the effective heat capacity are obtained from the expression (Dawit, 2018).

$$C_p = \begin{cases} C_{p.s}\, for\ T < T_s \\ C_{p.EEF}\, for\, T_s \leq T \leq T_L \\ C_{p.L}\ for\ T > T_L \end{cases} \quad \text{.......} 5.101$$

$$C_{p,EFF} = \frac{C_{p,s}+C_{p,L}}{2} + \frac{L_F}{T_L+T_s} \quad \text{.......} 5.102$$

The energy and continuity equations are given in Eqns. (5.101) and (5.102) were used to simulate the model. To include the effect of buoyancy ($\vec{V}$) and Darcy law's source term and reduce the complexity in solving the Navier-Stokes's equations, Boussinesq approximation was added to the momentum equation, which is given by (Niyas *et al.*, 2017):

$$\frac{\partial\vec{v}}{\partial t} + (\vec{v}.\nabla)\vec{v} = \frac{1}{\rho}(-\nabla P + \mu\nabla^2\vec{v} + \vec{F} + \overrightarrow{S}) \quad \text{.......} 5.103$$

$$\vec{F} = \rho\vec{g}\beta(T - T_m) \quad \text{.......} 5.104$$

$$\vec{S} = \frac{(1-\theta)^2}{(\theta^3+\varepsilon)} A_{mush}\vec{v} \quad \text{.........} 5.105$$

Where, A_{mush}, ε , θ, and β are mushy zone constant, a constant value of 0.001, melt fraction, and thermal expansion of the PCM respectively.

Phase change problems occur during a temperature interval and they are often called mushy region problems. The mushy zone constant defines the transition of velocity in the mushy region and values between 10^3 and 10^7 are recommended for most computations (Niyas *et al*., 2017).

5.11.4 Boundary Conditions used for the Thermal Energy Storage System

The boundary conditions used for the TES are: (i) there is no agglomeration or sedimentation in the shell, (ii) the flow of HTF is laminar with negligible viscous dissipation, (iii) the HTF is incompressible and Newtonian, (iv) the properties of thermal oil B is homogeneous and isotropic, (v) the heat loss through the outer wall of the shell is assumed to be negligible, (iv) the initial temperature of thermal oil B is taken to be uniform and the phase change during melting/solidification occurs within a temperature interval, (vii) fluid initialization of charging/discharging is done by assuming a constant temperature of 440K/298K followed by the constant velocity of the HTF and (viii) initially, there is no flow of through the tubes and all the domains are at a constant temperature of 298K/440K during the charging/discharging process, respectively.

CHAPTER SIX

EXPERIMENTAL SETUP AND PROCEDURE

6.1 Introduction

This chapter presents the description of the manufacturing process of experimental setup consisting parabolic trough solar collector, latent heat storage device, and bread baking machine and also presents the conceptual model of the whole experimental setup. The conceptual model of the system was developed using SOLID WORK 2019. The experimental setup and the measuring devices used are also presented.

6.2 Conceptual Model of Solar Thermal Bread Baking System

Figure 6.1 illustrates the schematic diagram of solar bread baker drawn using SOLID WORK 2019. The system consists of a parabolic trough collector, LHS unit, baking unit, frame, and support and closed-loop piping network as a connection for the whole system.

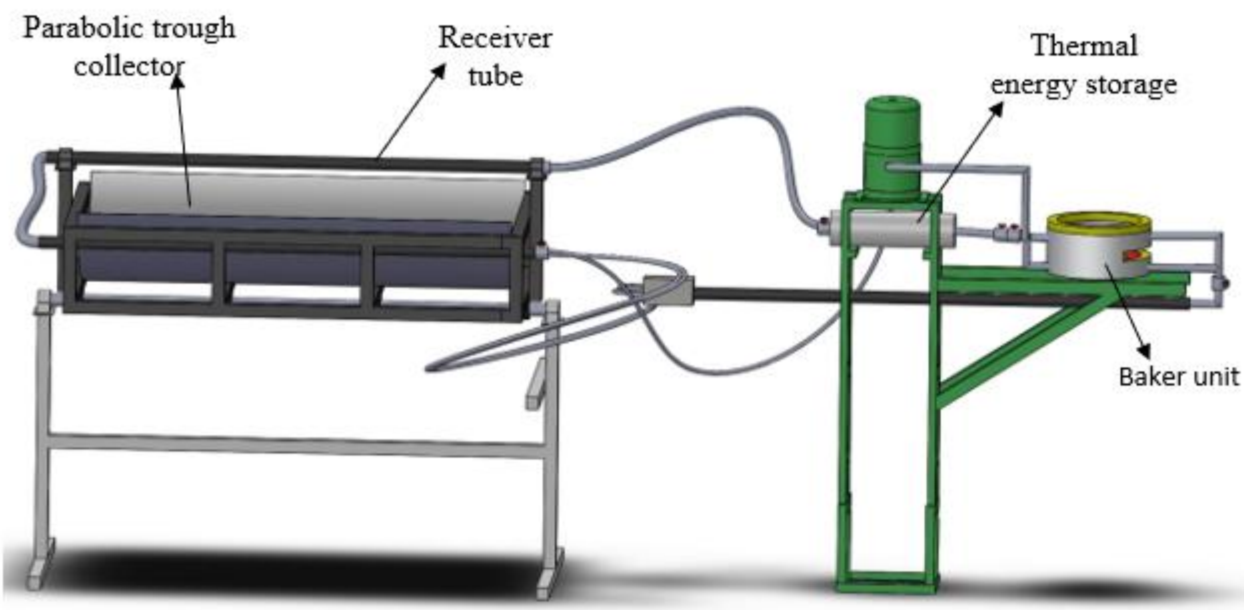

Figure 6. 1:-Conceptual schematic of a solar bread baker

6.3 Manufacturing of Parabolic Trough Collector

6.3.1 Parabolic Trough Solar Collector Supporter with Reflector

The parabolic trough concentrator supporter should be resisted different loads like wind load, stress loads, etc., so it should be a rigid body in design. This concentrator contains parabolas connected with a receiver tube. To support the parabolic concentrator the galvanized flat steel was used as material to form a parabolic shape in the prototype. In this work, flat steel is bent into a parabola with a length of 2 m and aperture width of 0.89 m. One steel sheet metal of dimension (2m× 1m) is used to form the parabolic shape in the prototype with the use of all dimensions calculated by parabolic trough collector. The steel sheet is used to provide mechanical strength to the parabola. The angle iron frame of 25mmx25mmx3mm was made and secured on top of the trough by a flat that was welded on the frame. The frame minimized the twisting of the trough. The mirror is then attached over to the galvanized sheet metal. The mirror is used because they have high reflectivity of 1.0.

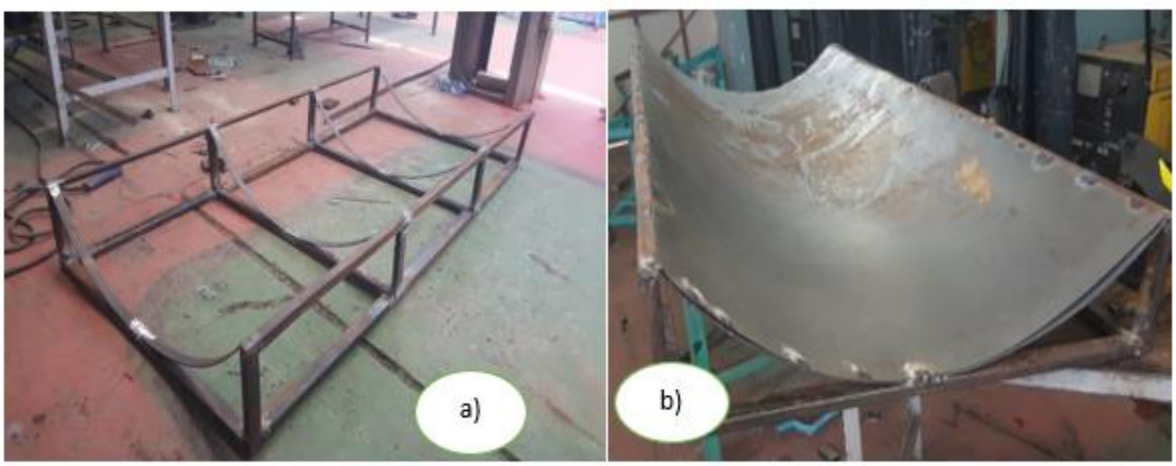

Figure 6. 2: - a) Supporter of the collector b) Supporter with a reflector of the collector

Enhanced of parabolic trough collector receiver: - during the manufacturing enhancement of receiver tube, radiation shield which has 2 mm thickness and length has 10mm is shown in figure 6.3 and its outer surface has 41 mm distance from the tube center and it covers one-third of the total periphery (120^o) as shown in figure 6.4.

Figure 6. 3: - Receiver internal fin

Figure 6. 4: - Parabolic trough collector receiver shield

6.4 The Latent Heat Storage Unit

The LHS unit's shell was manufactured of 355 mm X 760 mm mild steel sheet metal that was formed into a 100 mm diameter cylindrical shape using a rolling machine, as shown in Fig.6.5 (b). Carbon steel tubes were used to make five HTF tubes with a length of 700 mm. The HTF tubes' two ends were welded together using a circular plate with a diameter of 100 mm. As shown in Fig.6.5(a), the HTF tubes were inserted into the shell, and the two ends were welded and closed with a circular plate of 100 mm diameter. A hole was drilled on the outer surface of the shell to fill it with PCM, and an HTF inlet and outlet channel were constructed. To prevent leakage, epoxy mixed with hardener is applied to any possible openings in the shell, as well as both sides of the tube inlet and outlet connections. The shell was filled with 10 kg D-mannitol to store the heat and covered with a 30 mm thick foam insulation.

Figure 6. 5: - Manufacturing process of LHS (a) tube of LHS (b) shell of LHS (c) integrated of shell and tube and (d) PCM in container

6.5 The Baking Unit

The baking unit consists of the closed baking unit having a cylindrical galvanized sheet metal baker unit made of galvanized sheet metal with a dimension of 400 mm diameter and 230 mm height. To facilitate two tanks upper and lower and at the middle Patra space. In the flow of HTF, two holes were drilled on the upper side and bottom side of the tank for the inlet of HTF and the outlet of HTF from the tank by another side upper and bottom hole. The inlet side was used to connect the outlet pipe of the latent storage tank with the baking unit whereas the outlet side was used as a return pipe connection. The baking plate was equipped with a cleaning surface. To reduce heat loss from the baking unit with insulating fiberglass material. Figure 6.6 shows the baking unit assembly with thermal storage than, baking unit, connecting pipe, and thermal storage is well insulated.

Figure 6. 6: - Manufacturing process of baker unit (a) baker unit with HTF tank (b) bread Patra (c) insulated baker unit

6.6 Assembling of Fabricated PTC Integrated with Phase Change Material

Connecting tubes which is used to connect the closed circuit of the solar thermal bread baking system such as parabolic trough solar collector, thermal storage, pump, cold HTF tank, and baker unit. Those tubes are selected as they are easy to connect, available, corrosion-resistant, and can resist high pressure and temperature. Figure 6.7 indicates the connecting tubes insulated with fiber-glass to reduce heat loss.

Figure 6. 7: - Assembly of a solar thermal bread baker

The photograph of the complete setup for the LHS unit with its components and thermocouple positions is depicted in Figure 6.8. The inlet and outlet HTF temperature from the LHS and central and top surface temperature of the D-mannitol were measured with three K-type thermocouples (T1, T2, and T3) fixed at the inlet, outlet, and center of the thermal storage tank.

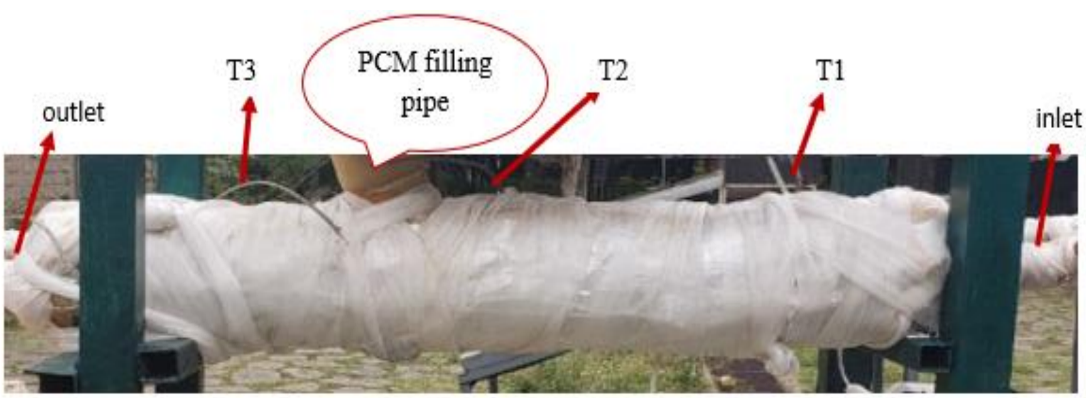

Figure 6. 8: - Setup of LHS unit and positions of thermocouples

6.7 Experimental Setup

For experimentally investigating the present solar thermal bread baking system, the setup was installed in the test field of ASTU, mechanical engineering department, Adama Ethiopia. The complete experimental setup of solar thermal bread baker consists of PTC, shell and tube LHS unit, and the baking unit which consists of the baking Patra and HTF tank and a closed-loop pipe network having HTF used as a connection for the whole system components. Figure 6.9 shows the photograph for the complete setup of the solar thermal baker. In the setup, the heat source for the baker is obtained from the PTC using terminal oil B as HTF which is circulated with the help of a drum pump connected between the collector and the baker unit.

The pump provides enough pressure to overcome the pressure drop in the circuit. To get a variable flow rate in the system the speed of the pump rotor is controlled using the speed controller of the pump. The measuring devices used in the experiment include a calibrated thermocouple thermometer based on the procedure described in APPENDIX D, nine K-type thermocouples fixed at different locations of the prototype to measure temperature at the collector, LHS, and backing plate surface. The photograph of the parabolic trough collector with solar baker is shown in Figure 6.9. It consists of a parabolic trough collector, thermal energy storage, a solar baker, and connecting pipes. The experiment is performed to investigate the thermal performance of PTC and phase change thermal storage units.

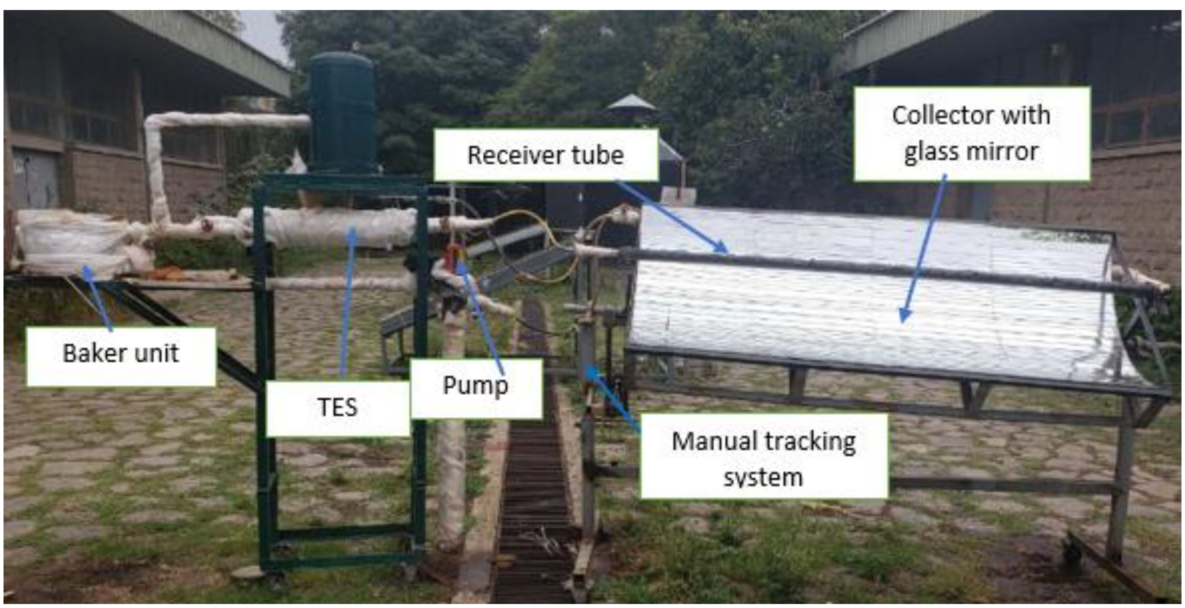

Figure 6. 9: - Experimental setup of the system

6.8 Experimental Measuring Instruments

Some instruments are used to measure the temperature of working fluid and the weight of PCM, bread gradient, and bread.

Thermocouples: The temperature during the experiments was measured by the thermocouples which are located along the length of the collector. K-type thermocouples are used in the setup. A data reader is used to read the temperature sensed by thermocouples and the values are recorded manually. The thermocouples can read values between -200 to 1350 °C.

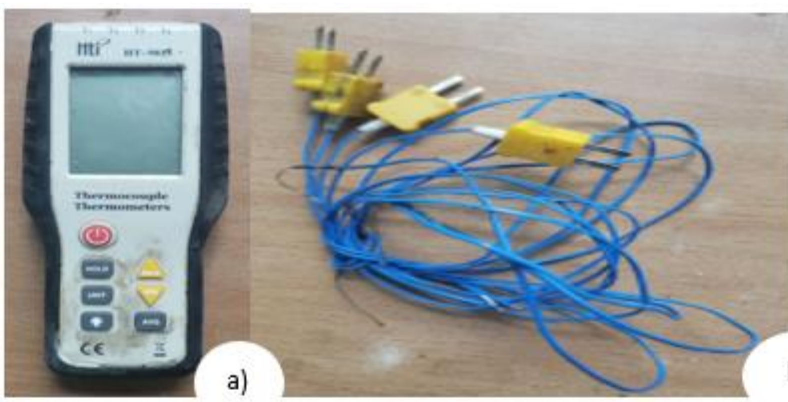

Figure 6. 10: - Temperature measuring devices a) Thermometer b) Thermocouple wires

Digital Weight Balance: Digital weight balance is used to measure the weight of the PCM, gradient, and bread.

Figure 6. 11: - Digital balance

CHAPTER SEVEN

RESULT AND DISCUSSION

7.1 Introduction

This chapter presents the results obtained from the experimental analysis of the PTC, LHS unit, and baking unit under different conditions. The first section presents the results of experimental investigations made on each component of the solar bread baker. The next section presents the numerical investigation of the LHS unit using finite element-based COMSOL Multiphysics software. The results of no-load, baking, and performance tests performed on the baking unit are also presented and discussed. Finally, the economic analysis of the solar bread baker is presented.

7.2 Solar Radiation

The amount of solar irradiance received affects the performance of the system, since the receiver temperature, HTF fluid outlet temperature, and others are directly related to solar irradiance. Thus, as solar radiation increases these temperature results also increase proportionally. The solar radiance increases to a maximum value at noontime and starts to decline in the afternoon.

From Figure 7.1 at 9:00 am, the solar intensity is 377.2 W/m^2, and as time passes, the intensity starts to rise until reaching the peak with a value of 845.9 W/m^2 around 12:00 pm. After that time, the intensity decreases to approximately 208.8 W/m^2 at 16:00 pm.

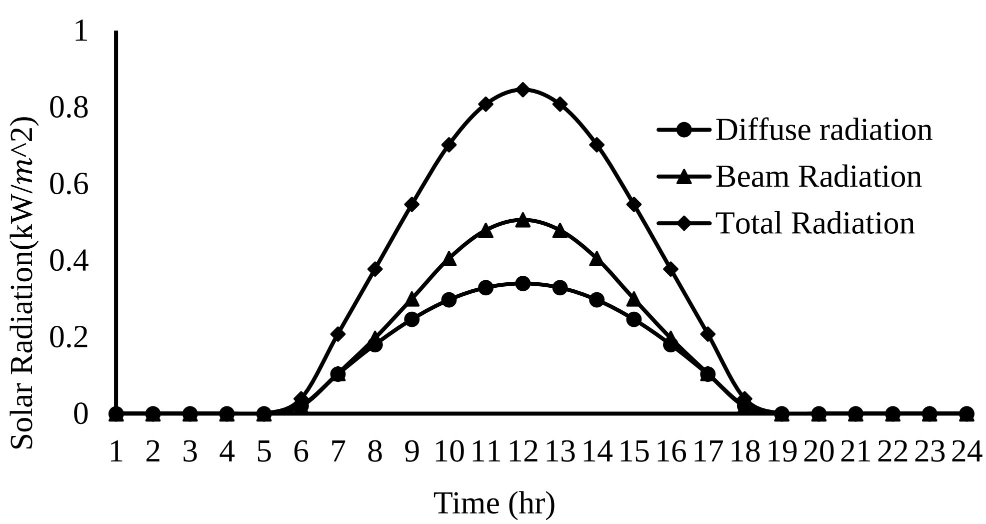

Figure 7. 1: Estimated hourly variation of solar radiation of Adama in June.

7.3 Ambient Temperature Profile

The ambient temperature of Adama measured during the test period were presented in the figure 7.2. The ambient temperature is the maximum value at noontime and starts to decline in the afternoon. Even if data measurement was taken 9:00 am to 17:00 pm time, but useful heat was extracted from 9:00 am to 17:00 pm. The variation of ambient temperature with time of the day was given in figure 7.2. The maximum ambient temperature measured between 11:45 am to 13:00 pm is found to be 306 K. The minimum temperature measured on the same day was 298.25 K, at 9:00.

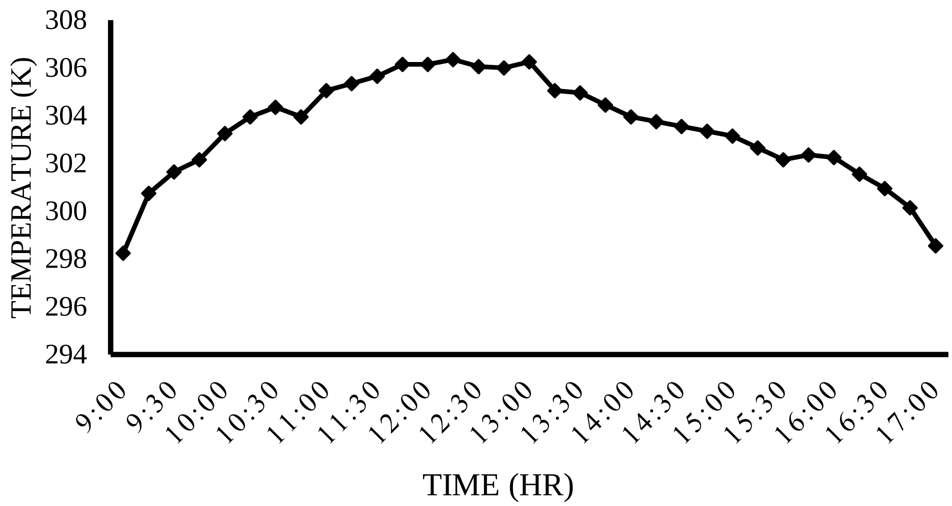

Figure 7. 2: - Average ambient temperature during experiment days

7.4 Experimental Results of the PTC without Receiver Fin and Shield

To examine the performance of PTC experimental tests were performed on June12^{th}, 13^{th}, 14^{th}, 16^{th}, 2021. The closed-loop test was started after performing the experimental procedure. After adjusting the experimental setup, several parameters were measured using thermocouples mounted at various points throughout the system. The next subsection presents and discusses the various results obtained.

7.4.1 Parabolic Trough Collector Outlet Temperature of Heat Transfer Fluid

During the experimental test, the variation in ambient temperature, collector output temperature, collector inlet temperature, and solar insolation with time is depicted in figure 7.3. At the start of the experiment, inlet and outlet temperatures rise at a high rate until 12:45 pm., when solar insolation also rises. After 12:45 pm., both inlet and outlet temperatures, as well as solar insolation, start to fall until the experiment is completed. The temperature of HTF released from the collector outlet is proportional to the amount of solar radiation reflected in the receiver tube. This is due to the heat capacity of HTF and the decrease in ambient air temperature, which increases convective heat loss for the receiver tube.

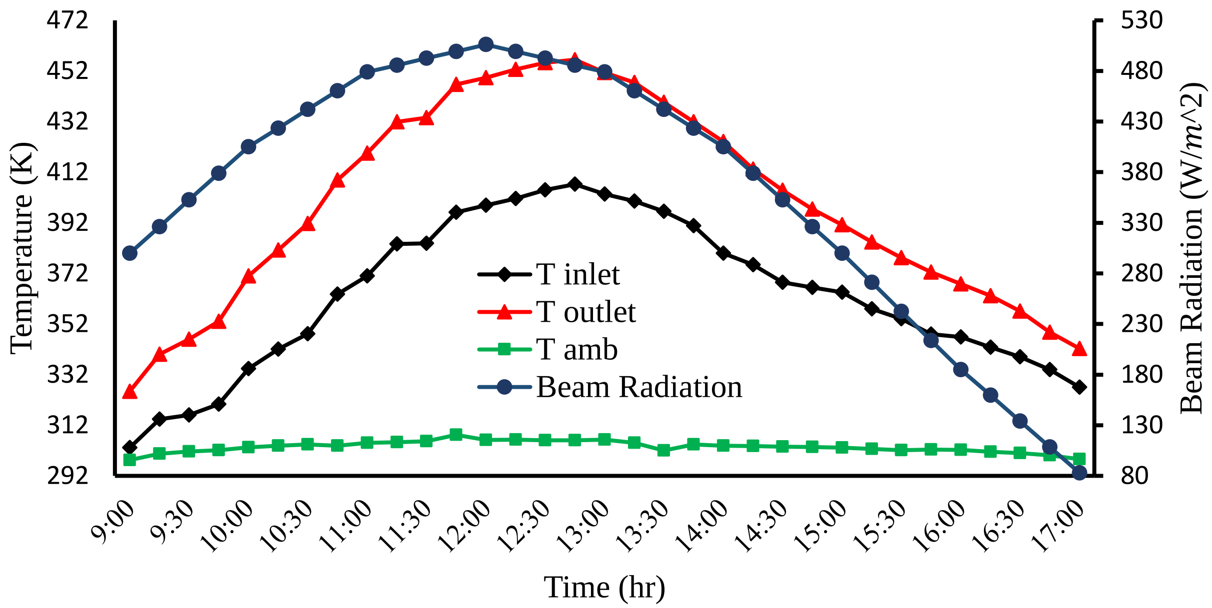

Figure 7. 3: Variation of inlet and outlet temperatures of the HTF with time

7.4.2 Useful Heat Energy of Parabolic Trough Collector

The useful heat gain is calculated from the measurements of the inlet and outlet HTF temperatures and mass flow rate as demonstrated in equation (5.60). Figures 7.4 show the useful heat gain for receiver without internal fin and shield. The experiments were carried out from 9:00 am to 16:00 pm for several days. However, the useful heat gains first increase, reach a peak value around noon, and then decrease. This is due to the fact that the useful heat gain is strongly influenced by the incident beam radiation and change of temperature.

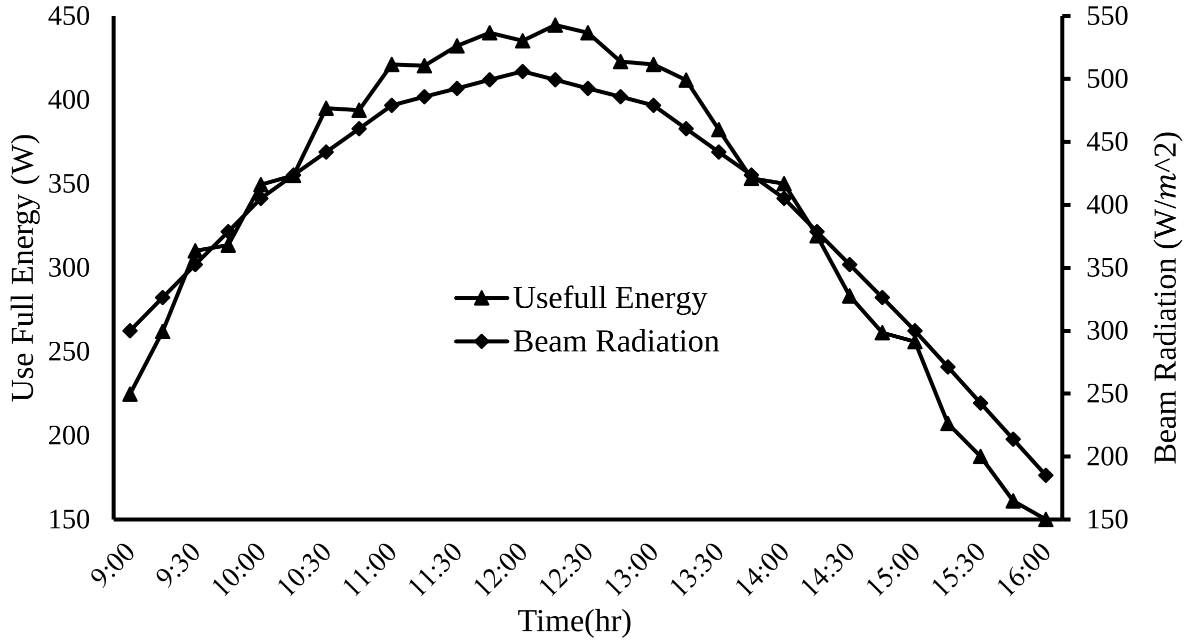

Figure 7. 4: - Variation of collected useful energy with respect to time

7.4.3 Thermal Efficiency of the Parabolic Trough Collector System

The variation in PTC thermal efficiency under the given input parameters of mass flow rate, ambient air temperature, and inlet and outlet HTF temperature is shown in Figure 7.5. The solar insolation received on the receiver tube follows a parabolic path, peaking in the mid of the day and gradually decreasing as time passed. The solar insolation was observed to be increasing throughout the day, peaking at 506.8 W. m^2 around 12:45 pm. The ambient temperature starts to rise at 9:00 am. and peaks at 12:45 pm. Similarly, the inlet HTF temperature increased from 298.57 K in the morning to 408.25 K at 12:45 pm. Because of the rising solar insolation and ambient temperature, the outlet HTF temperatures gradually increased from 9:00 am to 12:45 pm. Because of the lower solar insolation and ambient temperature after 12:45 pm., the outlet HTF temperature decreased.

Similarly, the peak thermal efficiency was 51.9 % at 13:15 p.m., and it dropped after 13:30 p.m. This was expected, as the change in HTF, the temperature was lowered as solar insolation decreased. Because of the decreasing solar insolation after 15:45 pm, the change in HTF temperature was small, decreasing the thermal efficiency.

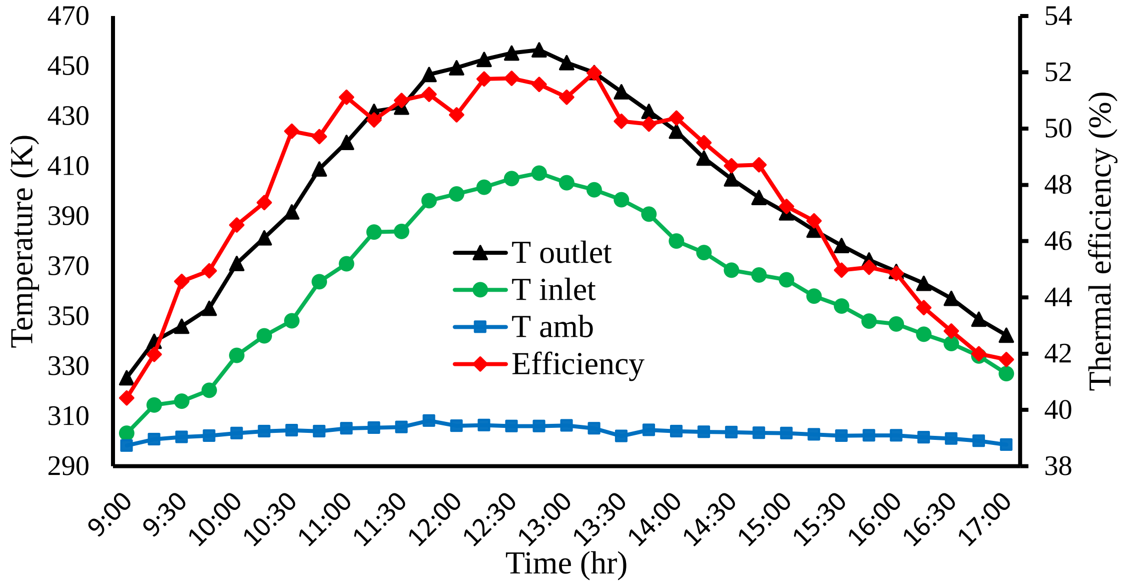

Figure 7. 5: - Variation of collector thermal efficiency with time

7.4.4 Exergy Efficiency of Parabolic Trough Collector

The amount of heat converted into useful work, which causes the rise in working fluid flow exergy, is measured by exergy efficiency, which is a true measure of solar collector performance. With a reference temperature of 303.15K and a sky temperature of 4500K, the Exergy efficiency of PTC was evaluated using Eqn.5.75. The change in exergy efficiency throughout time is depicted in Figure 7.6. The maximum exergy efficiency of 28.5 % was achieved with PTC at peak hours (12:00pm). Almost similar results were reported by Bellos and Tzivanidis (2017).

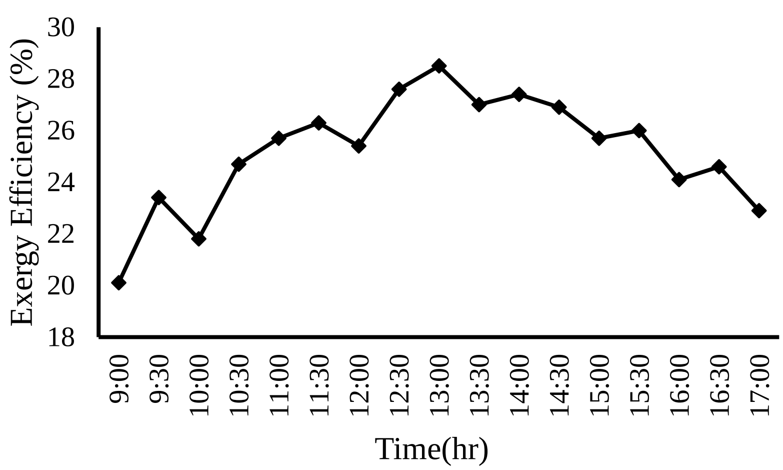

Figure 7. 6:-Exergy efficiency of PTC

7.5 Experimental Result of the Enhanced PTC

To examine the effect parabolic trough collector with inserting longitudinal fins in the down half of the receiver tube and receiver shield in the closed-loop experiment was performed with a PTC having five fins inside the receiver tube and shield one-third upper part of the receiver tube. After adjusting the experimental setup, several parameters were measured using thermocouples fixed at various points throughout the system. The following graphical results were obtained using the estimated value of hourly solar radiation, the calculated value of mass flow rate, and the measured ambient air temperature as input parameters.

7.5.1 Enhanced PTC Outlet Temperature of HTF

During the experiment period, Figure 7.7 describes the variation in ambient temperature, outlet temperature, inlet temperature, and solar insolation with time. The inlet and outlet temperatures begin to rise at a rapid rate from the start of the experiment and continue to do so until 12:45 pm. Then, after 12:45 pm, both inlet and outlet temperature decrease due to decrease solar intensity. The maximum outlet temperature of 465 K and 469 K for a receiver with fin and fin with shield, respectively.

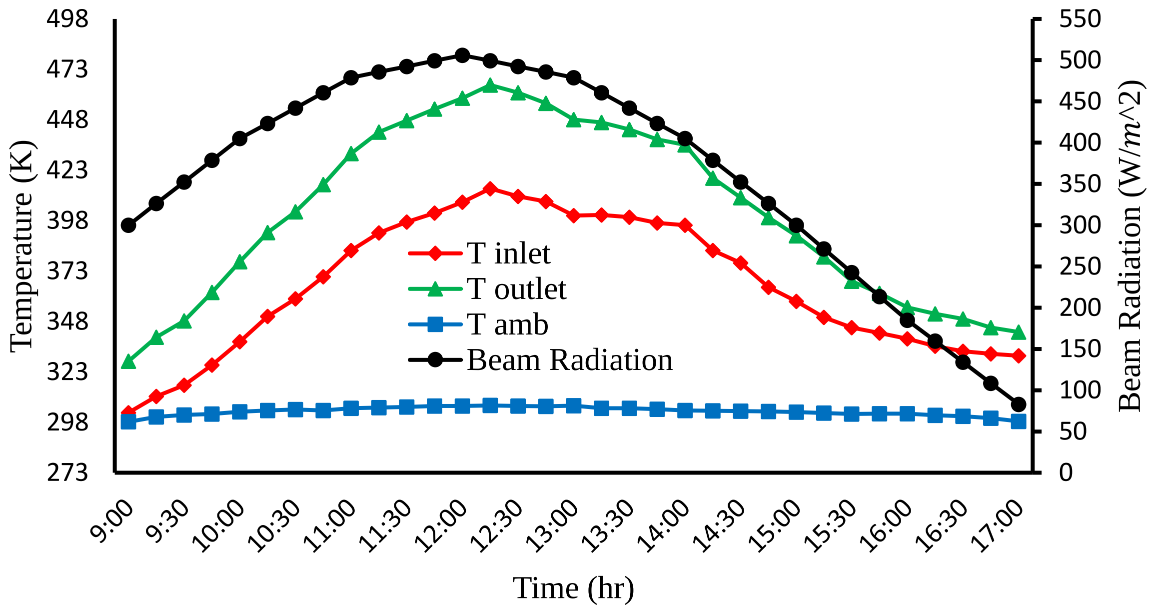

Figure 7. 7: - Variation of inlet and outlet temperatures of the HTF with time and receiver with fin

The test started at 9:00 am in the morning and it ended at 17:00 pm in the afternoon. The maximum temperature measured was 465.25 K at 12:15 pm and the minimum temperature measured is 327.28 K at 17:00 pm.

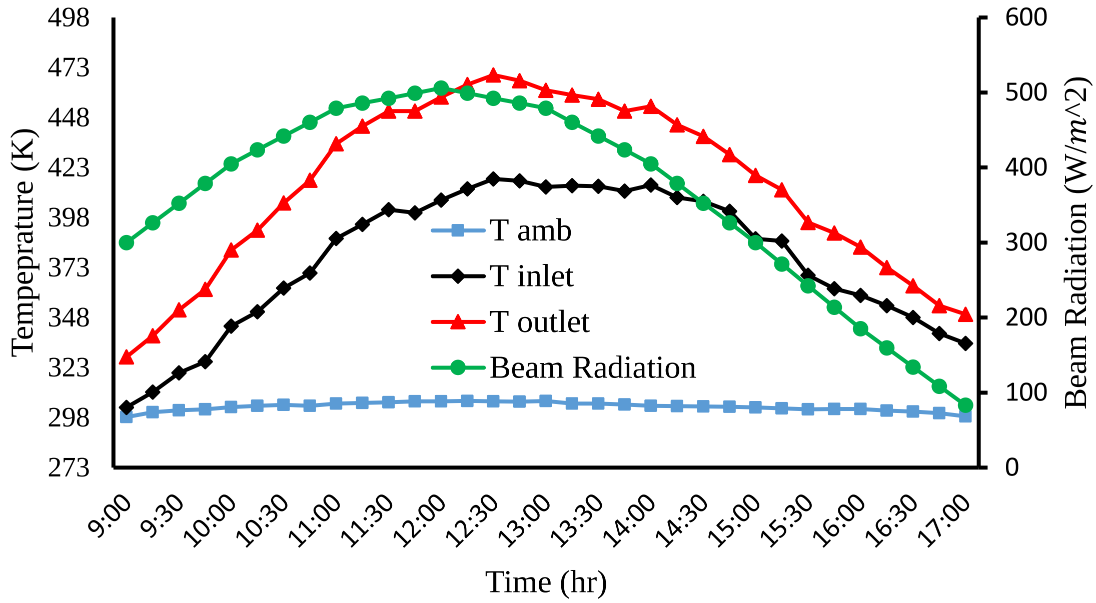

Figure 7. 8: - Variation of inlet and outlet temperatures of the HTF with time and with receiver fin with shield

The test started at 9:00 am in the morning and it ended at 16:00 pm in the afternoon. The maximum temperature measured was 469.85 K at 12:30 pm and the minimum temperature measured is 349.28 K at 17:00 pm.

7.5.2 Useful Heat Gain of Enhanced PTC

The performance of the solar collector is measured with its effectiveness to increase the temperature of inlet fluid flowing at a specific flow rate desired outlet temperature with a given aperture area and solar insolation. Figures 7.9 show the useful heat gain for an internal fin receiver and with the internal fin and sheid of the receiver, respectively. The experiments were carried out from 9:00 am to 16:00 pm for several days.

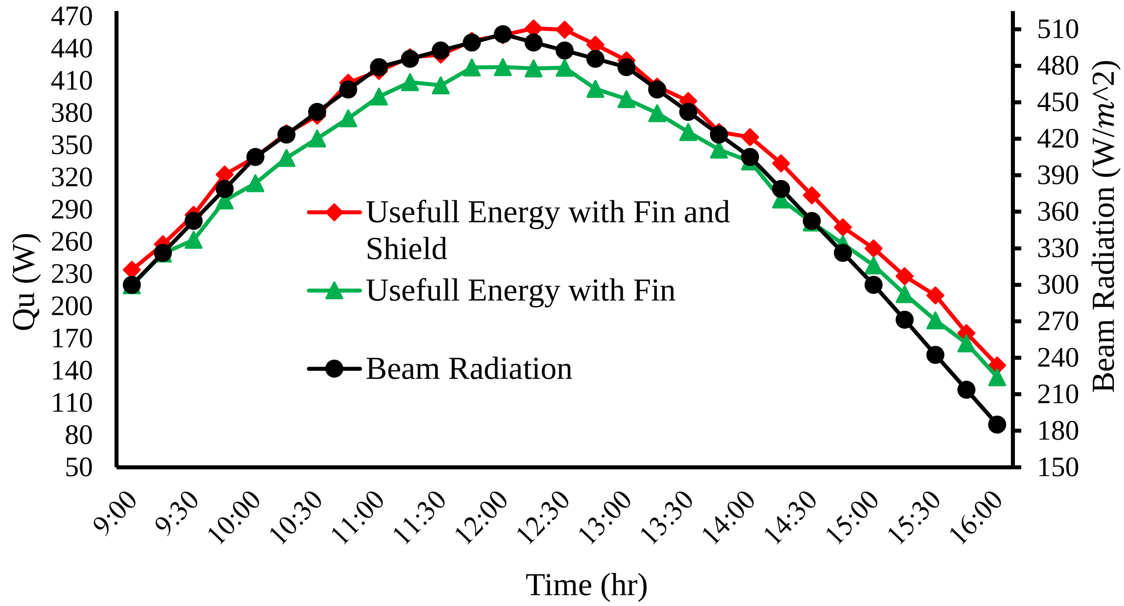

Figure 7. 9: - Variation of collected useful energy with respect to time

7.5.3 Thermal Efficiency of the Enhanced PTC

During the experiment test, Figure (7.10) and (7.11) shows that the collector efficiency of a receiver with internal fins and receiver with internal fin and sheild of is maximum thermal efficiency is 53.6 and 55.2%, respectively. Due to the use of an internal fin receiver and sheild one-thirds of the top receiver, this change is related to improved heat transfer of the collector receiver tube and reduce heat losses (convection and radiation).

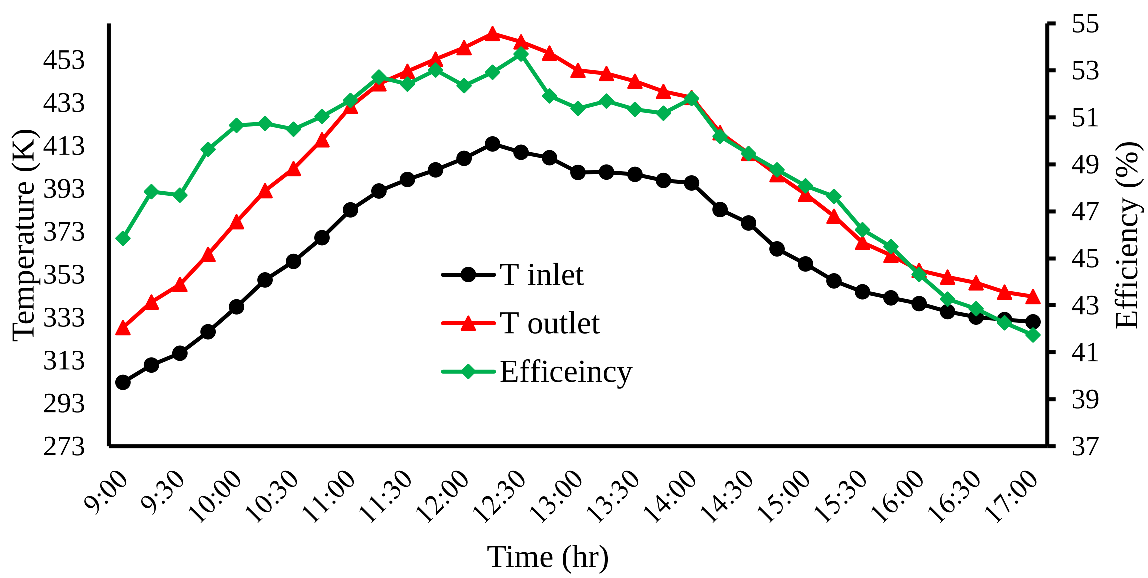

Figure 7. 10: - Variation of collector thermal efficiency with time and receiver with fin

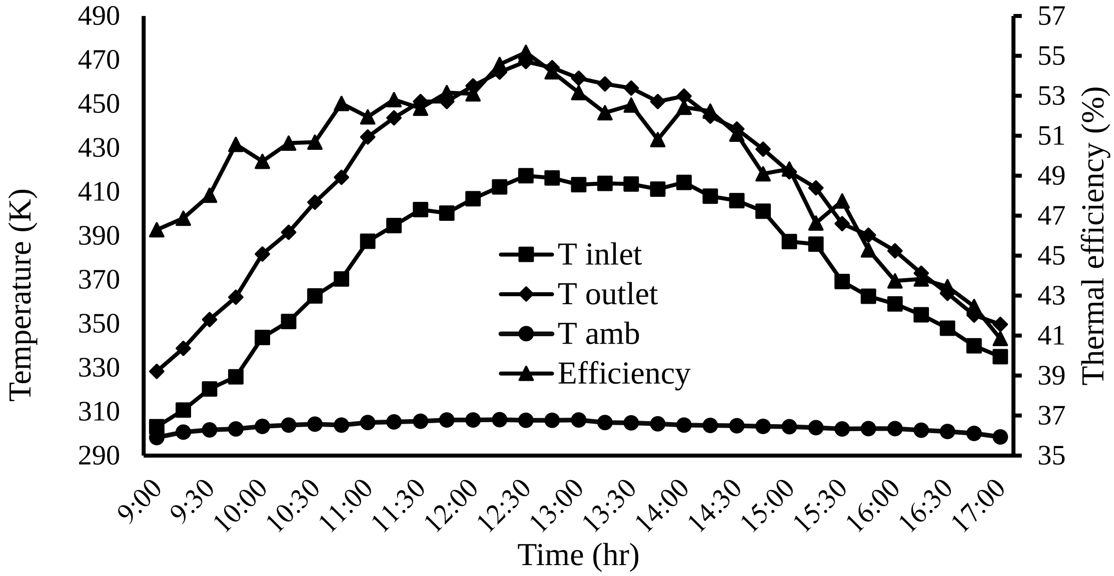

Figure 7. 11: - Variation of collector thermal efficiency with time and with receiver fin with shield

7.5.4 Exergy Efficiency of Enhanced PTC

Exergy efficiency is an accurate measure of a solar collector performance, indicating how much heat is transferred into useful work, increasing by working fluid flow exergy. Eqn.5.76 was used to calculate the exergy efficiency of PTC with a reference temperature of 303.15K and a sky temperature of 4500K. The fluctuation of exergy efficiency over time is depicted in Figure 7.12.

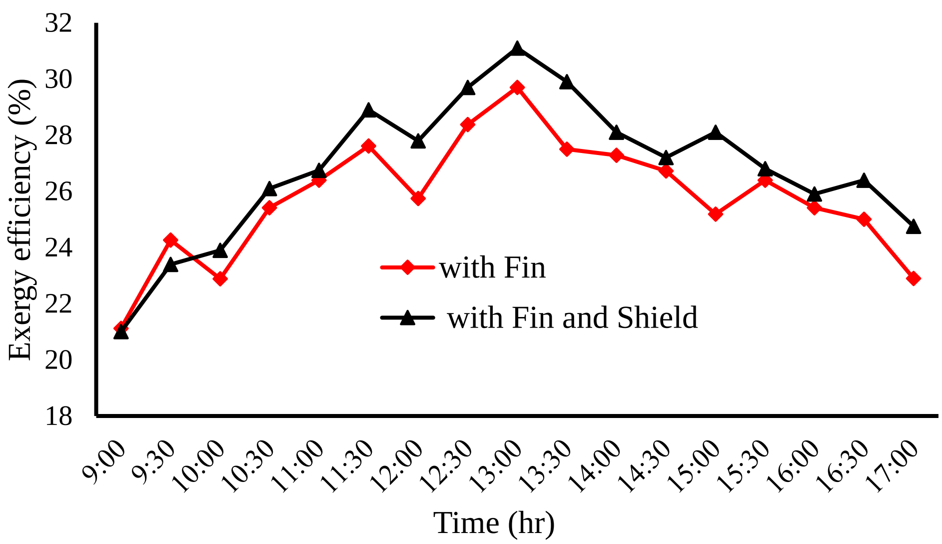

Figure 7. 12: - Exergy efficiency of modified PTC

7.6 Comparison of Various Performance Parameters for PTC with and Without Receiver Fin and Shield

In this subsection, the effect of adding a parabolic trough collector with longitudinal fins in the down half of the receiver tube and, receiver shield in a closed-loop experiment was investigated and addressed using a PTC with five fins inside the receiver and shield one-thirds upper part of the receiver tube. Different measurable performance parameters were used to make the comparison in the closed-loop experiment.

7.6.1 Comparison of Outlet Temperature of HTF from PTC with and without Receiver Fin and Shield

The purpose of adding an internal receiver fin and sheild the upper one-thirds of the receiver was to expand the PTC operating temperature range by reduces of receiver convection and radiation loss. The effects of adding a receiver fin and sheid on the temperature of the collector output are shown in figure 7.13. A maximum temperature differential of 13 K was reported between a receiver with fins and sheid and without. However, the thermos- physical properties of the HTF, and absorber losses play an important role in the performance of solar to thermal energy conversion of the receiver tube.

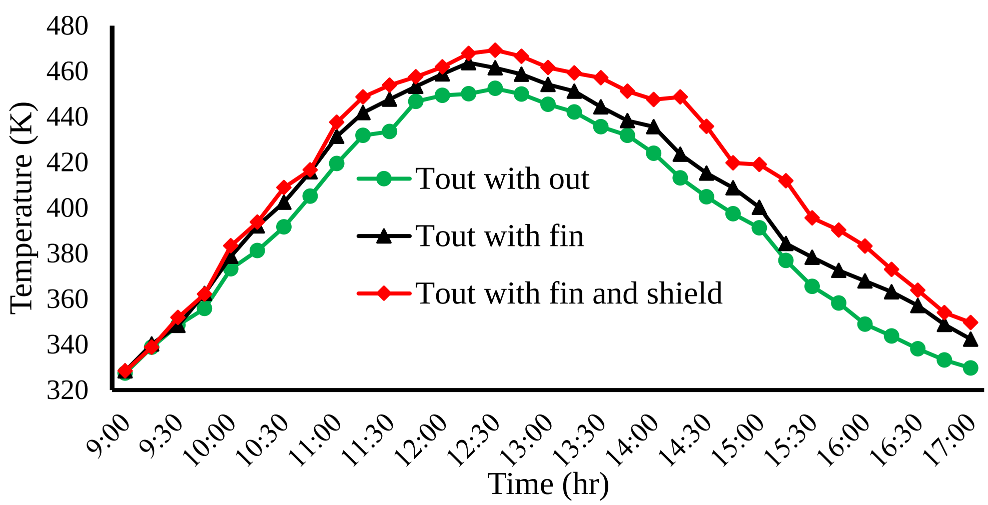

Figure 7. 13: - Effect of Internal Receiver Fin and the Receiver Shield on outlet temperature of HTF

7.6.2 Comparison of Efficiency of PTC with and Without Receiver Fin and Shield

The effect of adding an internal receiver fin and shield one-thirds of the upper receiver on PTC performance is shown in figure 7.14. As it can be seen the collector receiver with fin and shield had better performance than without. In the late morning and sunset, the efficiency of PTC without receiver fin and sheild are better as the difference in inlet and outlet temperature are relatively higher. The thermal efficiencies for those cases increased from the morning and reached a peak value at the mid-day followed by a continuous decrease due to a decrease in solar insolation. The peak solar thermal efficiencies of 51.9%, 53.6%, and 55.2% were achieved with and without the internal receiver fin and the receiver shield respectively.

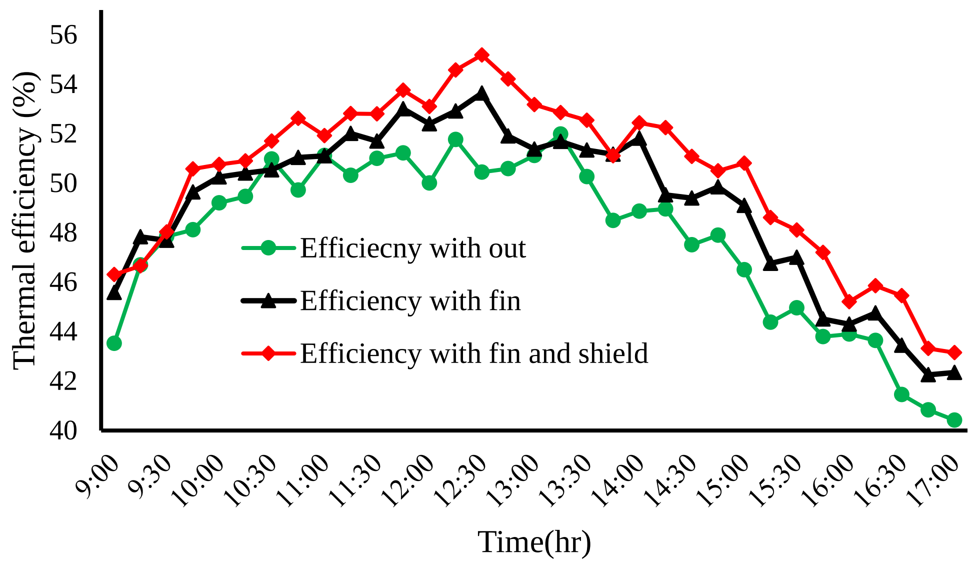

Figure 7. 14: - Effect of internal receiver fin and the receiver shield on thermal efficiency

Efficiency results from this experimental test are almost closer to those of other researches on parabolic trough collectors, for which peak thermal efficiency values of 51.5% (Wang *et al*., 2020), 52.9% (Yassen, 2012), and approximately 50.7% (Ktistis *et al*., 2021) have reported.

7.7 Experimental Result of Thermal Energy Storage System

Results of the experimental investigation of the thermal performance of the LHS system have been presented and discussed in this section. The results were obtained from a closed-loop experiment with no-load on the baker. The temperature of the HTF at the inlet and outlet of the LHS and the temperature of the D-mannitol at three different locations (inlet, at the center, and outlet) were measured, and the results are presented as follows.

7.7.1 Temperature Variation of D-mannitol During Charging and Discharging Process

The outlet temperature reading obtained from the parabolic trough collector was used for the thermal energy storage system. The temperature at three different locations of the storage was measured by K-type thermocouples. The temperature variation at the LHS inlet/outlet and the center of PCM is measured and reported. The input temperature of the LHS increases with time until solar noon, then begins to decline as the solar radiation intensity decreases, as seen in Figure 7.15. Similarly, the LHS outlet temperature rises slowly over time until the PCM melts. After the HTF temperature exceeds 440.15K, D-mannitol begins to melt. The PCM entirely melts after 2 hours once the HTF temperature hits 440.15K, as shown in the graph. As can be seen, the temperature of the input HTF reaches 440.15K between 11:30am and 13:30pm, and D-mannitol entirely melts when the temperature of the PCM at the center and outlet of the shell equalizes between 11:30 and 12:15. Since it holds latent heat until 13:00pm, the temperature of D-mannitol becomes constant. Beyond that, any increase in the inlet temperature of HTF after the PCM melts results in just sensible heat becoming stored, which is available until the inlet temperature decreases below the PCM melting point. Around 16:30 pm, the PCM temperature decreases to its melting point when the inflow temperature of HTF drops below 440.15K. Because it takes time to release the stored latent heat, the temperature of the PCM becomes practically constant after that. When the LHS inlet and outlet temperatures of HTF are compared after 16:30, the inlet temperature steadily drops. However, the HTF temperature at the LHS outlet was higher than at the input. This is because the output temperature absorbs heat from the PCM and maintains the same temperature as the PCM.

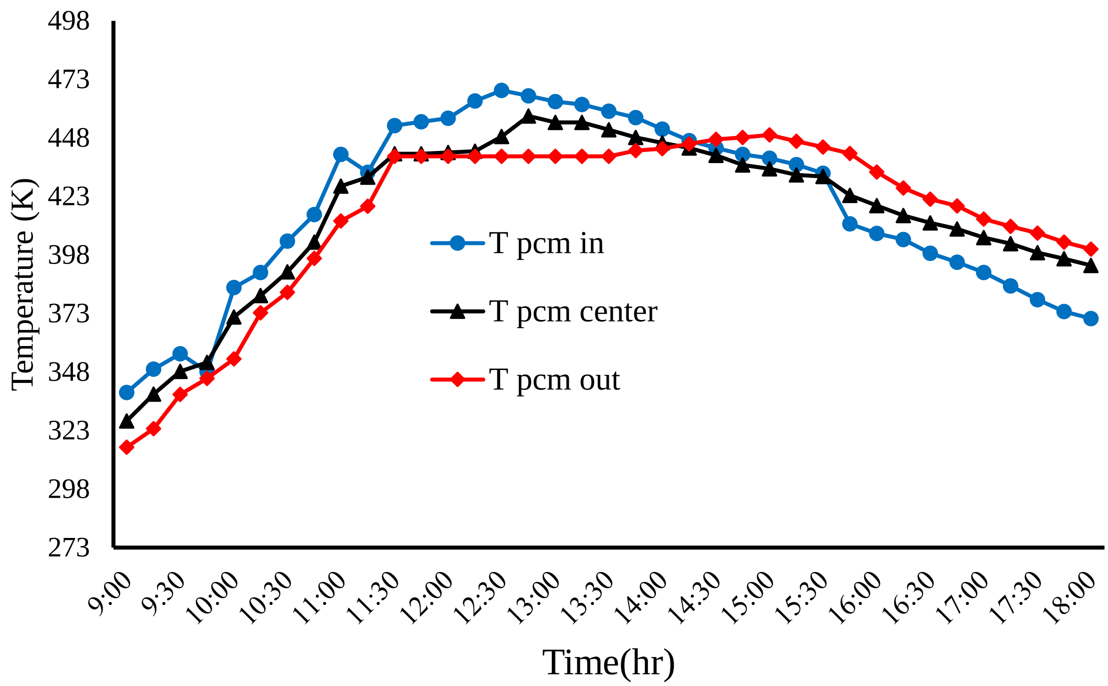

Figure 7.15: - Temperature variation of D-mannitol with time during the charging/discharging process

7.7.2 Energy Stored/Released During Charging/Discharging Processes

When the PCM is in the solid-state during charging, heat gets stored in the form of sensible heat only. Once the PCM reaches near the phase change temperature (440.15K), heat gets stored in the form of latent heat. Similarly, after melting of the PCM, further increment in temperature of PCM results heat to be stored in the form of sensible heat again. When the D-mannitol reaches its melting point during the charging process after the fluid temperature reaches 440.15k the amount of sensible, latent, and total energy stored in the PCM were 1.78MJ, 3.15MJ, and 4.93MJ respectively. During discharging process, on the other hand, the PCM is initially in liquid state 457.25K then the heat gets released inform of sensible heat until it reaches its melting point 440.15K. then the PCM starts to release its latent heat as the phase change occurs. The amount of sensible, latent, and total energy released during the discharging process was 1.41MJ, 2.85MJ, and 4.26MJ respectively.

7.8 Experiment of Bread baking Tests

Different types of tests were run on the baker and to see how the performed under various conditions.

(i) Experiment without bread baking of the baker unit. The purpose of this set of tests was to determine the effectiveness of the baker unit as well as the thermal capability of the integrated PCM storage unit for baking.

(ii) Experiment with bread baking. This set of experiments was carried out to confirm the results of the first experiment, which used a load with a high heat capacity and length of time for bread baking.

7.8.1 Experiment without Bread Baking

A no-load experiment was used to determine the performance of the HTF, charging, and discharging processes, as well as a general examination of the system when it was not doing bread baking. The HTF was only heated with no baking load added to the system. The current study used the whole setup of the experiment described in section 5.2 to conduct no-load tests. From 9:00am to 17:00pm, Figure 7.16 depicts the variation in HTF collector outlet temperature, HTF outlet from LHS ($T_{PCM-out}$), ambient air temperature (T_{amb}), solar beam radiation (I_b), and temperature at the surface of the baking plate (T_{plate}) as a function of time. The temperature of the collector output of the HTF in this test rises to 469.25K as time passes until solar noon. It then lowers as the afternoon solar intensity decreases. During the morning and afternoon, the HTF temperature from the LHS system and the temperature of the baking plate surface have the same trend.

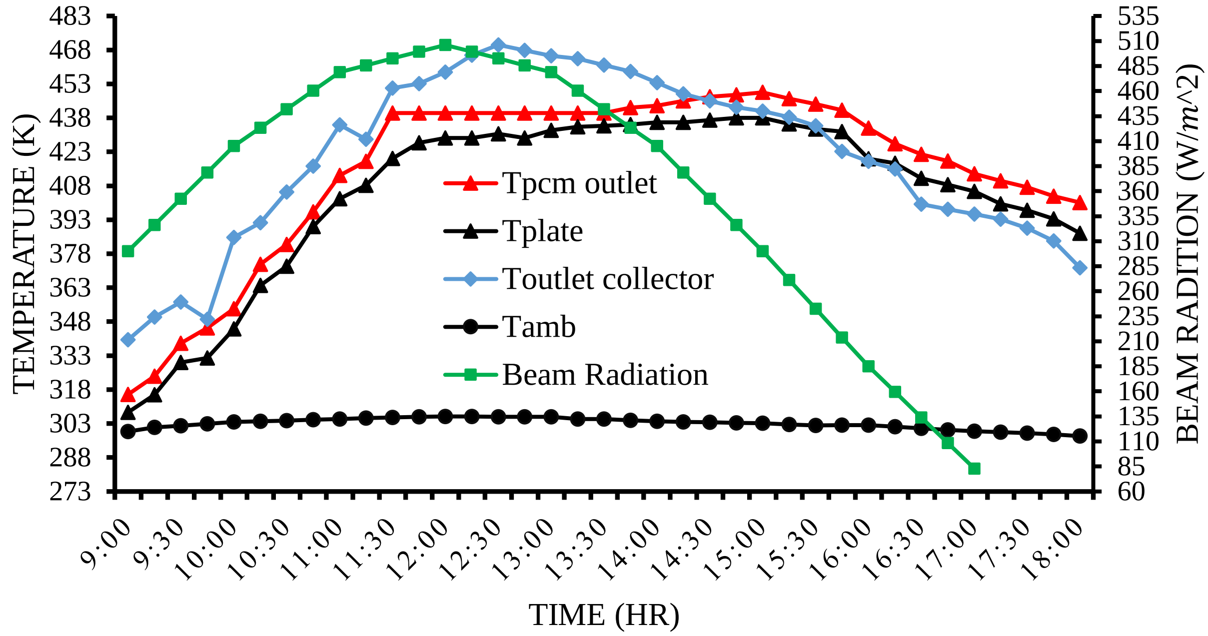

Figure 7. 16: - Experimental without baking parameters with time

7.8.2 Experiment with Bread Baking

Constructed on the results of the baking test, a final set of experiments has been conducted on the bread baker with actual baking loads on 18^{th}, 20^{th}, June 2021. The bread dough was 0.87 kg from this dough composition 58% of Wheat flour,40% of water, 0.8% of salt, and 0.6% of yeast this gradient list and the amount taken from small bread bakeries.

Table 7.1: - Actual gradient value for dough

Gradient	weight
Wheat flour	051 kg
water	0.34 kg
salt	0.007 kg
yeast	0.005 kg

This test was started at 12:00 pm with checked every 5min. The bread in the baker unit was taken out at 12:55pm and it was found that the bread was well baked. It takes more time than expected as the day was with fluctuating sunlight and partially cloudy. Maintaining the bread in the baker unit it was found that the baker was able to bake it even if it takes more time. Different photographs taken during the baking test are shown APPENDIX E.

The baking plate temperature attained was 433.15K and the corresponding baking time took was one hour which was comparable with that presented by El-Ghetany *et al.*, (2019) and Hailessilase Asfafaw, *et al.*, (2015). Therefore, the result shows that the possibility of baking plate temperature of 393.15-433.15K using the aluminum plate as baking plate.

Figure 7. 17: - Bread baking process (a) before baking (b)after baking

7.8.3 Temperature Profile of Bread

A thermocouple was inserted slightly on the dough at the center to record the temperature variation during the baking process as in Figure 7.18. The bread crumb/core temperature was measured at the center with the interval of baking time during the baking process and presented in Figure 7.17.

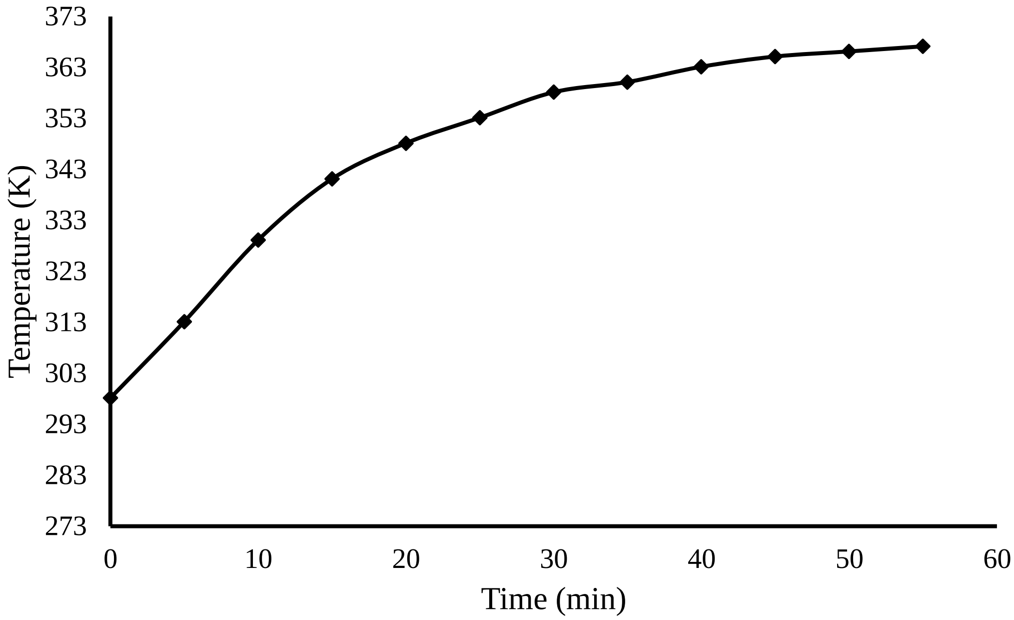

Figure 7. 18: - Temperature profile of bread core

The baking process ends after 55 minutes of baking time and as the crump temperature reached 366.15K. The bread surface temperature increases linearly during the first 30 minutes and the slow rise of temperature till the end of baking and the maximum crump temperature is limited to 373.15K. Thus, increasing from this maximum value could affect the physical attributes of bread.

7.8.4 Bread Weight Loss

Weight loss is the result of the evaporation of water from the dough during baking and depends on the baking temperature and baking time. The weight loss during the baking process was measured from the start to the end of baking. So that final baked bread sample weight was measured to be 0.72 kg with a loss of 0.12 kg from the initial weight of the dough sample (0.84kg). There was a weight loss of 14.28% which means the percentage of the initial weight of the dough removed during baking is in close agreement with the value suggested by (Nicolas *et al*., 2017).

7.9 Performance Evaluation of the System

The performance of a solar system depends on the efficiency of a solar concentrator, the efficiency of thermal storage and the efficiency of the baking plate as well. So that overall performance of the system is the product of these efficiencies. A baking experiment was performed to know the energy distribution and energy loss at various sections of the baking system such as energy absorbed by the receiver, amount of energy supplied to the storage, amount of energy stored and energy utilized for baking. As energy transfers from one medium to another energy loss should occur. It needs to calculate the amount of energy lost to optimize and improve the system performance.

7.10 Economic Analysis of Solar Thermal Bread Baker

The solar energy project is generally characterized by high initial costs and low operating costs. Thus, the basic economic problem is comparing an initial known investment with estimated future operating costs. Investments in buying solar energy equipment are important factors in solar process economics. Costs of installing this equipment must also be considered as these can match or exceed the purchase price. Also, to be included the costs of structures to support collectors and other alterations made necessary by the solar equipment. The total cost of solar thermal bread baker is the sum of the costs of its main components such as parabolic solar collector, Thermal energy storage, and baker unit.

The costs associated with these components include material, construction, labor and transport costs. The economic analysis of the CPCS with phase change material, therefore, requires the knowledge of these specific costs.

7.10.1 Net Present Value (NPV)

In finance, the net present value (NPV) or net present worth (NPW) of a time series of cash flows for both incoming and outgoing are defined as the sum of the present values (PVs) of the individual cash flows of the same entity. A positive NPV indicates that the benefits are higher than the costs that accumulate over the project life. The process of relating future amount to the present value is known as discounting and is expressed by the following equation (Kalogirou., 2009):

$$P = \frac{A}{(1+i)^n} \qquad \text{7.1}$$

Where, P= present sum of money, A= annual worth (value), n= number of years and, r= rate of interest Series present worth is given by (Kalogirou., 2009):

$$P = A\left[\frac{((1+r)^n-1)}{r(1+r)^n}\right] \qquad \text{7.2}$$

7.10.2 Benefit-Cost Ratio

The benefit-cost ratio (BCR) is another tool for assessing the profitability of a project. If the the ratio is greater than unity (i.e., B/C > 1.0) the project is profitable.

7.10.3 Simple Payback Period

The payback period is defined as the time needed for the fuel cost savings to equal the total initial investment of a project. The payback period of an investment taking into account the time value of money is given by the expression (Duffie and Beckman., 2013):

$$SSP = \frac{I_C}{A_S} \qquad 7.3$$

Where SPP= simple payback period, I_C = Initial cost and A_s= Annual saving (benefits)

7.10.4 Maintenance and Replacement Cost

The repair and maintenance costs are difficult to obtain, they are mostly dependent upon the manufacturers standard and quality of material used for construction of the total system. The average life of the storage tank is expected to vary between 9-12 years.

7.10.5 Total Cost of the Present Solar Thermal Bread Baker

The total initial investment cost of the present solar thermal bread baker includes the cost of the collector, storage system, baking units, and all other supporting and connecting units of the system. APPENDIX A summarizes the details of all the costs associated with the present solar thermal bread baker.

7.10.6 Economics Benefit of Solar Bread Baker Comparison with other Fuels

The other sources used for bread baking are firewood, electricity, petroleum, and charcoal. Firewood and charcoal are traditional methods whereas the others are modern baking systems. Now today in Ethiopia the biomass degradation is on the challenges of human life activity, so due to this case the costs of these fuels become increasing similarly the costs of electricity and petroleum becomes increasing. The following table shows the current price of different sources.

Table 7. 2: Current price of different fuel from Adama city market

Source type	Current cost
Wood price (Birr/kg)	6.00

Charcoal (Birr/kg)	12.0
Kerosene (Birr/lit)	25.4
Diesel (Birr/lit)	27.99
Electricity (Birr/KWh)	0.349

The solar thermal-based PCM integrated bread baking system was designed to target household bread (*Difo Dabo*) bakeries. In most parts of the country, *Difo Dabo* is baked using biomass (firewood) as a fuel source. The feasibility of bread baking using solar thermal systems and traditional biomass baking has been compared in this study. Manhiça *et al*., (2012) studied the analysis of wood-fired bakery ovens baking process and their wood consumption, and thus, the specific firewood consumption was found to be 0.95kg of wood per kg of wheat flour baked.

- Firewood consumption = (kg of wheat flour baked) × (specific wood consumption)

Therefore, it was known that 3kg of wheat flour was consumed during two cycles of baking, the firewood consumption estimated to be 2.85kg per day. Thus, about 85.5kg of firewood per month would be saved if solar energy was used as a heat source for baking instead.

The net present value, benefit-cost ratio, and simple payback period are given as follows. The present costs during the lifetime of the project are determined as:

$$P_C = I_C + A\left[\frac{((1+r)^n - 1)}{r(1+r)^n}\right] \ldots\ldots 7.4$$

Where I_C= initial cost = 14,882-Birr, A= Annual cost =1,100 Birr, r =discount rate = 10%, and n= 10 years

$$P_C = I_C + A\left[\frac{((1+r)^n - 1)}{r(1+r)^n}\right] \ldots\ldots 7.5$$

$$P_C = 21{,}591.5\ Birr$$

The annual benefit is 6,156 birr, so the present value of benefits during the lifetime of the project:

$$P_b = A\left[\frac{((1+r)^n - 1)}{r(1+r)^n}\right] \ldots\ldots 7.6$$

$$P_b = 37{,}828.62\ Birr$$

The Net present value is determined as NPV = $P_b - P_c = 16{,}237.12\ Birr$

The annual saving is: $A_s = A_b - A_c = 5{,}056\ Birr$

The simplest payback period is: $SPP = \frac{I_c}{A_s} = \ 2.93\ year$

Therefore; the payback of the present solar thermal bread baker is **2.93 years.**

The benefit-cost ratio: $BCR = \frac{P_b}{P_c} = \ 1.75\ > 1$

Generally, the initial cost of solar application is high as compared to other conventional bread baking systems but its operation and maintenance cost is negligible, hence the customer can get his money back in a short period payback period. And it is free from a health problem, environmental pollution, which is an eco-friendly and sustainable way of using a hug free solar energy don’t compare with the initial cost.

CHAPTER EIGHT

CONCLUSIONS AND RECOMMENDATIONS

8.1 Conclusions

Solar thermal-based bread baking system is the best alternative to shift the country's dependence on fossil fuels and minimize the environmental effect of burning fossil fuels. In this study experimental investigation of solar bread baking system with PCM thermal storage has been carried out. The system uses a parabolic trough collector used to concentrate the incoming solar irradiance to the receiver tube. To add the enhancement techniques on a PTC, the use of internal longitudinal fins and the use of a secondary shield reflector over the absorber. Every fin has 10 mm length and 2 mm thickness, while the shield covers one third (120^o) of the tube periphery. Thermal storage used was 10 kg of D-mannitol. The main challenges faced while conducting the experimental test of the system were the difficulty of managing heat transfer oil leaks and tracking errors due to manual tracking. The major aim of this thesis work was to size, manufacture, and conduct an experimental investigation on the performance of solar bread bakers. The following conclusions are drawn from this study:

- Based on the current status of the country a new method of solar energy application has been tested and new technical and technological opportunities of a solar energy application in solar thermal bread baking have been established.
- To reduces the dependence on biomass fuels and their adverse environmental effects.
- The maximum average outlet thermal oil B temperature, maximum energy, and exergy efficiency of PTC without receiver fin and shield were found to be 456 K, 51.9%, and 28.4% respectively.
- The maximum outlet thermal oil B temperature of PTC with receiver fin and receiver fin with shield was found to be 465 and 469 K respectively.
- The energy and exergy efficiency of the PTC increases with increasing solar radiation the intensity and the average energy and exergy efficiency of the PTC with receiver fin and receiver fin with shield was 53.6, 29.7 and 55.2, 31.1% respectively.
- The outlet HTF temperature of the PTC with receiver fin and shield configuration is 5 to 13 K higher than the receiver without fin and shield configuration and the energy and

exergy efficiency of the PTC with receiver fin with shield were 2.1 to 3.3% and 0.9 to 1.8% higher than the PTC without receiver fin and shield.

- The COMSOL simulation of D-mannitol filled LHS charging/discharging was achieved at 7200 sec/7920 sec.
- When the D-mannitol reaches its melting point during the charging process the amount of sensible, latent, and total energy stored in the PCM was 1.78MJ, 3.15MJ, and 4.93MJ respectively.
- The amount of sensible, latent, and total energy released during the discharging process were 1.41, 2.85, and 4.26 MJ respectively.
- The baking plate surface temperature in the experiment was measured and a temperature of about 441.25 K on the pan surface was registered; so that it was possible to bake nice bread. The baking cycle took about 55 minutes.
- The final baked bread sample weight was measured to be 0.72 kg with a loss of 0.12 kg from the initial weight of dough sample 0.84 kg that means 14.28% weight loss.
- The total investment cost of the baker was 14,832 Birrs with an annual energy saving of 6,156 Birrs with a pay-back period of 2.93 years.

8.2 Recommendations

Due to the limited access and rising cost to conventional energy sources, it is significant to shift to renewable energy for environmental sustainability. The solar thermal energy system is one of the promising renewable energy solution for sustainable energy utilization. Generally, this study shows that bread baking using solar thermal energy-based bakeries was possible by scaling up the system and creating awareness to the society about the benefits of the technology. Therefore, the main points to be recommended for future work based on the result of this study;

- An automatic tracking system should be incorporated in the PTC to minimize tracking errors and thus improve the efficiency.
- The receiver has to be an evacuated glass tube constructed in such a way that high radiation absorption and low thermal losses are realized.
- Further system analysis focuses on the temperature distribution of the baking plate surface.
- The utilization of renewable energy in Ethiopia should be increased, as there is a global concern that the developing nations could be faced with the energy crisis and global warming. It is expected that more damage and pollution of the environment will continue. Parabolic trough solar collector is one of the options for renewable energy and this technology should be adopted in rural area communities that utilize biomass and fossil fuel for solar thermal bread baker.
- Future work should focus on scaling up and demonstrating the systems to attract small scale bakeries.

Special Acknowledgement

This research project is funded by Adama Science and Technology University under the grand number

ASTU/SM-R/330/21

Adama, Ethiopia

References

Abbood, M. H., & Mohammed, M. M. (2019). Experimental characteristic of a solar parabolic trough collector with indirect steam generation system. International Journal of Energy and Environment, 10(2), 87-96.

Adem, K. D., & Ambie, D. A. (2017). A review of injera baking technologies in Ethiopia: Challenges and gaps. Energy for Sustainable Development, 41, 69-80.

Alguacil, M., Prieto, C., Rodriguez, A. and Lohr, J. (2014). Direct steam generation in parabolic trough collectors. Energy Procedia, 49, pp.21-29.

Alva, G., Lin, Y., & Fang, G. (2018). An overview of thermal energy storage systems. Energy, 144, 341-378.

American Thermal Insulation Manufacturers Association (ATIMA), (2005). "Energy Saving Guide,"

Amine, M. B., Allouhi, A., Kousksou, T., Jamil, A., & Lahrech, K. (2018). Yearly performance of low-enthalpy parabolic trough collectors in MENA region according to different sun-tracking strategies. Applied Thermal Engineering, 128, 1404-1419.

Arabacigil, B., Yuksel, N., & Avci, A. (2015). The use of paraffin wax in a new solar cooker with inner and outer reflectors. Thermal Science, 19(5), 1663-1671.

Argaw, N. (1996). Estimation of solar radiation energy of Ethiopia from sunshine data. International journal of solar energy, 18(2), 103-113.

Ayub, I., Munir, A., Ghafoor, A., Amjad, W., & Nasir, M. S. (2018). Solar thermal application for decentralized food baking using Scheffler reflector technology. Journal of Solar Energy Engineering, 140(6).

Bellos, E., & Tzivanidis, C. (2020). Enhancing the performance of a parabolic trough collector with combined thermal and optical techniques. Applied thermal engineering, 164, 114496.

Bellos, E., & Tzivanidis, C. (2017). A detailed exergetic analysis of parabolic trough collectors. Energy Conversion and Management, 149, 275-292.

Bhattacharya, S. C., & Leon, M. A. (2005, April). Prospects for biomass gasifiers for cooking applications in Asia. In World Renewable Energy Regional Conference, Jakarta, Indonesia, 18-21 April 2005.

Bilal, F. R., Arunachala, U. C., & Sandeep, H. M. (2018). Experimental validation of energy parameters in parabolic trough collector with plain absorber and analysis of heat transfer enhancement techniques. In Journal of Physics: Conference Series (Vol. 953, No. 1, p. 012030). IOP Publishing.

Bonacina, C., Comini, G., Fasano, A., & Primicerio, M. 1. (1973). Numerical solution of phase-change problems. International Journal of Heat and Mass Transfer, 16(10), 1825-1832.

Bouadila, S., Lazaar, M., Skouri, S., Kooli, S., & Farhat, A. (2014). Energy and exergy analysis of a new solar air heater with latent storage energy. international journal of hydrogen energy, 39(27), 15266-15274.

Boulet, M., Marcos, B., Dostie, M., & Moresoli, C. (2010). CFD modeling of heat transfer and flow field in a bakery pilot oven. Journal of food engineering, 97(3), 393-402.

Bredariol, P., Spatti, M., & Vanin, F. M. (2019). Different baking conditions may produce breads with similar physical qualities but unique starch gelatinization behaviour. Lwt, 111, 737-743.

Cengel, Y. A., & Boles, M. A. (2007). Energy, energy transfer, and general energy analysis. An Engineering Approach, McGraw-Hill, New York.

Chhanwal, N., Anishaparvin, A., Indrani, D., Raghavarao, K. S. M. S., & Anandharamakrishnan, C. (2010). Computational fluid dynamics (CFD) modeling of an electrical heating oven for bread-baking process. Journal of Food Engineering, 100(3), 452-460.

Chhanwal, N., Indrani, D., Raghavarao, K. S. M. S., & Anandharamakrishnan, C. (2011). Computational fluid dynamics modeling of bread baking process. Food Research International, 44(4), 978-983.

Dawit, G. D. (2018). Thermal Analysis of Solar Flat Plate Collector Coupled with Heat Storage (Doctoral dissertation).

Demagh, Y., Bordja, I., Kabar, Y., & Benmoussa, H. (2015). A design method of an S-curved parabolic trough collector absorber with a three-dimensional heat flux density distribution. Solar Energy, 122, 873-884.

Duffie, J. A., & Beckman, W. A. (2013). Solar Thermal Power Systems. Solar Engineering of Thermal Processes, Fourth Edition, John Wiley & Sons, Inc., Hoboken, NJ, USA. doi, 10, 9781118671603.

Eames, P., &. Da Cunha, J. P. (2016) Thermal energy storage for low and medium temperature applications using phase change materials–a review. Applied energy, 177, 227-238.

El-Ghetany, H. H., Hassan, S. A., & Metias, M. Z. (2019). Experimental Investigation of a Solar Baking System Using Parabolic Trough Solar Collector. International Journal of Emerging Technologies in Engineering Research (IJETER), 7(1).

ERKEK, T. Ü., & GÜNGÖR, A. (2013). EXPERIMENTAL PERFORMANCE EVALUATION OF PCM THERMAL STORAGE IN A PANEL RADIATOR

ETSAP, I. (2013). IRENA. Thermal Energy Storage-Insights for Policy Makers, 9.

Forson, F. K., Nazha, M. A. A., Akuffo, F. O., & Rajakaruna, H. (2007). Design of mixed-mode natural convection solar crop dryers: Application of principles and rules of thumb. Renewable energy, 32(14), 2306-2319.

Frank, I.P., DeWitt, D.P., Bergman, T.L. and Lavine, A.S. (2002). Fundamentals of heat and mass transfer (Vol. 6). New York: Wiley.

Gallagher, A. (2011). A solar fryer. Solar energy, 85(3), 496-505.

Garg, H. P. (2000). Solar energy: fundamentals and applications. Tata McGraw-Hill Education.

Genitha, I., Lakshmana, G. B. T., & John, D. R. (2014). Design, fabrication and performance evaluation of domestic gas oven. IOSR Journal of Engineering (IOSRJEN), 4(5), 35-38.

Ghazouani, K., Skouri, S., Bouadila, S., & Guizani, A. (2019). Thermal analysis of linear solar concentrator for indirect steam generation. Energy Procedia, 162, 136-145.

Gong, X., Wang, F., Wang, H., Tan, J., Lai, Q., & Han, H. (2017). Heat transfer enhancement analysis of tube receiver for parabolic trough solar collector with pin fin arrays inserting. Solar Energy, 144, 185-202.

Günther, M., Joemann, M., Csambor, S., Guizani, A. and Krüger, D. (2011). Parabolic trough technology. Advanced CSP teaching materials, pp.1-106.

Hailu, M. H., Kahsay, M. B., Tesfay, A. H., & Dawud, O. I. (2017). Energy consumption performance analysis of electrical mitad at mekelle city. Momona Ethiopian Journal of Science, 9(1), 43-65.

Hassan, A. (2010). Phase change materials for thermal regulation of building integrated photovoltaics.

Hassen, A. A., Kebede, S. B., & Wihib, N. M. (2016). Design and manufacturing of thermal energy based Injera baking glass pan. Energy Procedia, 93, 154-159.

Huang, Z., Yu, G. L., Li, Z. Y., & Tao, W. Q. (2015). Numerical study on heat transfer enhancement in a receiver tube of parabolic trough solar collector with dimples, protrusions and helical fins. Energy Procedia, 69, 1306-1316.

Islam, M. K., Hasanuzzaman, M., & Rahim, N. A. (2015). Modelling and analysis of the effect of different parameters on a parabolic-trough concentrating solar system. RSC advances, 5(46), 36540-36546.

Jesumathy, S. P., Udayakumar, M., Suresh, S., & Jegadheeswaran, S. (2014). An experimental study on heat transfer characteristics of paraffin wax in horizontal double pipe heat latent heat storage unit. Journal of the Taiwan Institute of Chemical Engineers, 45(4), 1298-1306.

John, G., König-Haagen, A., King'ondu, C. K., Brüggemann, D., & Nkhonjera, L. (2015). Galactitol as phase change material for latent heat storage of solar cookers: Investigating thermal behavior in bulk cycling. Solar Energy, 119, 415-421.

Kalogirou, S.A. (2009). Solar thermal power systems. Solar Energy Engineering, pp.521-552

Kalogirou, S.A. (2013). Solar energy engineering: processes and systems. Academic Press.

Kedir, M. F., Bekele, T., & Feleke, S. (2019). Problems of Mirt, and potentials of improved Gonzie and traditional open cook stoves in biomass consumption and end use emission in rural wooden houses of Southern Ethiopia. Scientific African, 3, e00064.

Keyanpour-Rad, M., Haghgou, H. R., Bahar, F., & Afshari, E. (2000). Feasibility study of the application of solar heating systems in Iran. Renewable energy, 20(3), 333-345.

Khadiran, T., Hussein, M. Z., Zainal, Z., & Rusli, R. (2015). Encapsulation techniques for organic phase change materials as thermal energy storage medium: A review. Solar Energy Materials and Solar Cells, 143, 78-98.

Kibaara, S., Chowdhury, S., & Chowdhury, S. P. (2012, May). A thermal analysis of parabolic trough CSP and biomass hybrid power system. In PES T&D 2012 (pp. 1-6). IEEE.

Kotas, T. J. (2013). The exergy method of thermal plant analysis. Elsevier.

Kotyla, J. (2017). Molten salt composition and composites for improved latent heat thermal energy storage. PAM Review Energy Science & Technology, 4, 46-58.

Kousksou, T., Strub, F., Lasvignottes, J. C., Jamil, A., & Bedecarrats, J. P. (2007). Second law analysis of latent thermal storage for solar system. Solar energy materials and solar cells, 91(14), 1275-1281.

Ktistis, P. K., Agathokleous, R. A., & Kalogirou, S. A. (2021). Experimental performance of a parabolic trough collector system for an industrial process heat application. Energy, 215, 119288.

Kumar, A., & Shukla, S. K. (2016). Mathematical modeling and optimization of a parabolic trough concentrator for the improvement of collection efficiency. Int. J. Innov. Res. Eng. Manage, 3, 375-380.

Laaraba, A., & Mebarki, G. (2020). Enhancing Thermal Performance of a Parabolic Trough Collector with Inserting Longitudinal Fins in the Down Half of the Receiver Tube. Journal of Thermal Science, 29(5), 1309-1321.

Li, P. W., & Chan, C. L. (2017). Thermal energy storage analyses and designs. Academic Press.

Lingayat, A. B., & Suple, Y. R. (2013). Review on phase change material as thermal energy storage medium: materials, application. International Journal of Engineering Research and Applications, 3(4), 916-921.

Le Houerou, H. N. (2012). The grazing land ecosystems of the African Sahel (Vol. 75). Springer Science & Business Media.

Lucas, C., Manhica, F. and Richards, T. (2012). Computational Fluid Dynamic Simulation of the flow field in wood-fired bakery ovens. International Journal of Applied Science and Technology, 7(2), pp.1-11.

Majeed, A. J., Najim, S. E., & Hammadi, S. H. (2014). SIMULATION SOLAR ELECTRICAL GENERATION POWER PLANT BY USING PARABOLIC TROUGH IN BASRA CITY. Al-Qadisiyah Journal for Engineering Sciences, 7(1), 1-11.

Manhiça, F. A., Lucas, C., & Richards, T. (2012). Wood consumption and analysis of the bread baking process in wood-fired bakery ovens. Applied thermal engineering, 47, 63-72.

Marif, Y., Benmoussa, H., Bouguettaia, H., Belhadj, M. M., & Zerrouki, M. (2014). Numerical simulation of solar parabolic trough collector performance in the Algeria Saharan region. Energy Conversion and Management, 85, 521-529.

Mazman, M., Cabeza, L. F., Mehling, H., Nogues, M., Evliya, H., & Paksoy, H. Ö. (2009). Utilization of phase change materials in solar domestic hot water systems. Renewable energy, 34(6), 1639-1643.

McLaughlin, R. P. (2020). Solar Thermal Energy System for Renewable Desalination.

Medrano, M., Gil, A., Martorell, I., Potau, X. and Cabeza, L.F. (2010). State of the art on high-temperature thermal energy storage for power generation. Part 2—Case studies. Renewable and Sustainable Energy Reviews, 14(1), pp.56-72.

Mekonnen, M. T. (2011). Design and manufacture of laboratory model for solar powered injera baking oven.

Mesfin, M., & Assefa, A. (2010). Modeling, simulation and performance evaluation of parabolic trough solar collector power generation system. Zede Journal, 27, 81-89.

Minaye, G. (2020). DESIGN AND EXPERIMENTAL TESTING OF SOLAR THERMAL BREAD BAKING SYSTEM (Doctoral dissertation).

Mishra, A., Powar, S., & Dhar, A. (2019). Solar Thermal Powered Bakery Oven. In Advances in Solar Energy Research (pp. 577-592). Springer, Singapore.

Mohamed, S. A., Al-Sulaiman, F. A., Ibrahim, N. I., Zahir, M. H., Al-Ahmed, A., Saidur, R., ... & Sahin, A. Z. (2017). A review on current status and challenges of inorganic phase change materials for thermal energy storage systems. Renewable and Sustainable Energy Reviews, 70, 1072-1089.

Mollahosseini, A., Abdelrasoul, A., Sheibany, S., Amini, M., & Salestan, S. K. (2019). Renewable energy-driven desalination opportunities–A case study. Journal of environmental management, 239, 187-197.

MORAKINYO, A. T., OMIDIJI, B., & OWOLABI, H. (2017). Development and optimization of operational parameters of a gas-fired baking oven. Leonardo Journal of Sciences, 31, 45-64.

Nath, D., Ansar, D., Das, B., & Bhuyan, S. (2018). Experimental analysis of solar water heater with compound parabolic concentrator. EAI Endorsed Transactions on Energy Web, 8(31), e8.

Newell, R., Raimi, D., & Aldana, G. (2019). Global energy outlook 2019: the next generation of energy. Resources for the Future, 8-19.

Nicolas, V., Glouannec, P., Ploteau, J. P., Salagnac, P., & Jury, V. (2017). Experiment and multiphysic simulation of dough baking by convection, infrared radiation and direct conduction. International Journal of Thermal Sciences, 115, 65-78.

Niyas, H., Rao, C. R. C., & Muthukumar, P. (2017). Performance investigation of a lab-scale latent heat storage prototype–experimental results. Solar Energy, 155, 971-984.

Okafor, B. E. (2014). Simple design of a dualpowered domestic oven. International Journal of Engineering and Technology, 4(5), 313-317.

Padhy, A., Vishal, B., Verma, P., Dwivedi, G., & Behura, A. K. (2021). Fabrication of parabolic trough hybrid solar PV-T collector using a-Si thin film solar cells in Indian perspective. Materials Today: Proceedings, 38, 56-62.

Patel, R., & Patel, V. (2020). Scheffler reflector for cooking application: a review. International Journal of Ambient Energy, 1-13.

Petrov, L. A. (2011). Solar Tracking Strategies. BSc (Hons) Dissertation, university of DUNDEE.

Pinelli, M., & Suman, A. (2017). Thermal and fluid dynamic analysis of an air-forced convection rotary bread-baking oven by means of an experimental and numerical approach. Applied Thermal Engineering, 117, 330-342.

Purlis, E. (2012). Baking process design based on modelling and simulation: Towards optimization of bread baking. Food control, 27(1), 45-52.

Sandeep, H. M., & Arunachala, U. C. (2017). Solar parabolic trough collectors: A review on heat transfer augmentation techniques. Renewable and Sustainable Energy Reviews, 69, 1218-1231.

Sarbu, I., & Sebarchievici, C. (2018). A comprehensive review of thermal energy storage. Sustainability, 10(1), 191.

Sedighi, M., & Salarian, H. (2017). A comprehensive review of technical aspects of biomass cookstoves. Renewable and Sustainable Energy Reviews, 70, 656-665.

Sekhar, T. V. R., Nandan, G., & Prakash, R. (2018). Parabolic trough solar collectors. Eur. J. Sci.(EJS), 1(1), 43-53.

Smith, J., Hinterberger, M., Schneider, C., & Koehler, J. (2016). Energy savings and increased electric vehicle range through improved battery thermal management. Applied Thermal Engineering, 101, 647-656.

Stutz, B., Le Pierrès, N., Kuznik, F., Johannes, K., Del Barrio, E. P., Bedecarrats, J. P., ... & Minh, D. P. (2017). Storage of thermal solar energy. Comptes Rendus Physique, 18(7-8), 401-414.

Swami, V. M., Autee, A. T., & Anil, T. R. (2018). Experimental analysis of solar fish dryer using phase change material. Journal of Energy Storage, 20, 310-315.

Tadesse, M. (2020). The Developmental Patterns of Injera Baking Stoves: Review on the Efficiency, and Energy Consumption in Ethiopia. International Journal of Mechanical Engineering, 7(1), 7-16.

Tesfay, A. H. (2015). Experimental Investigation of a Concentrating Solar Fryer with Heat Storage.

Tesfay, A. H., Kahsay, M. B., & Nydal, O. J. (2014). Solar-powered heat storage for Injera baking in Ethiopia. Energy Procedia, 57, 1603-1612.

Tian, Y., & Zhao, C. Y. (2013). A review of solar collectors and thermal energy storage in solar thermal applications. Applied energy, 104, 538-553.

Tijani, A. S., & Roslan, A. M. B. (2014). Simulation analysis of thermal losses of parabolic trough solar collector in Malaysia using computational fluid dynamics. Procedia Technology, 15, 841-848.

Tiwari, G. N., & Tiwari, A. (2016). Handbook of solar energy. Singapore: Springer.

Tsegay, M. (2011). Design and manufacture of a laboratory model for solar-powered Injera Baking Oven (Doctoral dissertation, MSc thesis, Addis Ababa Institute of Technology).

Tyagi, V. V., Buddhi, D., Kothari, R., & Tyagi, S. K. (2012). Phase change material (PCM) based thermal management system for cool energy storage application in building: An experimental study. Energy and Buildings, 51, 248-254.

M., Suresh, S., Jesumathy, S. P., Udayakumar, & Jegadheeswaran, S. (2014). An experimental study on heat transfer characteristics of paraffin wax in horizontal double pipe heat latent heat storage unit. Journal of the Taiwan Institute of Chemical Engineers, 45(4), 1298-1306.

Vignarooban, K., Xu, X., Arvay, A., Hsu, K. and Kannan, A.M. (2015). Heat transfer fluids for concentrating solar power systems–a review. Applied Energy, 146, pp.383-396.

Vijayan, S. N., & Kumar, S. S. (2017). Theoretical Review on Influencing Factors in the Design of Parabolic Trough Collector. World Academy of Science, Engineering, and Technology International Journal of Mechanical and Materials Engineering, 11(11).

Wang, Q., Yang, H., Zhong, S., Huang, Y., Hu, M., Cao, J., ... & Yang, H. (2020). Comprehensive experimental testing and analysis on parabolic trough solar receiver integrated with radiation shield. Applied Energy, 268, 115004.

Wang, W. W., Zhang, K., Wang, L. B., & He, Y. L. (2013). Numerical study of the heat charging and discharging characteristics of a shell-and-tube phase change heat storage unit. Applied Thermal Engineering, 58(1-2), 542-553.

Wang, Z., Qiu, F., Yang, W., & Zhao, X. (2015). Applications of solar water heating system with phase change material. Renewable and Sustainable Energy Reviews, 52, 645-652.

Wilberforce, T., Baroutaji, A., El Hassan, Z., Thompson, J., Soudan, B., & Olabi, A. G. (2019). Prospects and challenges of concentrated solar photovoltaics and enhanced geothermal energy technologies. Science of The Total Environment, 659, 851-861.

Williamson, M. E., & Wilson, D. I. (2009). Development of an improved heating system for industrial tunnel baking ovens. Journal of Food Engineering, 91(1), 64-71.

Yassen, T. A. (2012). Experimental and theoretical study of a parabolic trough solar collector. Anbar J. Eng. Sci, 5(1), 109-125.

Zhang, L., & Zhang, J. (2020). A systematic review on tourism energy consumption, sustainable tourism, and destination development: a behavioral perspective. Transport and Energy Research, 295-313.

APPENDIX A

Total costs of the solar bread baker

Table A. 1: Total cost of the project

No	Material cost		Qty	Price/ Cost in Birr	
	Material	Specification		Unit price	Total price
1	Glass mirror	1m×2m	1	700	700
2	Sheet metal	1m×2m	2	900	1800
3	Flat plat absorber	0.21×1.5m	1	200	200
4	Pipe	1/2" Diameter and 6m length	1	250	250
5	Gating valve	1/2" Diameter	8	60	480
6	Elbow and connectors	1/2" Diameter	18	20	360
7	Paint	1gal		170	170
8	RHS	40mm×40mm and 6m length	1	450	450
9	Flat iron	40mm×10mm and 6m length	1	200	400
10	Oil pump		1	1500	1500
10	Fiber glass	5kg		100	500
11	Phase change material tube	35mm Diameter and 6m length	1	200	200
12	D-mannitol	10kg	10	375	3750
13	Aluminum sheet	2m x1m	1		480
14	Thermic oil B	8 litter	8	129	1032
15	Receiver tube	2m		120	240
16	Labor and installation cost				1120
17	Transportation cost				200
18	Other cost				1000
Total investment cost in Birr					14882

APPENDIX B

Numerical Results of LHS System

The reports of a numerical simulation of the thermal performance of a D-mannitol -filled LHS unit are described in this section. The model grid independency test, average temperature variation, average melt fraction variation, and energy absorbed/released throughout the charging/discharging operation of the LHS have all been reported and examined.

Grid Independency Test

The numerical results of all models are highly affected by mesh element sizes. Simulations with varied mesh element sizes were done for both charging and discharging operations to assess the grid independence of the numerical outputs. The grid independence of the average temperature during charging procedures for 26286, 49210, and 77893 elements is shown in Figure 7.15 a. During the discharging process, grid independency testing of average melt fraction for 26286, 49210, and 77893 elements is shown in Figure 7.15 b.

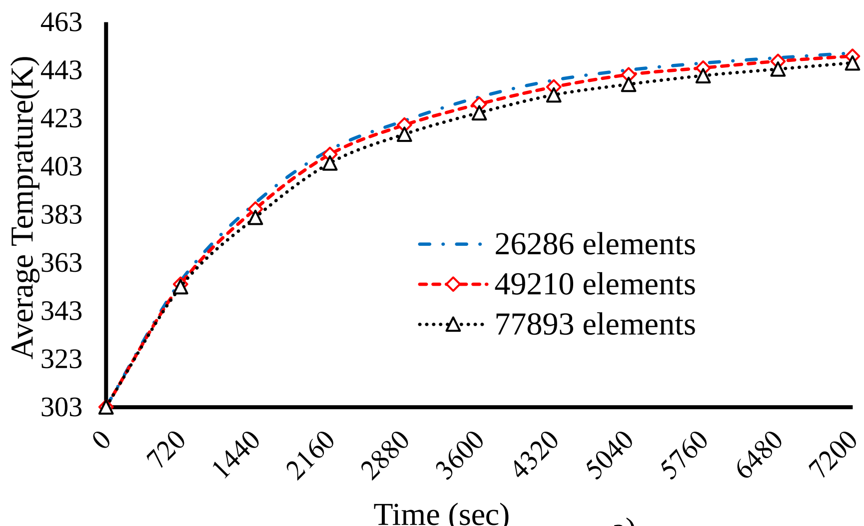

a)

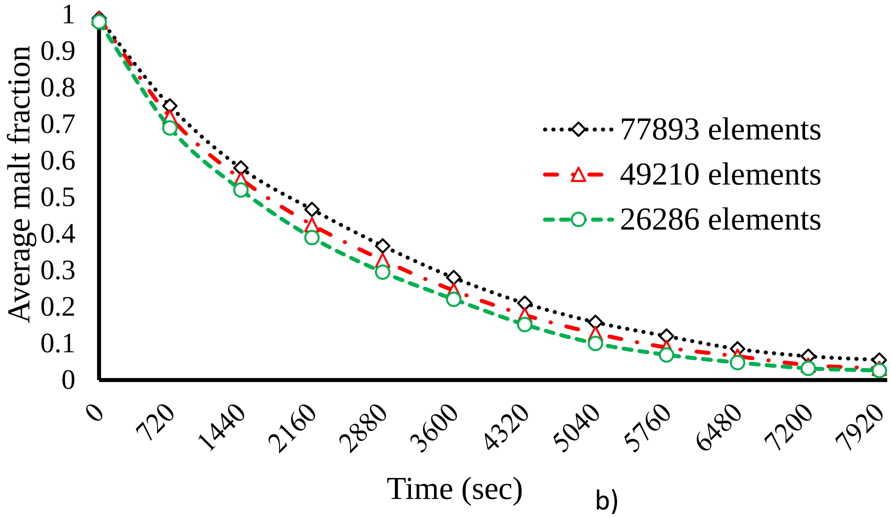

Figure B. 1:- Grid independency test with different mesh elements a) average temperature for charging and b) average melt fraction for discharging

Temperature Variation of PCM

Figure 7.16 (a) and (b) show the average temperature variation of the PCM during the charging and discharging periods. The volumetric average temperature of all the mesh elements in the numerical model is the average temperature. The temperature of PCM rises as it melts during the charging process when HTF from the collector at 460K flows through the HTF tubes, as shown in figure 7.16 (a). The discharge process begins when the sun is not shining or when it is cloudy, and it continues throughout the night as HTF at 303K flows through the HTF tubs, absorbing heat and lowering the temperature of the PCM until equilibrium is reached, as shown in figure 7.16 (b). Niyas *et al.*, (2017) and Dawit *et al.*, (2018) used oil and water as heat transfer fluids, respectively, and reported PCM temperature variations with similar trends.

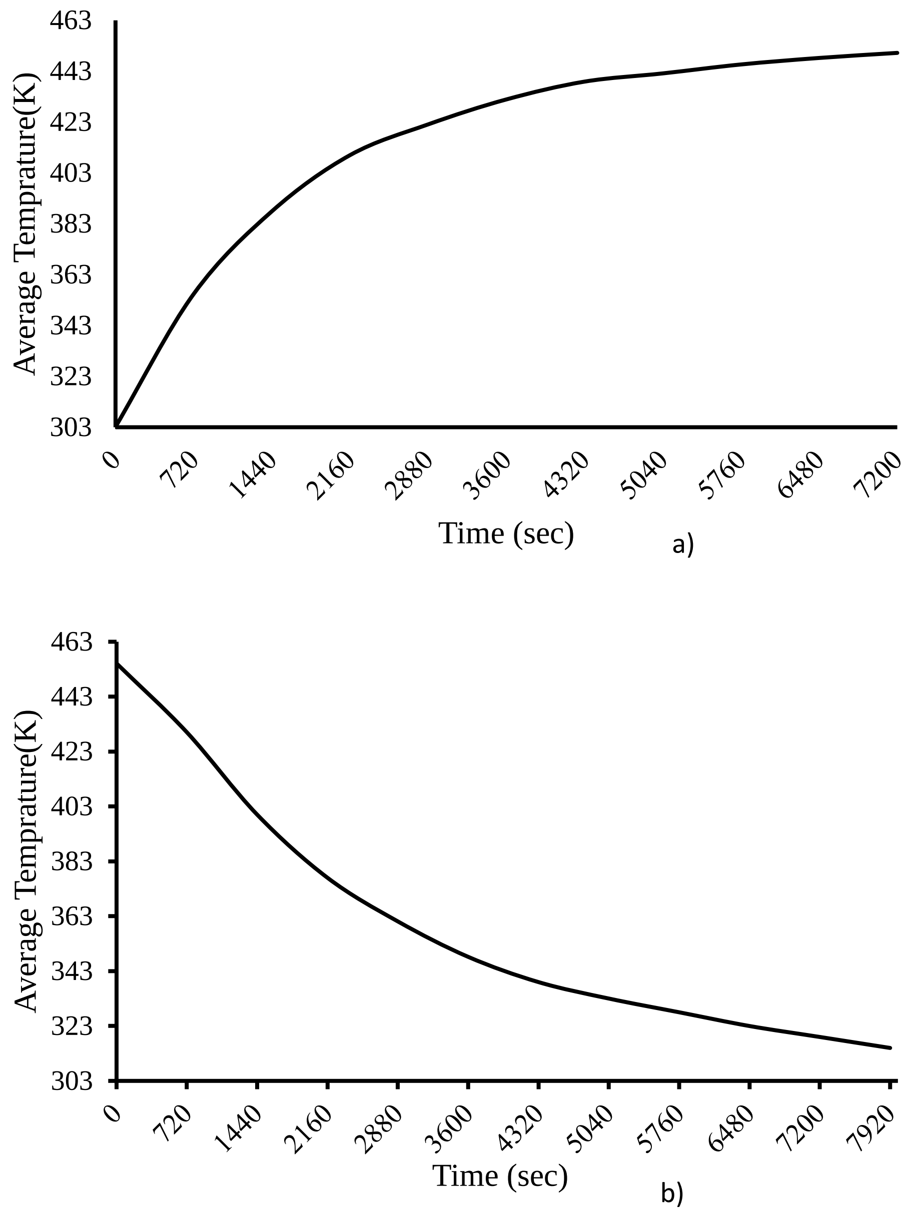

Figure B. 2:- Average temperature variation of shell and tube LHS systems a) Charging b) Discharging

Charging and Discharging Time

Melt fraction is the most important factor that influences the performance of any latent heat storage system during the melting/solidification process. The volumetric average melt percentage of all the meshed elements of the numerical model that varied between 0 and 1 is the average melt fraction in this case. Figure 7.17 indicates the changes in average melt fraction during the charging/discharging process.

The rise/fall of the average melt fraction of LHS during charging/discharging is faster at the beginning due to the presence of a higher heat transfer rate between the HTF and PCM, as shown in figure 7.17 (a) and (b). Due to the low heat transfer rate between the HTF and the PCM, this becomes slower over a specific amount of time. The charging/discharging period for the D-mannitol -filled LHS system was 7200 seconds and 7920 seconds, respectively.

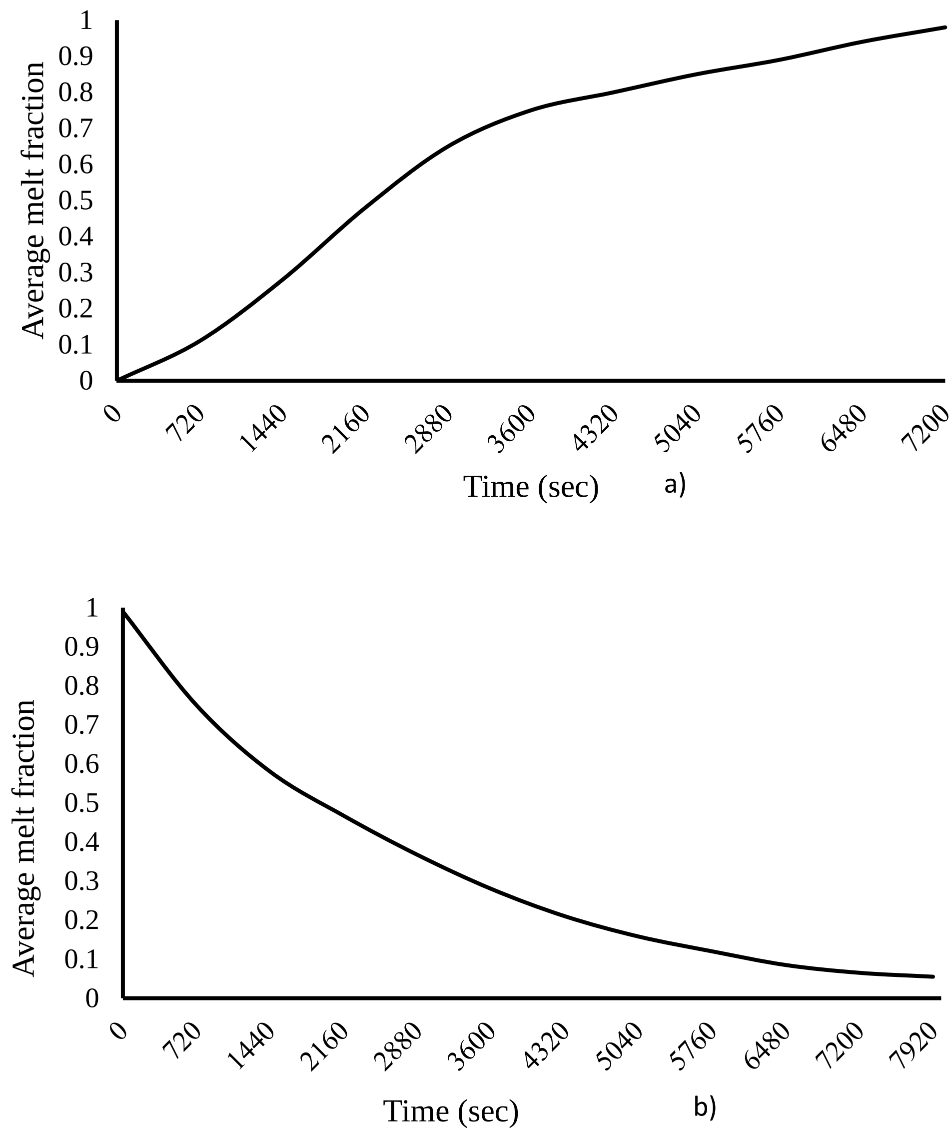

Figure B. 3:- a) charging melt fraction b) discharging melt fraction

Energy stored/discharged

The variation of rate of energy stored/discharged, i.e., sensible, latent, and total energy during the charging/discharging process is illustrated in Figure 7.18. during the charging/discharging process, the heat transfer fluid is circulated through the tube at a temperature of 450/303 K. due to this, heat transfer takes place between the HTF and the PCM. At the beginning of the charging/discharging process, the heat gets stored/discharged in the form of sensible heat only. Once the D-mannitol temperature reaches nearly the phase change temperature (420K), heat gets stored/discharged in the form of latent heat. The heat stored/discharged after complete phase change is also sensible energy. When the average temperature of the D-mannitol reaches 440K within 7200 seconds during the charging process, the amount of sensible, latent, and total energy in the LHS are 1.82MJ, 2.84MJ, and 4.66 MJ, respectively.

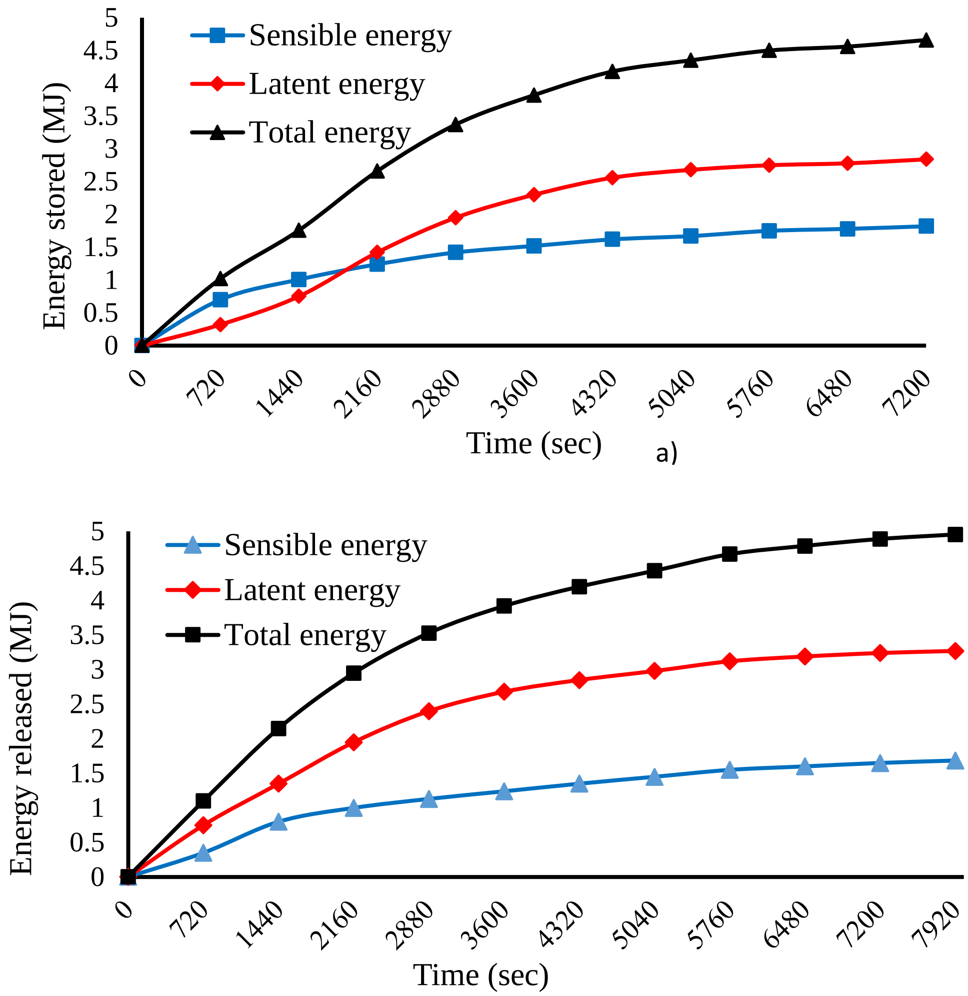

Figure B. 4:- a) Energy charging rate b) Energy discharging rate

Similarly, during the discharging process, when the temperature of the PCM reaches 303 K in 7920 seconds, the amount of sensible, latent, and total energy discharged from the Demannitol-filled LHS is 1.71 MJ, 2.79 MJ, and 4.5 MJ, respectively.

APPENDIX C

Design of Baking Unit Heat Transfer Fluid Gallery

To transfer heat energy assume uniformly from the heat transfer oil. The oil inlet and outlet ports were drilled with1/2 inch diameter size on opposite sides of the housing of the gallery; pipes with 1/2 inch diameter were connected to the drilled inlet and outlet ports. To increase the contact between the hot heat transfer oil with the pan supporting plate. To decrease heat loss, the oil gallery was insulated by a fiberglass insulation system which has about 3 cm thickness from below, upper, and the sidewall.

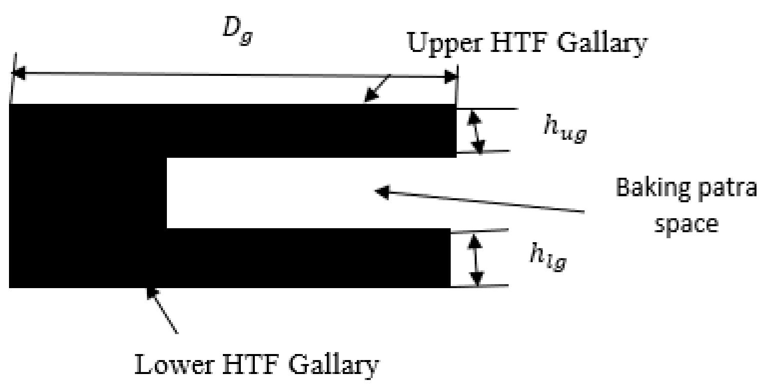

Figure C.1:- Baking unit schematic

The volume of the oil gallery can be determined as follows:

Lower HTF Gallary

$V_g = \frac{\pi}{4} D_g^2 h_g$……………………………………………………………………..C.1

$$V_g = \frac{\pi}{4} 0.04^2 \times 0.028 = 0.0035m^3$$

Upper HTF Gallary

$$V_g = \frac{\pi}{4} 0.04^2 \times 0.02 = 0.0025 m^3$$

APPENDIX D

Calibration of the Thermocouple Thermometer

Calibration of thermometers can be carried out using a reference thermometer in a temperature calibration test by comparing both measurement values of a reference thermometer and other thermometers Calibration test for a four-channel digital K-type thermocouple was conducted in the chemical laboratory with a weber thermometer by using 0.3 kg water boiling and cooling test for 35 minutes.

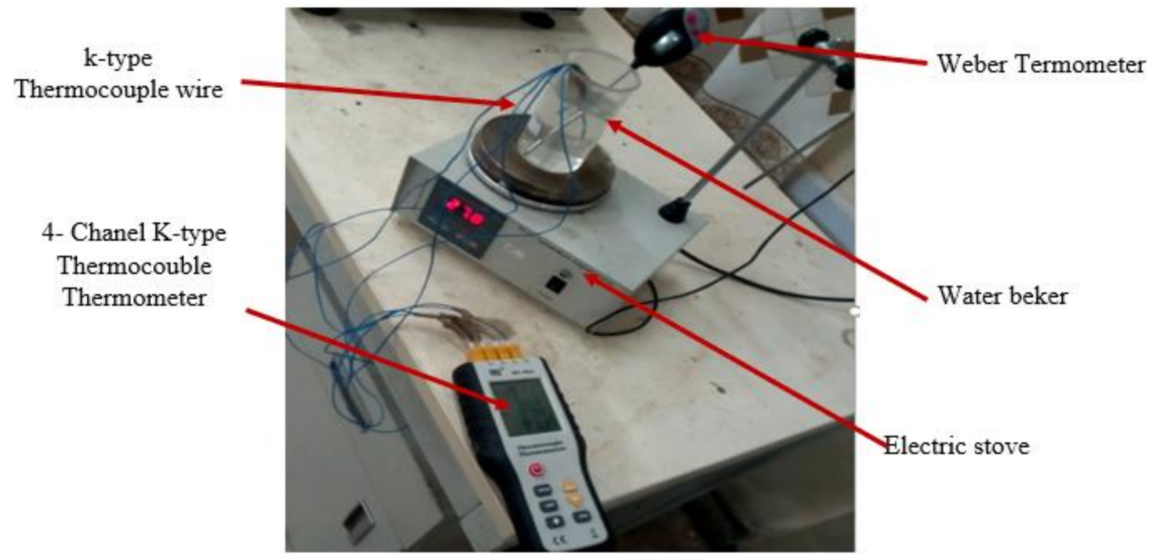

Figure D-1: Calibration Setup

Table D. 1: Water temperature measuring test by using K-type thermocouples

Time	T_1 weber thermometer (°C)	T_2 (K-type thermocouple) (°C)	Uncertainty (%) $\frac{T_1-T_2}{T_{w2}} * 100$
1	24.8	24.6	0.8065
3	31.2	30.9	0.9615
5	38.8	38.5	0.7732

7	42.6	42.3	0.7042
9	51.3	51	0.5848
11	60.2	59.8	0.6645
13	63.5	63	0.7874
15	69	68.5	0.7246
17	71.2	70.8	0.5618
19	73.1	72.8	0.4104
21	77.1	76.6	0.6485
21	81.2	80.6	0.7389
23	82.2	81.8	0.4866
25	83.5	83	0.5988
27	87.5	87.1	0.4571
29	89.3	88.8	0.5599
31	91.1	90.8	0.3293
33	92	91.6	0.4348
35	92.9	92.5	0.4306
Average uncertainty%			0.6139

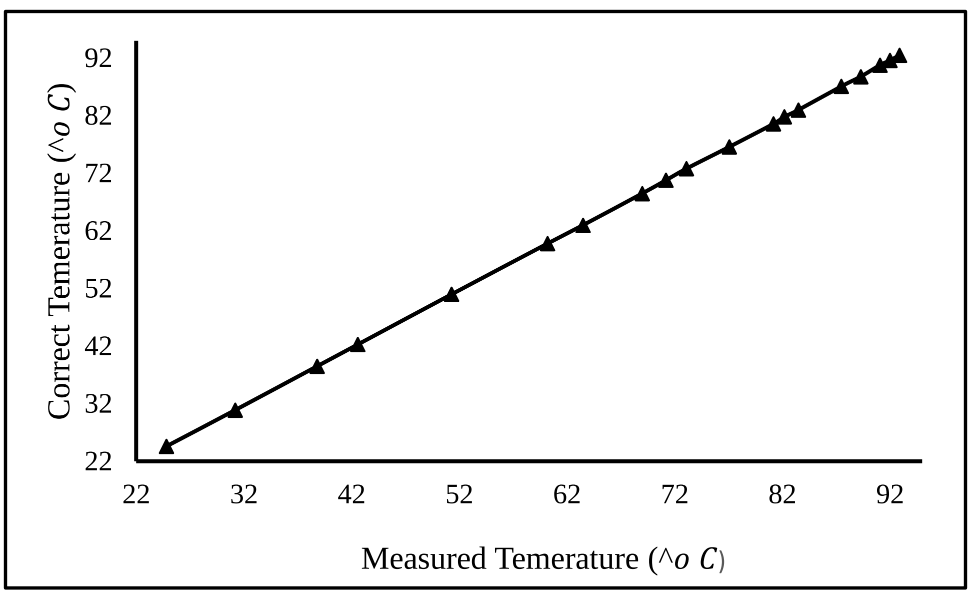

Figure D-2: Measured Temperature versus Corrected Temperature

Four-Channel Digital Thermometer Specifications

- Serial number: HT-9815
- Temperature range:0-800℃
- Power supply: 9V
- Weight: approx. 250g

APPENDIX E

Experimental setup during the baking time

Figure E.1:-Photographs during bread baking time

APPENDIX F

Drawing of solar baker parts

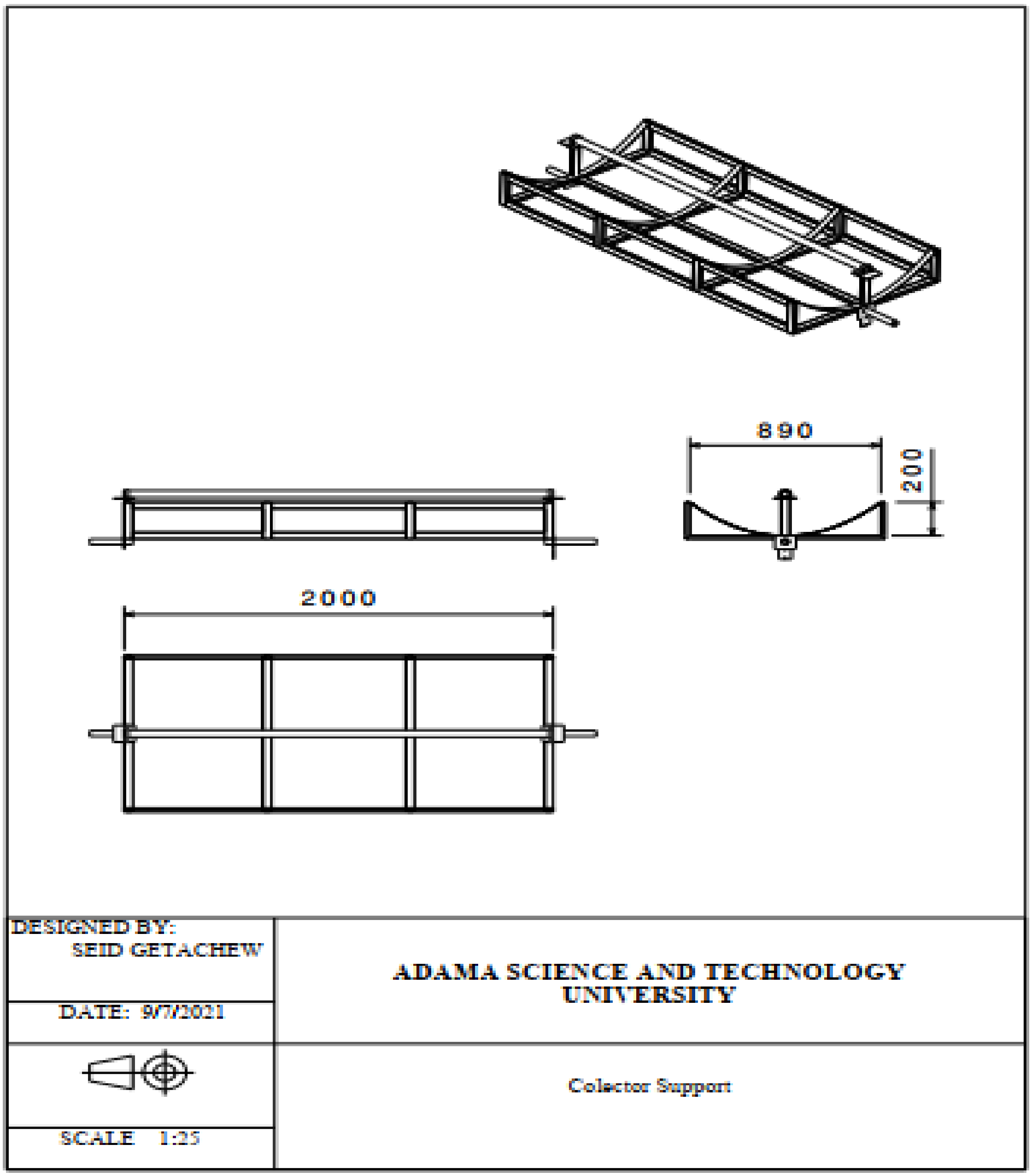

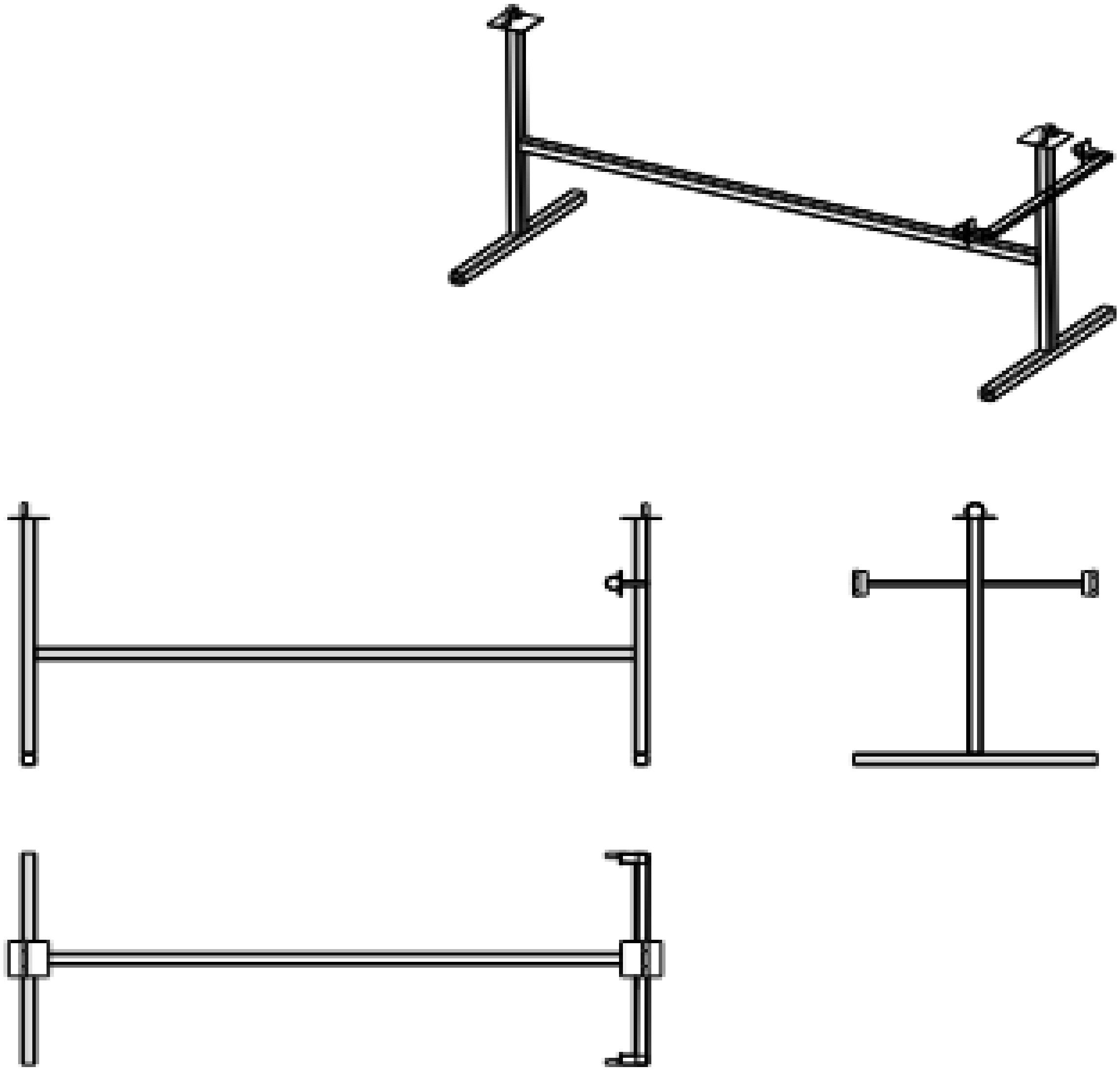

DESIGNED BY: SEID GETACHEW	ADAMA SCIENCE AND TECHNOLOGY UNIVERSITY
DATE: 9/7/2021	
	Tracking and frame Assembly of collector
SCALE 1:25	

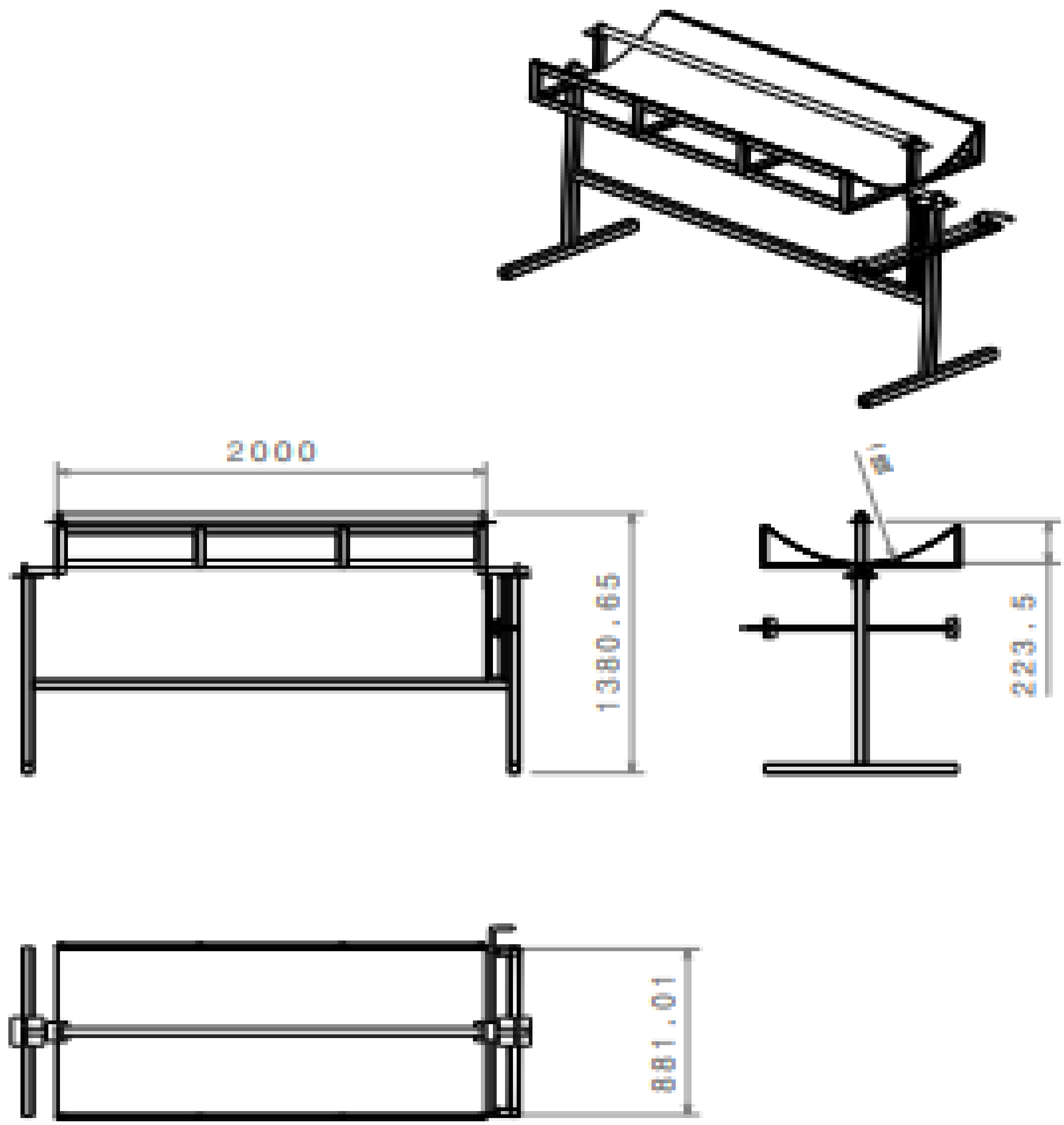

DESIGNED BY: SEID GETACHEW	ADAMA SCIENCE AND TECHNOLOGY UNIVERSITY
DATE: 9/7/2021	
	Parabolic Trough Solar Colector Assembly
SCALE 1:25	

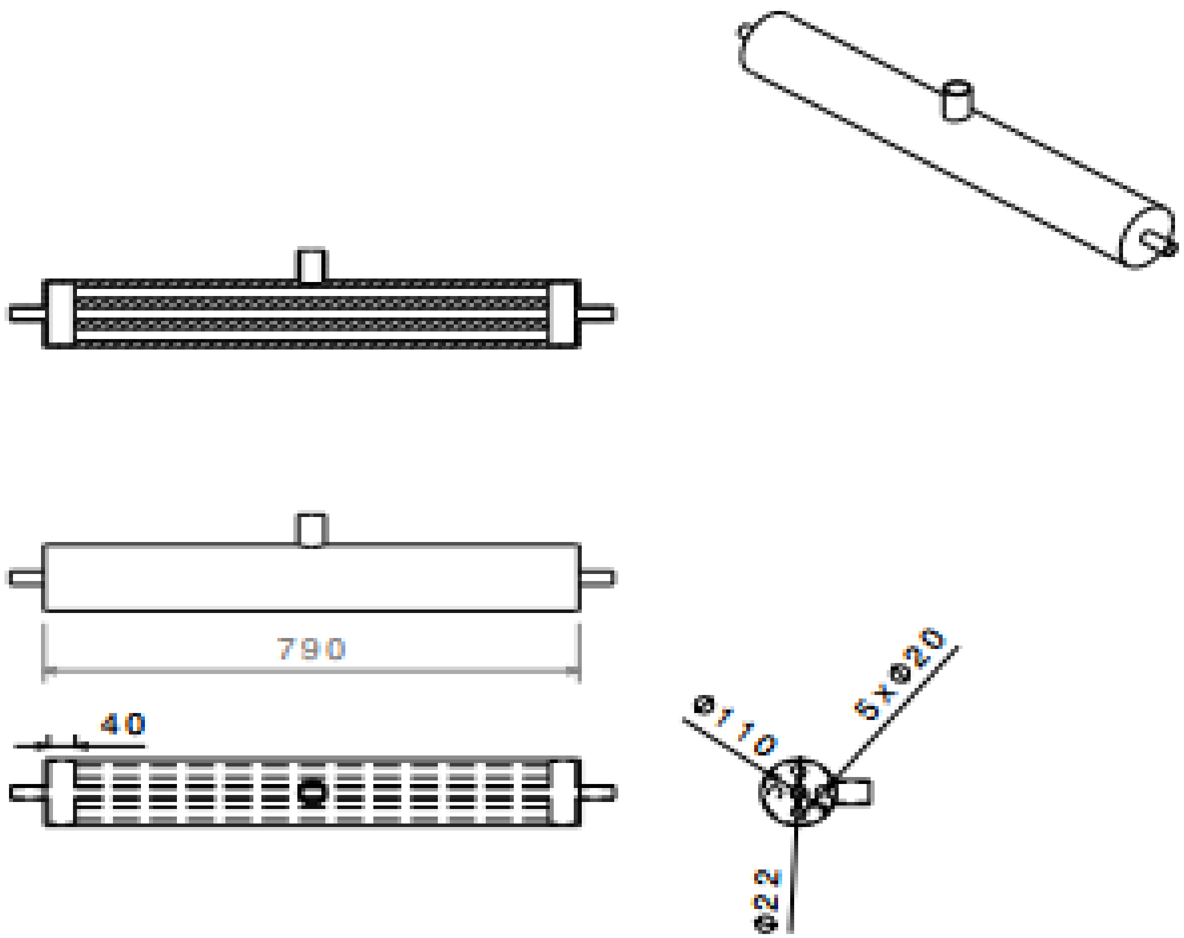

DESIGNED BY: SEID GETACHEW	ADAMA SCIENCE AND TECHNOLOGY UNIVERSITY
DATE: 9/7/2021	
	Thermal Energy Storage
SCALE 1:25	

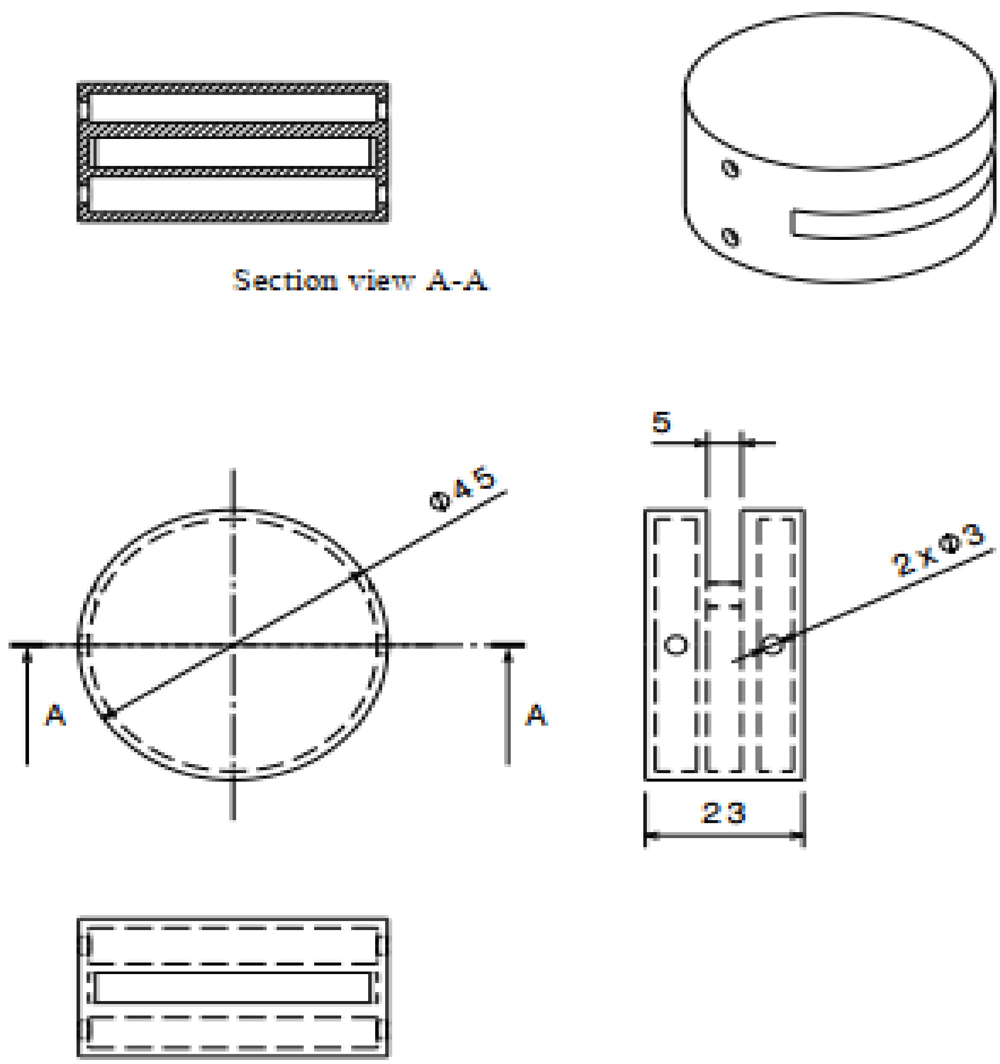

DESIGNED BY: SEID GETACHEW	ADAMA SCIENCE AND TECHNOLOGY UNIVERSITY
DATE: 9/7/2021	
	Baker Unit
SCALE 1:25	